



Summary of geological information relevant to  
development of the porphyry Cu-Mo Resolution deposit,  
Arizona.

Dr Armelle Kloppenburg  
*4DGeo - Applied Structural Geology*  
*Daal en Bergselaan 80, 2565AH The Hague*  
*The Netherlands*

For Resolution Copper Mining LLC  
Superior, Arizona.

May 2017

Table of Contents

<b>1. GENERAL CHARACTERISTICS OF PORPHYRY COPPER DEPOSITS .....</b>	<b>5</b>
1.1 Geological characteristics .....	5
1.2 Economic Considerations.....	6
<b>2. PHYSIOGRAPHY .....</b>	<b>8</b>
<b>3. STRATIGRAPHY .....</b>	<b>9</b>
3.1 Lithological units .....	11
3.1.1 Early to Middle Proterozoic plutonic and metamorphic rocks .....	12
3.1.2 Middle Proterozoic rocks of the Apache Group and associated diabase .....	13
3.1.3 Paleozoic rocks .....	14
3.1.4 Cretaceous intrusive and extrusive rocks .....	15
3.1.5 Middle Tertiary rocks.....	16
3.1.6 Upper Cenozoic deposits (unconsolidated) .....	19
<b>4. ECONOMIC GEOLOGY .....</b>	<b>20</b>
4.1 Metallic mineral occurrences.....	21
4.2 Non-metallic and industrial minerals .....	22
<b>5. GEOLOGICAL SETTING .....</b>	<b>23</b>
5.1 Tectonic context.....	23
5.2 District structures and structural history .....	24
5.2.1 Inherited basement architecture .....	25
5.2.2 Proterozoic diabase emplacement dikes and sills along extensional faults .....	25
5.2.3 Palaeozoic extensional faults.....	25
5.2.4 Laramide orogeny, folds and thrust, intrusions and erosion .....	25
5.2.5 Tertiary Basin and Range extension, listric faults, (half) grabens and rotated fault blocks ....	26
5.2.6 Newly documented regional faults, structures and kinematics .....	27
5.3 Present-day tectonics, stresses and seismicity .....	36
5.3.1 Regional tectonic stresses .....	36
5.3.2 Measured in situ stresses at Resolution .....	37
5.3.3 Regional seismicity .....	39
<b>6. DEPOSIT-SCALE GEOLOGY AND STRUCTURES .....</b>	<b>41</b>
6.1 Background .....	41
6.2 Input data .....	42
6.2.1 Data sets used for the geological model.....	42
6.2.2 Types of data sets used in alteration and mineralization modelling .....	44
6.3 Modeling techniques, constraints and assumptions, handling uncertainty .....	45
6.3.1 Modeling of stratigraphic domains .....	45

6.3.2	<i>Modeling of intrusive bodies</i> .....	45
6.3.3	<i>Modeling of breccia bodies</i> .....	45
6.3.4	<i>Modeling of structures and orientation data</i> .....	46
6.3.4.1	Discretisation of Faults.....	46
6.3.4.2	Annealed vs Non-annealed Faults.....	47
6.3.5	<i>Constraints and assumptions for the 2D and 3D modelling of faults</i> .....	47
6.3.6	<i>From section interpretation to 3D geological framework model</i> .....	48
<b>6.4</b>	<b>The 3D geological framework model</b> .....	<b>48</b>
6.4.1	<i>Interpreted geological units</i> .....	49
6.4.2	<i>Interpreted faults and fault blocks</i> .....	52
6.4.3	<i>Concept for the structural evolution of the Resolution “graben”</i> .....	54
6.4.3.1	Pre-mineralization extensional faulting .....	55
6.4.3.2	Syn - mineralization releasing bend and fault-bounded pull-apart graben .....	55
6.4.3.3	Post-mineralization Basin and Range Extensional faults .....	55
6.4.3.4	Post-mineralisation compressional structures and present-day stresses.....	55
<b>7.</b>	<b>REFERENCES</b> .....	<b>57</b>

APPENDIX 1. Geological map compiled for the project area at 1: 15,000 scale (W. Hart, Resolution Copper, 2016).

APPENDIX 2. Element abundance of the Resolution Copper Orebody (multi-element geochemical analysis) compared to average crustal abundance (Data from: MWH, 2013)

## Preface

This report summarizes geological information as available from regional geology maps and accompanying explanatory notes (USGS), relevant peer-reviewed scientific publications, and Resolution Copper in-house peer-reviewed studies.

It aims to provide a basis for describing the character of the Resolution deposit, the present-day conditions of the regional geology, structures and features to help inform the NEPA process of evaluating impacts and alternatives for the Mine Plan of Operations.

This report has a high level of geological detail, due to the nature of the deposit, the infrastructure development required to mine the deposit and its potential impacts on mining operations and sensitive receptors.

The Resolution deposit is an approximately 64 million year old porphyry Cu-Mo deposit that sits 4,500 to 7,000 ft (1,370-2,100 m) below ground surface. Like many world-class porphyry copper deposits globally, Resolution is a large volume, low concentration ore body. The ore is hosted by Proterozoic and Paleozoic quartzite and carbonate units, Proterozoic diabase sills, and Cretaceous sandstones, volcanoclastic rocks and tuffs as well as felsic porphyry intrusions. The location and the geometry of the mineralization are both strongly structurally controlled, with pre-, syn-, and post mineralization faults, tilted fault blocks, intrusions and angular unconformities forming testimony to a complex history. The known deposit as a whole is tilted approximately 25 degrees (deg) to the east-northeast, but has not been significantly dismembered by Tertiary Basin and Range extension/faulting.

The geological information presented in this document starts with a description of geologic characteristics of porphyry copper deposits world-wide. Chapter 2 then describes how the present-day landform of the project area strongly results from the underlying geology. Chapter 3 provides an up-to-date geological map, with a detailed description of the full sequence of rock types present, from the oldest 1.7 Ga metamorphic Pinal Schist to the youngest deposits of surficial, unconsolidated erosional material. A summary of metallic and non-metallic mineral occurrences, as well as industrial minerals, is presented in Chapter 4. An outline of the tectonic evolution forms the context for a description of the regional structural development, the main tectonic phases and the character of the associated structures at the scale of the district (Chapter 5). Chapter 6 then zooms into the geology of the Resolution deposit, the current understanding, the knowns, the unknowns, and the methods and assumptions used to construct the geological framework model in digital 3D space – largely from drill hole data. The model describes the host rock configuration and characteristics including mechanical properties, the potential connectivity of faults and fault blocks for fluid flow, the mineralization volumes and grade, and other mineralization-related characteristics to be taken into account in the development of the resource.

The geological information aims to cover all geological aspects that may have an influence on the environmental impact of the project.

# 1. General Characteristics of Porphyry Copper Deposits

Porphyry copper deposits are found around the world, most commonly in areas with active or ancient volcanism associated with active continental (Andean-type) margins or island arcs. The porphyry intrusion provides a pathway for energy and metals from deeper-seated magma chambers. Porphyry copper deposits typically are low grade, large tonnage deposits that require bulk mining techniques (John and others, 2010). Because of their large size their mine lives typically span decades. Geologic characteristics of porphyry copper deposits have been described by Seedorff et al. (2005), Sinclair (2007), and Berger et al. (2008), and have more recently been reviewed by John et al. (2010). Below is a summary of the characteristics most relevant for environmental impact studies and follows Seal (2012).

## 1.1 Geological characteristics

Primary (hypogene) ore minerals found in porphyry copper deposits are structurally controlled and genetically associated with felsic to intermediate composition; porphyritic intrusions that typically were emplaced at shallow levels in the crust. Mineralization commonly occurs both within the associated intrusions and in zones within the surrounding wall rocks (Figure 1). The primary minerals fill veins, veinlets, stockworks and breccias. The main copper-sulfide ore minerals are chalcopyrite ( $CuFeS_2$ ) and bornite ( $Cu_5FeS_4$ ). A number of other minor copper sulfide minerals are commonly found; most notable from an environmental perspective is the arsenic-bearing mineral enargite ( $Cu_3AsS_4$ ). Molybdenite ( $MoS_2$ ) is the main molybdenum mineral. Gold in porphyry copper deposits can be associated in appreciable amounts with bornite, chalcopyrite, and pyrite; the gold may occur as a trace element within these sulfide minerals or as micrometer-scale grains of native gold (Kesler and others, 2002).

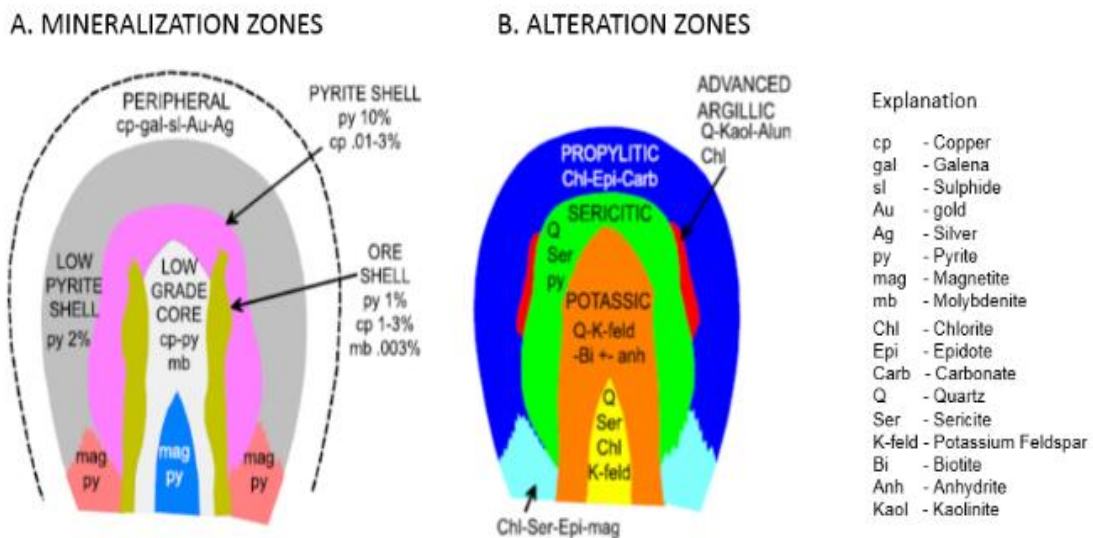


Figure 1: Cross section through an idealized porphyry copper deposit showing the relationship of the ore shell to various alteration types. A. Distribution of ore mineral assemblages; B. Distribution of alteration types, with the causative intrusion corresponding to the potassic alteration zone. From John and others (2010), modified from Lowell and Guilbert (1970).

Hydrothermal mineralization produces hydrothermal alteration haloes that are much larger than the actual ore deposit. The classic alteration zonation includes a potassium feldspar-biotite rich core, surrounded by a muscovite/illite sericitic (phyllitic) alteration zone, which is surrounded by a clay-rich argillic alteration zone and finally by a chlorite-epidote rich propylitic zone (Lowell and Gilbert, 1970). The ore zones generally coincide with the potassic and sericitic alteration zones. From an environmental perspective, the importance of these alteration types is that the sericitic and argillic alteration tends to destroy the acid-

neutralizing potential of the rock, while enhancing the acid-generating potential through the addition of pyrite. In contrast, the outer portion of the propylitic zone tends to have enhanced acid-neutralizing potential due to the introduction of trace amounts of carbonate minerals.

Supergene (weathering) processes, which occur long after the initial hydrothermal mineralizing events, can lead to zones of supergene enrichment near the tops of these deposits (John and others, 2010). The supergene enrichment zones can be either oxide- or sulfide-dominated depending on the prevailing oxidation state at the site of formation, the depth of the water table, and climate.

Porphyry copper deposits can be divided into three subtypes on the basis of their Au to Mo ratios: (i) porphyry Cu, (ii) porphyry Cu-Mo, and (iii) porphyry Cu-Au deposits, where Cu-Au deposits have Au/Mo ratios greater than or equal to 30, Cu-Mo deposits have Au/Mo ratios less than or equal to 3, and Cu deposits are all other deposits not within these bounds (Sinclair, 2007; Singer and others, 2008). On the basis of these criteria, the Resolution deposit would be classified as a porphyry Cu-Mo deposit.

At Resolution the mineralisation and alteration patterns are largely intact and integrally tilted to the east by displacement on post-mineralization Basin and Range extensional faults (Figure 2).

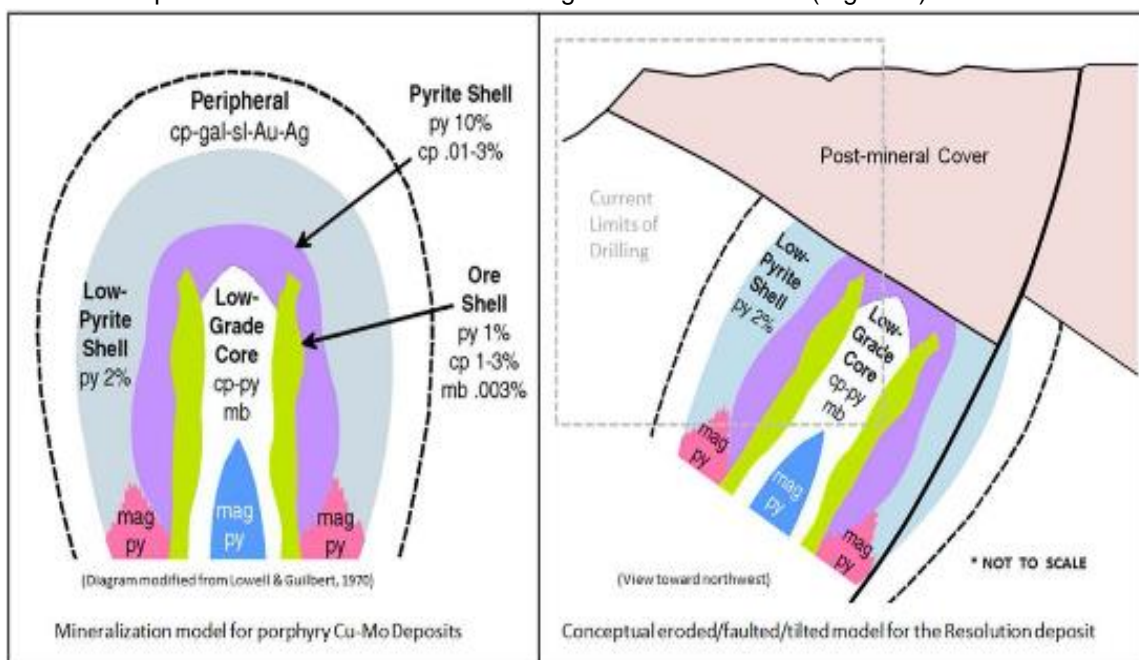


Figure 2: (Left) Idealized cross section through a porphyry copper-molybdenum deposit. (Right) At Resolution, Basin and Range extension on west- or southwest-dipping faults has caused an overall tilt of the deposit to the east-northeast (Internal RCC report, 2016; modified from Lowell & Guilbert, 1970).

## 1.2 Economic Considerations

The grade and tonnage of porphyry copper deposits vary widely (Table 1, Singer et al., 2008), but copper deposits are generally of low grade and high tonnage. Summary statistics compiled for 256 porphyry copper deposits world-wide are visualised and provide context for the Resolution deposit with an estimated total Cu inferred resource of 1,766 million tonnes, and a copper and molybdenum percentage of 1.51% and 0.035% respectively per the 2015 Rio Tinto annual report, (Figure 3 amended from Singer et al., op cit). This diagram also shows that that the total contained metal at Resolution is of similar order of magnitude as the largest well-known Cu-Mo deposits.

Table 1. Global copper and molybdenum grade and tonnage summary statistics for porphyry copper deposits (n = 256; Model 17, Singer et al., 2008) compared to the Resolution deposit.

Parameter	10th Percentile	50th Percentile	90th Percentile	Resolution
Tonnage (Mt)	1,400	250	30	1766
Cu grade (%)	0.73	0.44	0.26	1.51
Mo grade (%)	0.023	0.004	0	0.035

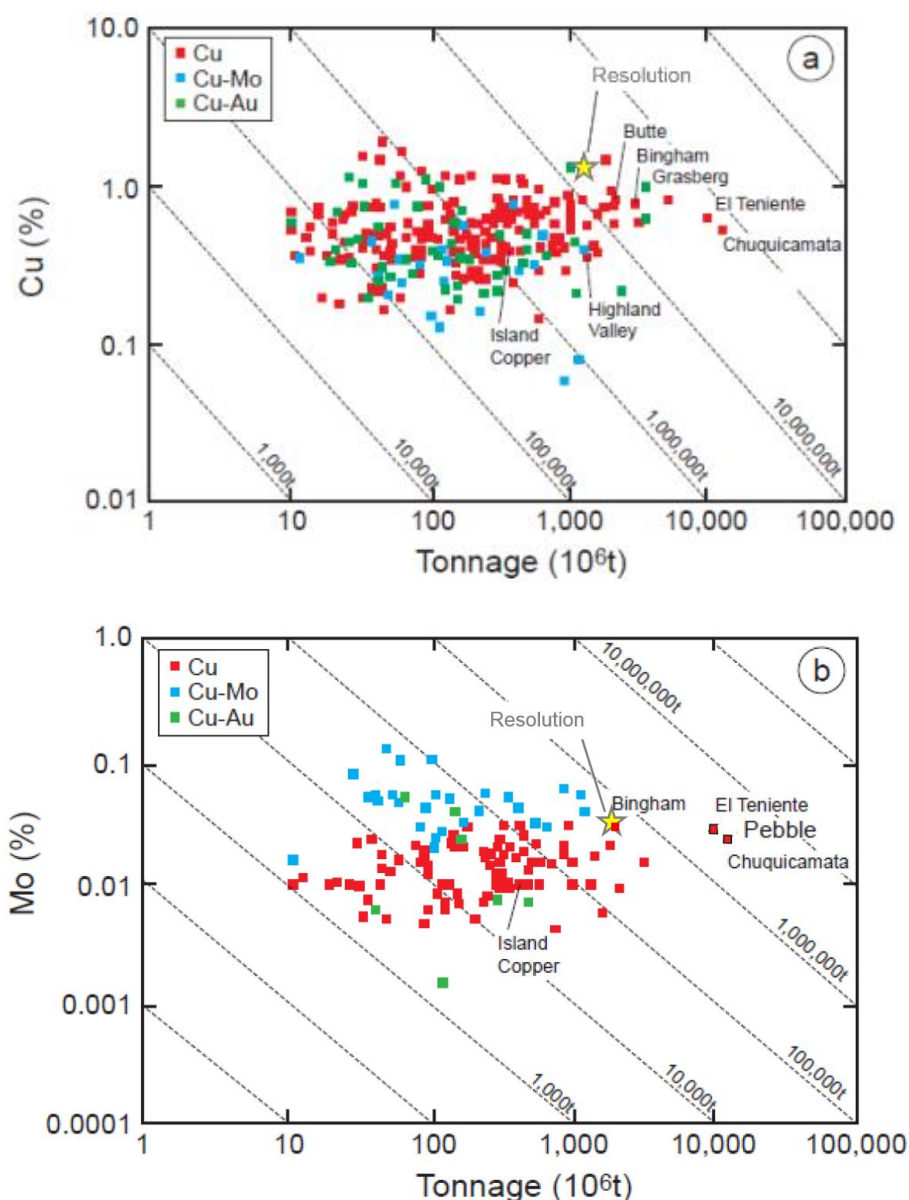


Figure 3: Grade and tonnage characteristics of the Resolution deposit compared to other porphyry-type deposits world-wide, copper (top), molybdenum (bottom). Selected, noteworthy deposits are labeled. The dashed diagonal lines represent the total contained metal. Modified from Seal (2012) and Sinclair (2007).

## 2. Physiography

The project area includes the historic Superior (formerly Pioneer) mining district, which lies on the north-eastern edge of the Basin and Range physiographic region (Figure 4). The topographic expression of many of the geological and structural features is strong.

The eastern part of the area, which includes the Resolution deposit, is part of one of the easternmost Basin and Range mountain ranges, the rugged Oak Flat plateau of 4000 to 4600 ft (1200-1400 m) elevation located just east of the town of Superior. Oak Flat's western edge is delineated by the prominent Apache Leap escarpment, with high peaks of around 4760 ft (1450 m) elevation, which overlook the town.

The western portion of the project area includes the Superior basin, with generally low relief but with local mountain ridges formed by variably eroded fault blocks of older rocks, which are tilted to the SE and which locally protrude from beneath younger, gently dipping basin sediments. These small ridges separate intervening valleys, many filled with Quaternary aged alluvial deposits. The valleys are relatively narrow at higher elevations and widen as elevation decreases toward Queen Creek, the main drainage in the project area. Elevations in the Tailings Storage Facility range from approximately 2,240 ft (683 m) in the southwestern portion to 2,920 ft (890 m) above mean sea level. This area is flanked to the south by Picketpost Mountain, a remnant volcanic vent complex of Tertiary age forming an isolated erosional butte with a maximum elevation of 4,378 ft (1,334 m).

The main channel of Queen Creek trends roughly east-west across the project area, at a high angle to the west-facing range front. From its upper reaches on the northern periphery of Oak Flat, the channel passes southwest-ward across the plateau, then steepens in grade and bends westward as it transects the Apache Leap escarpment, crossing the Superior basin through the town of Superior, and then the Queen Valley circa 13 miles (20 km) farther west. Most of the other drainages in the project area on Oak Flat, and within the Superior basin are tributaries of Queen Creek. The southern part of Oak Flat within the project area drains toward the southeast primarily via Rio Rancho Creek, then southward along Devils Canyon and ultimately Mineral Creek. Areas farther east drain primarily southward to Devils Canyon which drains into Mineral Creek. Mineral Creek is impounded by Big Box Dam and diverted through a tunnel around the Asarco-Ray open pit.

The project area is located in a zone with a low level of present-day seismicity (see Section 5.3).

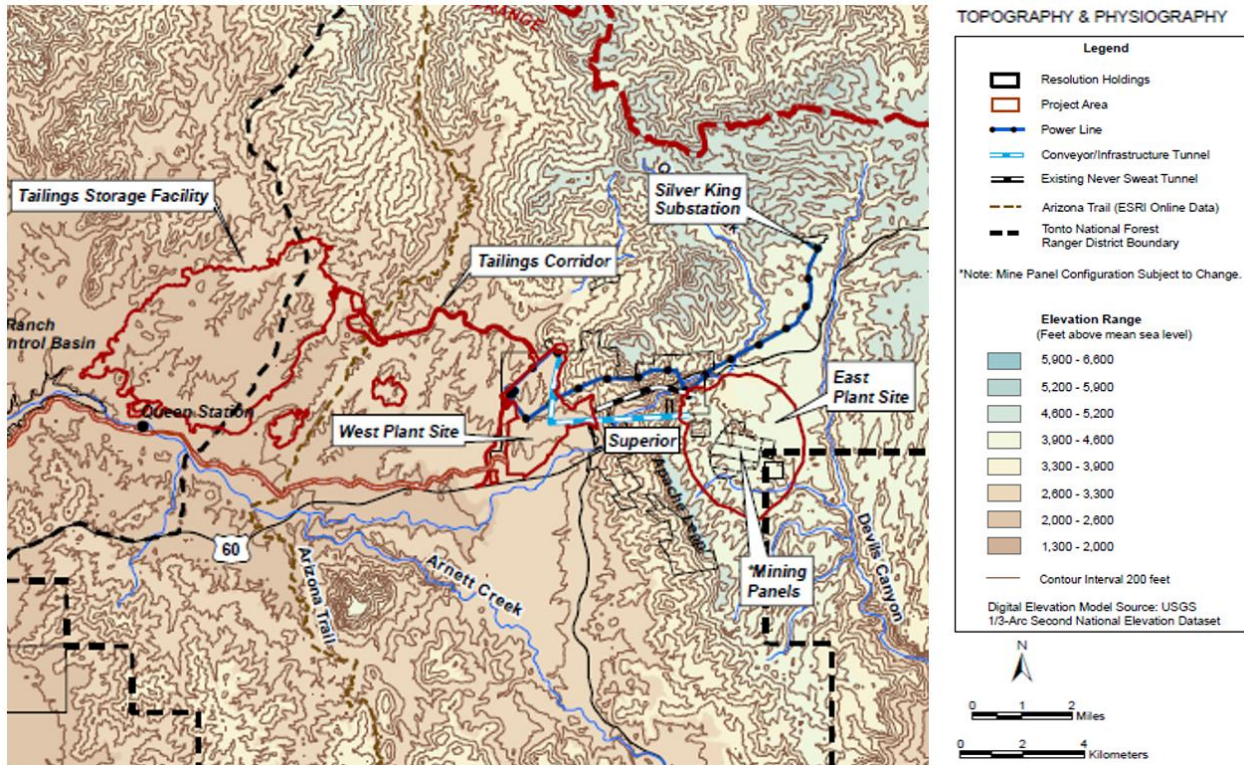


Figure 4: Topography and physiography of the project area, showing the Town of Superior, Queen Creek, the outline of the deposit and tailings storage facility. After: Resolution Copper General Plan of Operations Figure 2.2-1.

### 3. Stratigraphy

An up to date geological map for the project area (Figure 5, and Appendix 1) has been compiled by W. Hart (Resolution Copper Company, December 2016) by merging a recent in-house project-scale (1:12,000) geologic map and significant portions of the following published 1:24,000 scale 7.5 minute geologic quadrangle maps: 1) Geology of the Picketpost Mountain and the southern part of the Iron Mountain quadrangles (Spencer and Richard, 1995), 2) Geology of the Superior quadrangle, 3) Geology of the Pinal Ranch quadrangle. The project-scale map was produced by digitizing and merging a collection of unpublished detailed maps:

1966-1993, D. Hammer - Hammer remapped all area previously mapped by others within the Magma mine mineral holdings in more detail, and extended a 1-mile-wide belt of mapping approximately 3.5 miles south of the east-west trending Magma vein, to eventually include mining claims and surface workings of numerous small-production MnOx-Ag-Cu mines gradually acquired by Magma which had been either mined out or abandoned by 1957.

2003-2005, J. Gant, J. Wilkins (Kennecott Exploration Company) – Field mapping and 1:12,000 scale geologic maps produced for the Oak Flat area (covering the Resolution deposit); produced primarily for geotechnical evaluations, as part of the first Order of Magnitude study.

2007, A. Schwarz and field assistants (RCC) – Field mapping traverses with true thickness measurements of stratigraphic sections along the range front immediately east of Superior town.

The rocks in the project area span an age range of at least 1700 million years, from 1700 million year old metamorphosed sediments that now form the Pinal Schist, to the Miocene (<22 Ma) sequence of volcanic rocks, and Quaternary-aged erosional deposits. The legend and geological unit identifier codes largely follow the stratigraphic sequence of the published Picketpost Mountain map (Spencer and Richard, 1995). Newly mapped units include sub-units of the Tertiary Apache Leap tuff (Tal), some of which are described in a separate publication (Peterson, 1961), and later mapped in-house by Kennecott and Resolution Copper Company geologists. Additional unexposed stratigraphic units of hydrothermal breccia bodies of late Cretaceous age units were recognized in drill holes only, and their descriptions follow Hehnke et al. (2012).

A description of each geological unit is given in the section below, starting with the youngest units, with radiometric age dates provided where available.

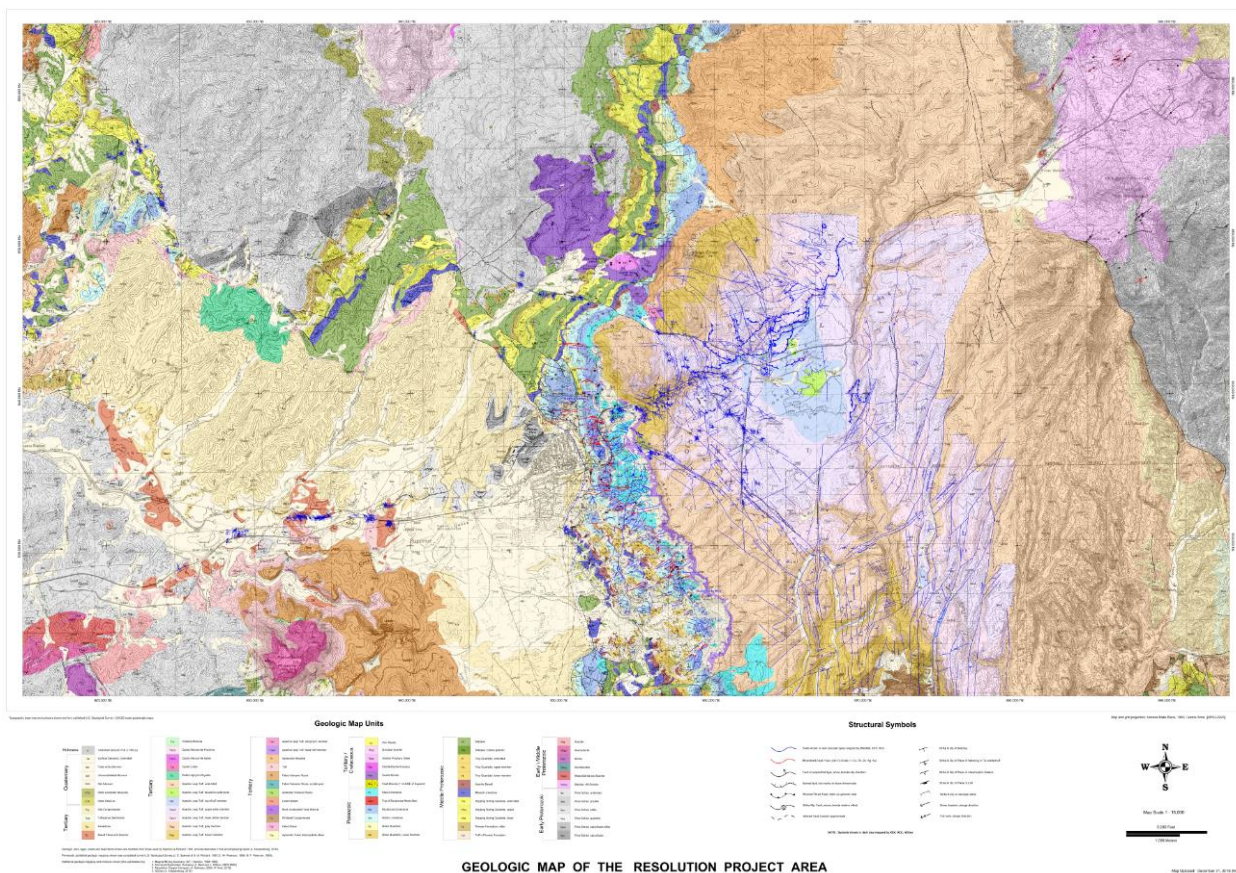


*Figure 5: Thumbnail of the 1: 15,000 compiled geological map (W. Hart, Resolution Copper, 2016) covering the project area. The full-sized resolution map is presented in Appendix 1. The geology is based on the 1:24,000 USGS Picketpost and Superior quadrangle geological maps merged with additional detailed in-house mapping of lithology and structures near the deposit. Showing published faults in black and newly documented faults and other structures in dark blue.*

An overview of mapped geological units and identifier codes, including selected published and unpublished geochronological age constraints, is given in Table 2. A full description of all lithological units is provided in Section 3.1.

An associated updated (tectono-) stratigraphic column is presented in Figure 6, showing deposition, erosion, (angular) unconformities, and intrusive relationships. It serves to illustrate the relationship between stratigraphy, igneous activity and tectonic events, further discussed in Section 5.1.

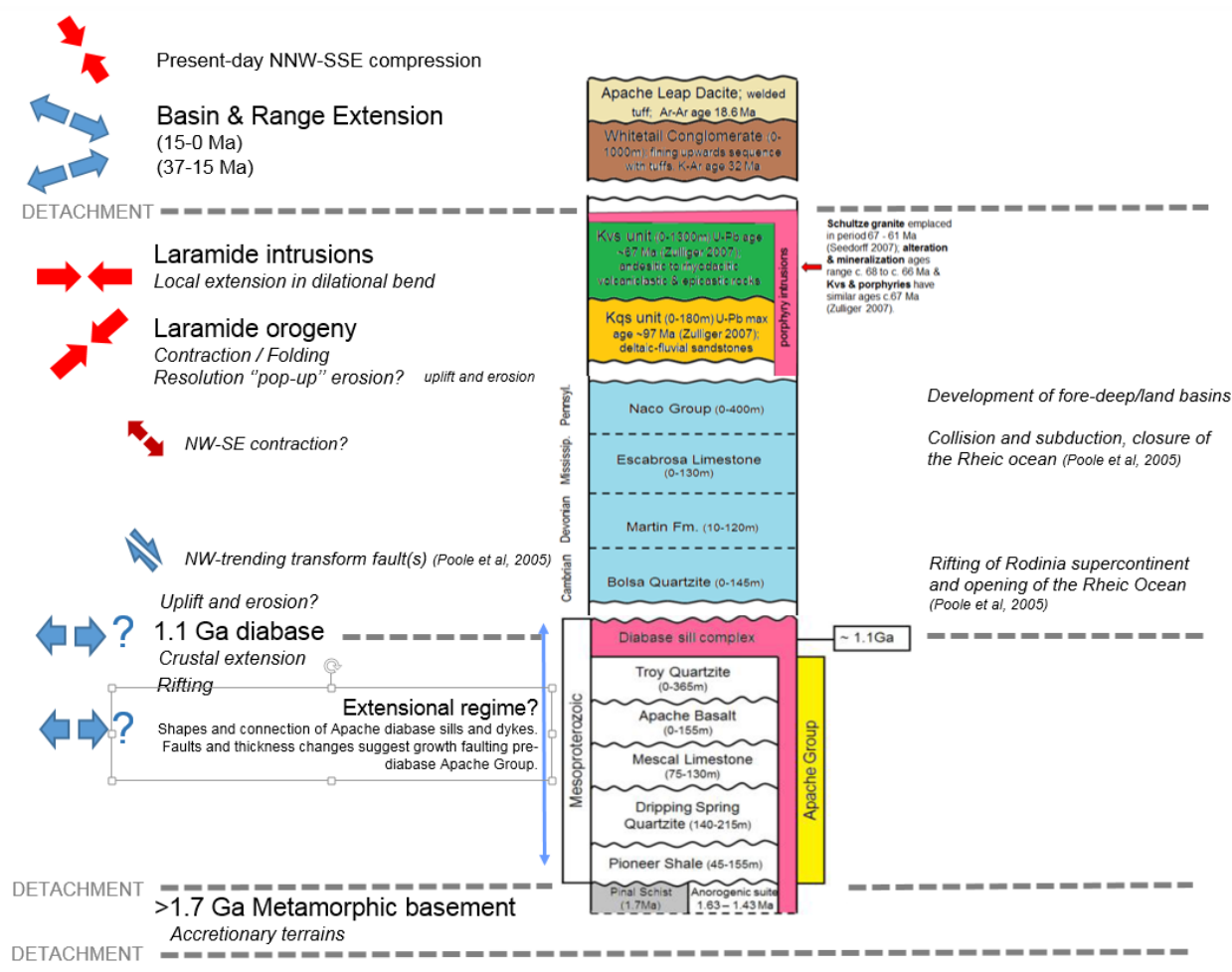


Figure 6: Tectono-stratigraphic column, illustrating the relationship between the timing of main tectonic phases and associated sedimentation, as well as (erosional) unconformities, intrusion relationships, and the mechanically weaker stratigraphic layers that have acted as detachments. The Laramide orogeny involved first NE-SW compression, which then with time progressively rotated to E-W (Bird, 2002), causing belt-parallel folding and thrusting, as well as strike slip reactivation of the ENE-trending Salt River – Jemez Geophysical Lineament. Basin and Range extension initiated as ENE-WSW, and then rotated with time to NW-SE extension as a result of changing subducting plate configurations (Bird, 2002). The continent-scale tectonic compilation of Poole et al. (2005) describes the pre-Laramide rifting and opening of the Rheic Ocean with development of NW-trending transform faults in the basement, followed by closing of the Rheic Ocean, continent collision and the NW-SE compression during deposition of the Escabrosa and Naco Group carbonates.

### 3.1 Lithological units

The lithological units that comprise the map (Figure 5, and Appendix 1) are described below. They are divided into age groups and a general description of the sequence per era, and the geological significance for the project area is given, after which each unit is described in detail. An overview of the stratigraphy is presented in Table 2.

Period	Map Unit codes	Rock type(s)	Age	Age (Ref)
Upper Cenozoic	d	Disturbed ground / fill (<200 yr)		
	Qal	Active stream channel alluvium		
	Qs, Qtc, Ooa	Older alluvial fan and terrace deposits		
	Qls, QTIs, QTs	Landslide deposits		
Middle Tertiary	Tcg, Tss	Conglomerate and sandstone		
	Tb, Tvx, Tql, Tp,	Gila Group volcanic and intrusive rocks and equivalent units (younger than Apache Leap Tuff)	18.4±0.5 Ma	K-Ar cooling age biotite (ref)
	Tal	Apache Leap Tuff	18.58 + 0.03 Ma	<sup>40</sup> Ar/ <sup>39</sup> Ar cooling age (Ferguson et al., 1998)
	Tf, Tt, Tfp, Tfa, Tbl, Tdf, Tda, Tdb	Superstition Group volcanic rocks and equivalent units (older than Apache Leap Tuff)		
	Tw	Whitetail Conglomerate	24.29±0.12 Ma, 21.97±0.06 Ma, 21.77±0.32 Ma	<sup>40</sup> Ar/ <sup>39</sup> Ar cooling age, Sanidine (Hehnke et al, 2012).
	Tda	Dacite dikes		
Cretaceous-Tertiary	(not on map)	Laramide Porphyry intrusive (QEP)	73 - 64 Ma	U-Pb, zircon (Seedorff et al., 2005b; Stavast, 2006; Zulliger, 2007).
Cretaceous	(not on map)	Kvs - Volcaniclastic sediments	74 - 64 Ma	U-Pb, zircon
	(not on map)	Kqs - Quartzose sandstones, local conglom.	Max 97 Ma. - Min 74 Ma.	U-Pb, detrital zircon (Zulliger, 2007).
	Kd	Diorite porphyry and quartz diorite (Silver King stock)	74.83±0.33 Ma	<sup>40</sup> Ar/ <sup>39</sup> Ar cooling age biotite (Hehnke et al, 2012)
Palaeozoic	Pn, Mem Dm, Cb	Naco Formation Escabrosa Limestone Martin Formation Bolsa Quartzite	Pennsylvanian (323 Ma -299 Ma) Mississippian (359 Ma - 323 Ma) Devonian (420 Ma - 359 Ma) Cambrian (541 Ma - 485 Ma)	
Middle Proterozoic	Yd	Diabase	1.1 Ga	
	Yt	Troy Formation orthoquartzite		
	Ym, Yds (Ydsu, Ydsl, Ydsb), Yp, Ypt	Apache Group: Mescal Limestone Dripping Springs Quartzite ( <i>Upper DSQ, Lower DSQ, Barnes Conglomerate</i> ) Pioneer Shale ( <i>Tuff in Pioneer Shale</i> )	1.6 Ga	
Early to Middle Proterozoic	Yg, Yxg, Yxgd, Yxd, Yxh, Yxgm	Granite, granodiorite, diorite, hornblende, mixed schist/granite		
	Xp	Pinal Schist	pre-1.7 Ga	

Table 2: Mapped geological units and identifier codes as used on the geological map in Figure 5, with published geochronological age constraints.

Unless otherwise noted, geologic unit codes and descriptions herein are from: Geologic Map of the Picketpost Mountain and southern part of the Iron Mountain 7.5 minute quadrangles (Spencer and Richard, 1995). Equivalent geologic unit codes shown on Geology of the Superior Quadrangle (D. Peterson, 1969) and Geology of the Pinal Ranch Quadrangle (N.P. Peterson, 1947, and 1957-59) are shown in italic font within parentheses, where applicable.

### 3.1.1 Early to Middle Proterozoic plutonic and metamorphic rocks

The oldest rocks in the project area belong to the metamorphic Pinal Schist (Xp), developed from >1.7 Ga Paleoproterozoic turbidites (Keep, 1996). The Pinal schist contains a series of Early to Middle Proterozoic intrusions.

**YXg** Granite (early or middle Proterozoic) -- Equigranular, unfoliated, medium to fine grained granite or granodiorite with local marginal aplitic zones. Generally contains 7-10% mica, including both biotite and muscovite, but their relative abundance varies greatly. More muscovite-rich granite, common south of Queen Creek, appears to have assimilated more Pinal Schist and is generally associated with gradational assimilation zones and broader contact aureoles. The northeast-trending

elongated body in the northeast part of the map area generally has sharp contact with a few screens of schist near the contact, and no apparent contact metamorphic aureole. The granite near the contacts in this pluton is slightly foliated.

- YXgd** Granodiorite (early or middle Proterozoic) -- Similar to YXg, but contains more abundant biotite and has slightly darker color index.
- YXd** Diorite (early or middle Proterozoic) -- Fine to medium grained dark gray equigranular diorite, composed of hornblende or pyroxene and plagioclase.
- YXh** Hornblendite (early or middle Proterozoic) -- Fine to coarse grained hornblendite, consisting of 70 – 90% hornblende with anhedral plagioclase, and common secondary(?) epidote. Rock is black.
- YXgm** Mixed schist and granite (early or middle Proterozoic) -- YXg or YXgd with abundant screens and pendants of Pinal Schist.
- YXmg** Granite on Manitou Hill (early or middle Proterozoic) — Sill-like bodies of granite intruding Pinal Schist. YXg or YXgd with abundant screens and pendants of Pinal Schist.
- Xp (pCp)** Pinal Schist, undivided (early Proterozoic) -- Dominantly phyllitic schist in northern areas and dominantly psammitic schist in southern exposures. Metamorphic grade appears to be higher in northern areas where metamorphic very fine grained to microcrystalline phyllosilicates impart a reflective sheen and schistosity to phyllitic rocks, whereas phyllitic schist in southern areas is only slightly higher grade than a slate. Northern exposures generally consist of bluish gray, fine grained, phyllosilicate-rich schist with numerous, variably folded hydrothermal quartz stringers. Foliation is defined by compositional layering, phyllosilicate orientation, and quartz segregations. Quartz stringers are commonly irregular in thickness and tightly folded.

### 3.1.2 Middle Proterozoic rocks of the Apache Group and associated diabase

Unconformably overlying the Pinal Schist is the Proterozoic Apache Group: a >500m thick conformable sequence of sedimentary and volcanic formations. The main outcrop of these rocks is in the range front where they are well exposed partly because they are tilted to the east. The sequence includes, from oldest to youngest: the Pioneer Formation, Dripping Spring Quartzite, and Mescal Limestone with unnamed basalt flows locally overlying the Mescal Limestone. The Middle Proterozoic Troy Quartzite unconformably overlies the Apache Group. Diabase sills and dikes intruded all of these sedimentary units regionally extensively, locally causing inflation of the sequence of up to a 100%. The diabase has yielded a range of ages all clustering around 1.1 Ga. See Wrucke (1989) and Donadini et al. (2011) for an overview of available age dates for the diabase across Arizona. Faults that are exploited by the diabase and therefore must be older than the intrusions that trend NE and NW.

- Yd (pCdb)** Diabase (middle Proterozoic) -- Abundant 1-3 millimeter (mm) plagioclase crystals in black groundmass. Locally crude layering is defined by variation in ratio of plagioclase to groundmass and in size of plagioclase crystals. Generally is highly fractured and typically forms fragments less than 20 centimeter (cm) diameter. In many areas is deeply weathered to form a characteristic red-brown granular soil with no exposed rock. A sill nearby Miami was dated at  $1040 \pm 30$  Ma, and  $1140 \pm 40$  Ma by K-Ar on biotite (Banks et al, 1972).
- Yt (pCt)** Troy Quartzite (middle Proterozoic) — Upper member is chiefly fine-grained, locally medium- to coarse-grained quartzite and arkosic quartzite. Weathers to resistant, blocky ledges. Bedding medium, generally planar, but locally wavy. White to light gray where fresh, light gray to light brownish-gray where weathered. Chiefly rounded to sub-rounded, well-sorted grains; beds locally contain scattered quartz granules and small pebbles. Many beds contain clots of powdery hematite interstitial to grains, giving the rock a spotted appearance. Lower member consists of alternating beds of conglomerate, poorly sorted coarse-grained feldspathic quartzite and arkose, and siltstone;

conglomerate beds most abundant near base; beds are lenticular and have highly variable thicknesses. Crossbedding and local Liesegang banding are common. In upper part, a medium-grained feldspathic sandstone bed as much as 50 feet thick shows well-developed convolute laminations.

**Yb (pCb)** Apache Basalt (middle Proterozoic) — Dark-gray to dark-brown aphanitic rock composed of microscopic plagioclase tablets partly altered to clay and calcite, and pyroxene and olivine largely altered to opaque oxides, serpentine, calcite, iddingsite, and other products. Locally vesicular and/or amygdaloidal. Some layers are volcanic breccia consisting of angular basalt blocks in a matrix of basaltic lava (D.W. Peterson, 1969)

**Ym (pCm)** Mescal Limestone (middle Proterozoic) -- Massive to wavy laminated, light gray limestone (Spencer and Richard, 1995).

**Yds (pCds)** Dripping Spring Quartzite (Middle Proterozoic).

Ydsu Dripping Spring Quartzite, upper unit (middle Proterozoic)--Reddish brown to brownish red, thin bedded to laminated siltstone and very fine grained sandstone that readily parts along bedding planes. Locally the middle part is a black, laminated argillite. Some red-brown units contain 1-2 cm diameter light tan or gray reduction spots, similar to those in the Pioneer Formation, but in the upper Dripping Spring, the spots tend to be larger in diameter and less abundant than in the Pioneer.

Ydsl Dripping Spring Quartzite, lower unit (middle Proterozoic)--Tan to pink medium to thin bedded feldspathic quartz arenite or feldspathic quartzite. Low- to moderate-angle trough cross beds are common. Ranges from coarse- to fine-grained, forming a fining upward sequence. In western exposures (west of Hewett Canyon) basal 5-10 meters consists of pale orange, medium to coarse grained, well bedded, partially cross bedded (10-40 cm thick cross bedded beds) quartzose sandstone with sparse, typically isolated quartzite pebbles and cobbles up to 5 cm diameter. Local pebble beds contain subrounded to rounded clasts of bull quartz, tan to brown quartzite, red jasper(?), and, possibly, brown silicic metavolcanic rocks. Prominent bluffs form the top of this unit in Whitford Canyon.

**Yp (pCp)** Pioneer Shale (middle Proterozoic) -- Reddish brown to purple siltstone and fine grained sandstone with basal Scanlon conglomerate that is 20 to 200 cm thick and consists of clasts of underlying Pinal Schist. Ubiquitous, light gray circular or elliptical reduction spots, generally less than 1 cm in diameter, distinguish sandy parts of the Pioneer from the upper Dripping Spring Quartzite.

**Ypt** Tuff in Pioneer Formation (middle Proterozoic) -- Pale tan to pale gray, hard, massive, very fine grained siliceous hornfels. Contains sparse 1-2mm feldspar phenocrysts. This resistant unit forms a prominent ledge in outcrop where it is present. The bed is 2-5 m thick in the Whitford Canyon area, thinner or absent in the western part of the map area.

### 3.1.3 Paleozoic rocks

Unconformably overlying the Proterozoic Apache Group and Troy Quartzite is a sequence of Paleozoic conformable sedimentary formations that include, from oldest to youngest, Bolsa Quartzite, the Martin Formation, Escabrosa Limestone, and Naco Limestone. These units are extensively present in the range front and in the area of the Magma Mine north of Resolution, but partly eroded in the deposit graben itself, and fully eroded further towards the south, near the Ray Mine.

**Pn** Naco Limestone (Pennsylvanian) -- Medium- to thin-bedded light gray, white, pale blue and pink limestone that locally contains irregular light-brown chert nodules and layers. Bedding planes distinct and most are flat, though some are wavy. Fossils that are common and locally abundant include fusulinids, brachiopods, corals, bryozoan. Base of formation generally marked by 4-meter

bed of dusky red to purple fissile shale; similar shale is sporadically interbedded with limestone higher in section. Thin discontinuous beds of chert conglomerate crop out locally below the shale and mark the base. Variability of thickness due to post-Naco erosion that occurred before deposition of overlying Tertiary rocks (Peterson, 1969). Variability of thickness due to post-Naco erosion that occurred before deposition of overlying Tertiary rocks (Peterson, 1969).

- Me** Escabrosa Limestone (Mississippian) -- Bluff forming, resistant, thick bedded to massive dolomitic limestone and limestone. Lower part is dolomitic, grades upward into pale gray to bluish gray, slightly cherty limestone with small crinoid columnals.
- Dm** Martin Limestone (Devonian) -- Martin Limestone consists, in ascending order, of tan dolomite, gray petroliferous limestone, light gray, slightly cherty limestone, thick graded sandstone bed with very well rounded quartz grains, coarse at base and fine at top, well bedded, fossiliferous gray limestone containing crinoids, shells, and coral, grading into thick bedded limestone.
- Cb** Bolsa Quartzite (Cambrian) -- Coarse to fine grained to locally silty, well-bedded, blocky weathering, typically cross bedded quartzite. Color is dark and light brown to dark brownish-red to orangish-tan, and color banding is typical. Degree of sorting varies greatly. Some beds that contain coarse grains are so poorly sorted they are best described as grit. Crossbeds are common, range from a few cm to perhaps 50 cm thick, and locally contain very coarse (up to 8mm) quartz grains and sparse, 2-4 mm pink potassium(?) feldspar grains. In general, at lower stratigraphic levels the Bolsa Quartzite is darker colored, and contains locally abundant magnetite laminations and local dark lithic fragments probably derived from Apache diabase. Much of the Bolsa Quartzite contains tan, medium to coarse quartz-rich sandstone massive or crudely graded beds interbedded with medium to fine grained, cross bedded and plane bedded sandstone with dark tan to brown laminations. Upper Bolsa Quartzite is tan to light gray to pinkish light gray, medium to fine grained to locally coarse grained orthoquartzite without dark laminations.
- Cbl** Bolsa Quartzite, lower unit (Cambrian) — Medium to coarse-grained darker brown and brownish-red quartzite and conglomerate; contains locally abundant magnetite laminations, clasts of quartzite, siltite, vein quartz, limestone and local dark lithic fragments probably derived from Apache diabase.

#### 3.1.4 Cretaceous intrusive and extrusive rocks

Cretaceous quartz-rich sandstone (Kqs) and an overlying volcanoclastic sequence (Kvs) are found in drill core only *within* the graben that hosts the Resolution deposit, and not in outcrop elsewhere in the project area. The thickness of both units increases towards an adjacent fault, and structural analysis of oriented bedding data from multiple drill holes shows a classic “fan” distribution of orientations. Taken together this information provides strong evidence that deposition occurred during active tectonics in a fault-bounded half-graben. This is interpreted to indicate that these sedimentary units were either never deposited outside the graben or were completely eroded prior to deposition of the Tertiary-aged “cover” units (Tw, Tal). Mesozoic felsic intrusions within the project area include the Silver King Quartz Diorite.

- Kvs** Andesitic/felsic volcanoclastic rocks (Cretaceous) – *Subsurface occurrence only*. Restricted to the west and northwest sector of the graben and comprises a sequence of up to 1 km of graywacke, conglomerate, and lesser lava flows and tuff (Manske and Paul, 2002; Ballantyne et al., 2003; Zulliger, 2007). The upper part of the section is dominated by andesitic to basaltic volcanoclastic rocks, whereas the lower part has a transition into discontinuous conglomerate beds containing cobbles of quartzite with less common limestone cobbles; clasts of Pinal (Hehnke, 2012).
- Kqs** Quartzose sandstone (Cretaceous) – *Subsurface occurrence only*. The basal Cretaceous section comprises interbedded quartzose sandstone and siltstone up to 150 m thick lying on the Paleozoic or Precambrian formations with a slight angular unconformity. This unit is absent from the southern and eastern sectors of the graben. U-Pb ages for sedimentary zircons from the sandstone define a maximum age of ~97 Ma (Zulliger, 2007) (Hehnke et al, 2012).

**Kdp (dp)** Diorite or dacite porphyry (Late Cretaceous) — Sills, dikes, and small irregular hypabyssal bodies of light- to medium-gray porphyritic altered dikes, sills and a single small stock cutting the Silver King Quartz diorite stock and older strata exposed in the northwestern quadrant of the Superior quadrangle. Phenocrysts that constitute 20-60 percent of rock consist chiefly of euhedral and subhedral plagioclase, 1-10 mm in diameter, and euhedral hornblende prisms ½ -15 mm long. Groundmass aphanitic to very fine grained, chiefly plagioclase, K-feldspar, hornblende, biotite, locally pyroxene; quartz generally absent but locally abundant. Partly to completely altered to sericite, clay, calcite, and chlorite. A small plug that intrudes the Silver King quartz diorite stock is exposed at the Silver King mine contains disseminated pyrite (Peterson, 1969), and has been dated at 73.6±1.6 Ma by U-Pb for zircons (Hehnke et al, 2012). Porphyritic dikes of similar composition were mapped in the underground Magma mine and one sample yielded a U-Pb zircon date of 69.1±4.0 Ma (Seedorff, et al. 2005b).

**Kqd (qd)** Quartz diorite (Late Cretaceous) -- **Silver King quartz diorite stock** exposed in the Superior quadrangle (Peterson, 1969), dated at 74.83±0.33 Ma by <sup>40</sup>Ar/<sup>39</sup>Ar on biotite (Hehnke et al, 2012) and quartz diorite of Arnett Creek exposed in the Picketpost Mountain quadrangle, (Balla, 1972) dated at 73.5±2.3 Ma by K-Ar on biotite (Balla, 1972). Original unit codes “Kd” and “qd” seen, respectively on the Picketpost Mountain and Superior quadrangles changed to “Kqd” for consistency (this publication). Tertiary – Cretaceous intrusive rocks

**TKsg** **Schultze granite** (Early Tertiary to Late Cretaceous)—Irregular, multi-lobed stock of pink-gray to pale lavender (weathers tan) porphyritic biotite-quartz monzonite grading locally into granite porphyry phases (Peterson, N.P., 1963). U-Pb zircon ages for the granite range from 67 to 61 Ma (Seedorff et al., 2005b; Stavast, 2006).

**TKgp** Granite porphyry dikes (Early Tertiary to Late Cretaceous)—scattered dikes of granite porphyry connected with or spatially associated with a major lobe of the Schultze granite stock exposed in the northwestern quadrant of the Pinal Ranch quadrangle (Peterson, N.P., 1963).

### 3.1.5 Middle Tertiary rocks

Oligo-Miocene (24-22 Ma) Whitetail Conglomerate (Tw) was deposited after Cu-mineralisation. It is a coarse basin fill comprising fragments of most of the older rock types. It is thin and locally absent in the range front, but has filled a Basin & Range graben over the deposit, bound to the East by the Devil’s Canyon fault, forming a wedge up to 1.5 km thick, in an early Basin and Range listric extensional half-graben.

Overlying the Whitetail Conglomerate and volumetrically the most significant Tertiary unit is the Miocene (~18.4 Ma) Apache Leap dacitic welded tuff. It is largely formed by crystal-rich quartz latite ash flows and forms the Apache Leap escarpment. In-house mapping has divided the Apache leap tuff into eight separate units.

**Tcg (QTg)** Gila Conglomerate (middle Tertiary) -- Coarse, gravel and generally subrounded cobbles to boulders, with minor amounts of finer-grained material, that form deeply (5-10 m) incised surfaces near major drainages). Clasts consist of Pinal Schist, granitoids, Apache Group, Paleozoic carbonate and clastic strata, and Tertiary volcanic rocks. Intra-unit dash-dot contact at east edge of southern part of map area marks base of conglomerate that is similar to Tcg, elsewhere but contains conspicuously more detritus derived from the Apache Group, principally Dripping Spring Quartzite, which gives slopes on the unit a tan color as opposed to the gray color typical of Tcg.

**Tcgt** Tuffaceous sediments (middle Tertiary) — Tuffaceous sediments and tuff layers within the Gila Conglomerate (Tcg), locally crystal tuff with little or no non-volcanic component (modified from “QTgt”, Geology of the Pinal Ranch quadrangle, AZ, Peterson, N.P., 1963).

- Tss** Sandstone (middle Tertiary) -- Tan to pale brown, poorly sorted and poorly bedded medium to fine grained sandstone that grades stratigraphically upward into conglomerate of map unit Tcg. Contact placed at base of area where conglomerate constitutes greater than 50% of outcrop.
- Tb (QTb)** Basalt (middle Tertiary) -- Basalt lava flows and flow breccias near Queen Creek in the southern part of the Picketpost Mountain map.
- Tvx** Volcanogenic breccia (middle Tertiary) -- Described by D. Peterson (1966) as angular blocks and fragments of tuff and other lithic material such as diabase, rhyolite, and schist in a heterogeneous pyroclastic matrix. The breccia forms a steep dike that has intruded along the contact between tuff and rhyolite and cuts across tuff beds at nearly right angles. Exposed only on the north flank of Picketpost Mountain.
- Tqmp** Quartz monzonite porphyry (middle Tertiary) -- Identified as the Wood Camp Canyon aplitic granite by Shafiqullah et al. in the northeast corner of the Picketpost Mountain quadrangle who derived a K-Ar biotite date of  $18.35 \pm 0.4$  Ma from this unit (1980). Mapped as "Tg". (Spencer and Richard, 1995). Originally mapped as "qmp" in the northwest corner of the Superior quadrangle (Peterson, D., 1969). Based on this age, for consistency, this unit code revised to "Tqmp" (this publication).
- Tqma** Quartz monzonite aplite (middle Tertiary) — Finer-grained/aphanitic border phase of the Tqmp unit. Originally mapped as "qma" in the northwest corner of the Superior quadrangle (Peterson, D., 1969). Based on this age, for consistency, this unit code revised to "Tqma" (this publication).
- Tql** Quartz latite (middle Tertiary) -- Described by Peterson (1966) as lava flows and shallow vent-filling intrusion that forms the top of Picketpost Mountain and a small plug on the northwest flank. Quartz latite is flow banded to brecciated and contains 25 to 30% phenocrysts of plagioclase, quartz, biotite, sanidine, and minor hornblende. (See Peterson (1966) for a detailed description). Biotite from this unit yielded a K-Ar date of  $18.4 \pm 0.5$  Ma (Shafiqullah et al., 1980).
- Tp** Perlitic aphyric rhyolite (middle Tertiary) -- Pale gray, glassy, aphyric rhyolite, tan weathering, with spheroidal weathering texture that probably reflects devitrification. Layered character on weathered surfaces and parallel fractures on fresh surfaces vary from planar to convoluted and may be disrupted by what appears to be flow brecciation. Layering and parallel fractures are inferred to reflect flow of lava.
- Tal (Td)** Apache Leap tuff (Miocene) -- Massive, moderately to strongly welded crystal-rich ash-flow tuff. Crystals of biotite, plagioclase, quartz and minor sanidine. Fiamme are typically obscure except near the base of the unit. Pink-gray or pale lavender in color. The Apache Leap tuff has been dated by the  $^{40}\text{Ar}/^{39}\text{Ar}$  method to be 18.6 Ma (Ferguson et al., 1998). Densely welded vitrophyre locally present at base. Overlies lavas of unit Tf, Apache Group strata, and Pinal schist on a surface with significant (10's of meters) of topographic relief, and even greater structural relief. The following informal sub-units (members) of the Apache Leap tuff, first recognized by D. Peterson, USGS (1961 and 1968) and mapped by geologists of Resolution Copper Company (formerly Kennecott Exploration Company, 2003-2004) on Oak Flat plateau, east of the town of Superior, are described here:
- Ts** Tuffaceous Lacustrine Sediments (Miocene) -- moderately to poorly consolidated, tan to buff (weathered to yellowish-buff), bedded to finely laminated graded sandstone, siltstone and pebble conglomerate, alternating with interbeds of lithic-crystal dacite tuff and thin layers of accretionary lapilli tuff. Individual accretionary lapilli may locally exceed 3 cm in diameter. Scattered clasts of pre-Tal country rock lithologies. Rare bleached freshwater (?) gastropod shells and shell fragments 2-5 mm (W. Hart, Resolution Copper Company, 2016).

- Talt** “Top of Tuff” (Miocene) -- well consolidated but relatively soft, massive to widely jointed white to light gray (weathered to brown, gray, or yellowish-gray) lithic crystal tuff, finely porphyritic crystal lithic lapilli tuff/ignimbrite and volcanic agglomerate/breccia with mostly volcanic clasts or blocks locally commonly exceeding 20 cm in diameter, commonly irregular in shape, with abundant xenoliths of all pre-Tal country rock units. Both normal and reverse grading is observed. On freshly broken weathered outcroppings, the white tuffaceous matrix to the agglomerate is locally difficult to distinguish from white/ bleached volcanic clasts/blocks (W. Hart, Resolution Copper Company, 2016).
- Talw2** White Tuff, upper member (Miocene) -- Well consolidated white to light gray (weathered to brownish-gray or pinkish-gray), non-welded and weakly welded finely porphyritic crystal tuff and lapilli tuff, locally spherulitic, and with common scattered xenoliths, up to 10 cm in diameter. Lapilli are dacitic “pumice lumps with a mean diameter of up to 15 cm”, some of which appear to be slightly flattened, (Peterson, 1961).
- Talw1** White Tuff, lower member (Miocene) -- White to light gray (weathered to brownish-gray or pinkish-gray), weakly to moderately welded lapilli tuff and finely porphyritic crystal tuff. Dacitic buff to gray colored pumice lapilli are weakly to moderately flattened with a long dimension locally up to 20 cm. Common scattered xenoliths up to 5 cm in diameter (Peterson, 1961).
- Talg** Gray Tuff (Miocene) -- Pinkish-gray (weathered to brownish- or pinkish-gray), firmly welded finely porphyritic lapilli tuff with light gray flattened dacitic pumice lapilli up to 10 cm diameter in the horizontal plane, but with thicknesses decreasing downward from 2 or 3 cm in the upper part to less than 1 mm thick near the base due to progressive flattening down-section. Common scattered xenoliths up to 5 cm in diameter. Unit is gradational with the underlying Brown Tuff (Peterson, 1961).
- Talb** Brown Tuff (Miocene) -- Light, reddish- to yellowish brown (weathered to brown and grayish brown), welded finely porphyritic tuff with common, lighter colored streaks which are extremely flattened, lapilli. Near the base of the unit, the flattened lapilli are discernable only with microscope as fine lamina which appear to merge with the porphyritic matrix. Abundant xenoliths locally exceeding 30 cm in diameter constitute 10-25% of the rock volume (Peterson, 1961).
- Talv** Vitrophyre (Miocene) -- Medium to very dark gray (weathered to gray-brown), generally highly resistant, translucent to opaque glassy-textured welded tuff. Outcroppings locally exhibit pronounced columnar jointing which is crudely to distinctly polygonal when viewed in horizontal section. Xenoliths constitute 5-10% of the rock volume. A sub-horizontal zone of distinctive, crudely spherical nodular masses of vitric and devitrified vitric tuff, ranging in size from a few centimeters up to over 1 meter in diameter, occur at or near the top of the vitrophyre unit at many locations (Peterson, 1961).
- Talbt** Basal Tuff (Miocene) -- Light gray to white (weathered to light gray, yellowish-gray or medium red), medium to fine-grained non-welded finely porphyritic crystal tuff, commonly intercalated or interlayered with pre-Tal clastic sediments which were probably unconsolidated prior to entrainment within the tuff (Peterson, 1961).
- Tr** Spherulitic rhyolite (middle Tertiary) -- Light gray weathering, crystal-poor rhyolite(?), with very well developed flow banding, and abundant gas cavities and spherulitic devitrification. Typically caps volcanic sequence in the Millsite-Hewett canyon area of the Picketpost Mountain quadrangle. Stratigraphically above Tw (Whitetail conglomerate) and below Tal (Apache Leap tuff) within the north-central portion of the Superior Quadrangle.
- Tt** Tuff (middle Tertiary) -- Massive and bedded tuff that may contain phenocrysts of biotite, quartz, sanidine, and hornblende and variable amounts of volcanic lithic fragments. Locally spheroidal

weathering and typically weathers to tan to orangish brown color. Tuff in southwest part of map area that underlies aphyric perlitic rhyolite contains up to 40% lithic fragments that include Pinal Schist and quartzose sandstone.

- Tf** Felsic volcanic rocks, undivided (middle Tertiary) -- Massive and flow banded, aphyric to porphyritic rhyolite to, possibly, dacite lavas. Variable phenocryst content of porphyritic varieties commonly includes biotite and sanidine. Vitrophyre present locally and brecciated character in some areas may be product of devitrification. Unit locally includes interbedded tuffaceous rocks. The unit was not studied in detail. It appears to consist of several thick, but not widely distributed lava flows with associated auto breccia and block and ash deposits. Similar felsic lavas and tuffs mapped in Superior quadrangle include "QTvl" and "QTvt" (Peterson, 1969).
- Tfp** Crystal poor felsic volcanic rocks (middle Tertiary) -- Prominent flow banding with very few phenocrysts.
- Tfa** Andesitic volcanic rocks (middle Tertiary) -- Dark red brown lavas with plagioclase, biotite and pyroxene crystals; commonly flow banded.
- Tbl** Lower basalt (middle Tertiary) -- Basaltic flows and flow breccias with 1-3% 1-3 mm pits containing iron oxides that probably represent relict olivine, and 1% 2-4 mm dark green clinopyroxene(?). Aphyric vesicular basalt at east edge of Picketpost Mountain quadrangle map rests concordantly on Mescal Limestone and is possibly, but not likely, middle Proterozoic.
- Tx** Rock avalanche or talus breccia (middle Tertiary) -- Clast supported monolithologic breccia with subangular clasts up to 50 cm diameter, exposed near the base of Picketpost Mountain on the west flank. Breccia consists of a lower unit of quartzite clasts and an upper unit of diabase clasts.
- Tw** Whitetail conglomerate (early Tertiary) -- Poorly sorted, crudely bedded to massive conglomerate containing sub- rounded to subangular clasts up to 40 cm diameter of Apache Group rocks and Paleozoic carbonates and quartzites. Reddish brown sandy matrix is poorly cemented.  $^{40}\text{Ar}/^{39}\text{Ar}$  age dates determined for tuff beds within the Whitetail conglomerate (Hehnke, et al., 2012) include: 24.29±0.12 Ma (80 m above base), 21.97±0.06 Ma (170 m above base), 21.77±0.32 Ma (350 m above base).
- Tdf** Felsic dikes (Middle or Early Tertiary or Cretaceous) -- Undifferentiated felsic dikes, locally porphyritic, in the Picketpost Mountain quadrangle (Spencer and Richard, 1995), and a single, northeast-striking, aphanitic and finely porphyritic felsic dike known locally as "Grandfather lead". The dike, locally faulted, is mapped over a 2-mile strike length, cutting Pinal Schist and the north lobe of the Silver King Quartz diorite stock, in the northwest quadrant of the Superior quadrangle. Dike is composed of light-gray aphanitic rock largely altered to clay, mica, and calcite. Relict phenocrysts of plagioclase discernible. Forms prominent outcrops (Peterson, 1969). The dike is displaced approximately 1000 feet in an apparent right-lateral sense by the Conley Spring fault (W. Hart, Resolution Copper Company, 2016).
- Tda** Aphanitic felsic to intermediate dikes (Middle Tertiary)
- Tg** Granite (middle Tertiary) -- Identified as the Wood Camp Canyon aplitic granite by Shafiqullah et al. (1980) who derived a K-Ar biotite date of 18.35±0.4 Ma from this unit.

### **3.1.6 Upper Cenozoic deposits (unconsolidated)**

Quaternary alluvium (Qal) generally lies unconformably on all the other formations. It consists of recent and near-recent stream deposits in basins, fans, terraces, floodplains, and channel deposits. It is composed of gravel, sand, silt, and clay. Although alluvium is present along many of the drainages, for

clarity, deposits less than approximately 30 ft (10 m) thick and of limited areal extent are not shown on the geologic map.

- d (Qf)** Disturbed ground (Holocene) -- Unconsolidated surficial deposits consisting of excavated material including mine waste and land fill produced by human activity.
- vq (q)** Vein quartz (Uncertain) — White “bull” quartz vein, forming prominent outcrops. No metallic minerals detected (D. Peterson, 1969).
- Qs** Undivided surficial deposits (Quaternary) -- Slightly to moderately consolidated alluvial deposits forming dissected and undissected surfaces, and unconsolidated sand and gravel in washes and streambeds.
- Qtc (Qt)** Talus and colluvium (Quaternary) -- Unconsolidated sediment on hillsides.
- Qal (Qal)** Unconsolidated alluvium (Quaternary) -- Unconsolidated sand and gravel in unvegetated or sparsely vegetated active stream channels and forming vegetated flats up to 2 m above adjacent stream channels.
- Qoa (Qal)** Old alluvium (Quaternary) -- Weakly consolidated cobble to boulder conglomerate capped by surfaces generally 2-5 m above active stream channels. Geomorphic surface on deposit is generally well preserved.
- QTIs** Older landslide deposits (Quaternary or Tertiary) -- Similar to QIs, but scarps in headwall of the landslide are degraded and revegetated. Typically these are much larger landslides than QIs deposits, involving entire mountain sides, particularly in upper Reeves Trail Canyon.
- QTs (QTg)** Older alluvium (early Quaternary to late Tertiary) -- Coarse gravel and generally sub-rounded cobbles to boulders, with minor amounts of finer-grained material, that form deeply (5-10 m) incised surfaces near major drainages).

#### 4. Economic Geology

Mineral occurrences in and around the Resolution project area include a range of metallic, non-metallic and industrial minerals. There is a long history of silver and copper mining in the near vicinity of Resolution. Mining operations continue to play a major role in driving the region’s economy. In addition to the Magma Mine, a series of major mines (both active and inactive) are located within a 30 mi (48 km)

radius of the project area in an area known as the Copper Triangle (Figure 7). They include: the Pinto Valley Mine and Concentrator, Carlota Mine, Miami Mine and Smelter Complex, Ray Mine and Concentrator and Hayden Concentrator and Smelter Complex. Overall, at least 31 mines are located in the vicinity of the Copper Triangle, representing a range of mining operations that include copper, gypsum, and marble mining.

Detailed overviews of the economic geology including historic mining activities in the Superior district are documented amongst other by Peterson (1962), Hammer and Peterson (1968), Peterson (1969) and Manske and Paul (2005). Below is a short summary, limited to the project area.

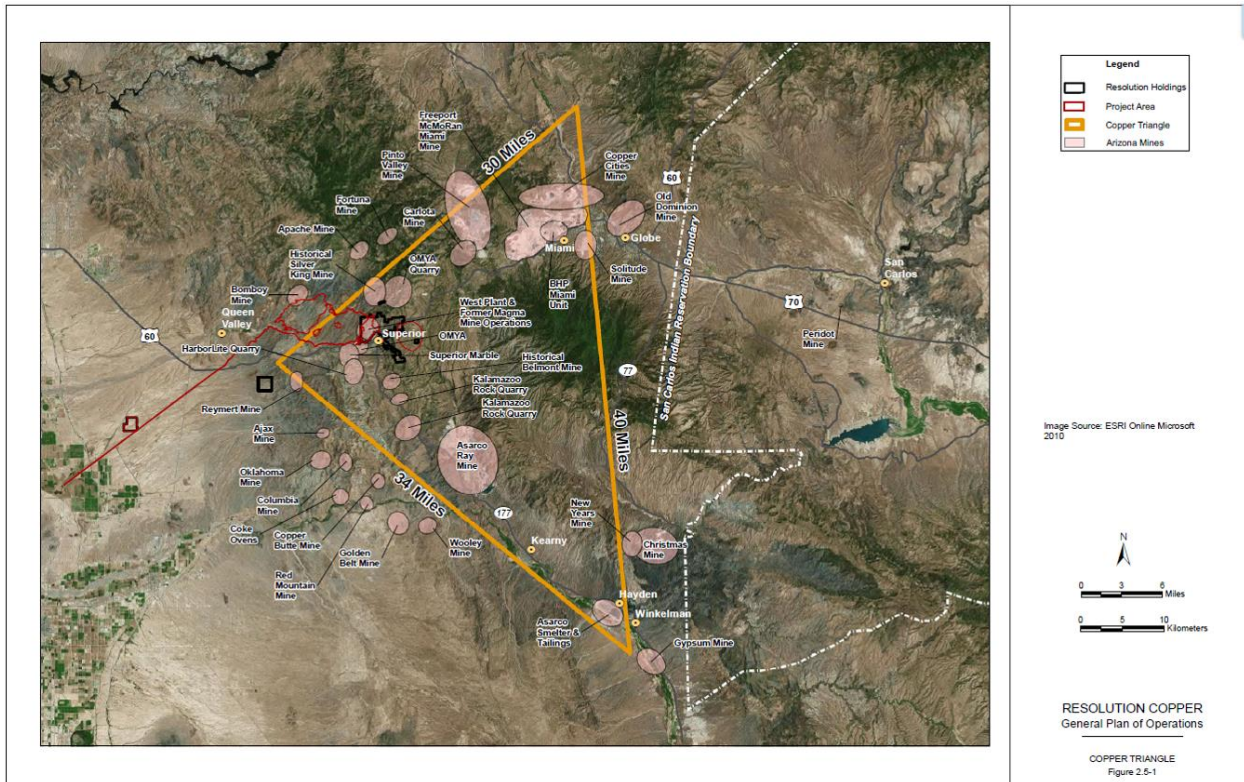


Figure 7: Map of the Copper Triangle showing active and inactive mining operations in the vicinity of the Resolution project area.

#### 4.1 Metallic mineral occurrences

The most significant deposit mined in the vicinity was the historic Magma Mine, with copper and minor Au, Ag, Zn, Pb mined – some 2 km north of the Resolution deposit - for almost 90 years, from 1910 to 1996. The Magma main orebody was an E-W trending vein and related veins in rocks of Palaeozoic age (Peterson, 1969). It was a relatively narrow orebody only 12-15 m wide, but with 25 M tonnes mined at a high average grade of 5% Cu (Manske and Paul, 2005).

The Silver King Mine produced silver for 25 years (1875 – 1890, and from 1918 - 1928) from a stock work of veinlets within the diorite porphyry in a quartz-diorite stock approximately 1-2.5 miles (2-4 km) northwest of Resolution. This deposit also contained Zn, Pb and Cu sulphides (Peterson, 1969). Like Magma, this deposit was of limited extent, but with high average silver grades. After a small tonnage of secondary enriched capping of free milling and direct shipping ore grading up to 1,700 troy ounces per ton was depleted around 1882, approximate average grades then reportedly ranged from 55 troy ounces per ton (1883), to 21 troy ounces per ton (1887) (Tenney, 1929 in Short, et al., 1943). Assuming an approximate average grade of 40 troy ounces per ton for the main, early period of mining (1875-1989), and based on a reported nominal milling rate of 50 tons per day during this time, an approximate total milled tonnage of 148,000 has calculated, (Hammer, 2011, unpublished report). A similar calculation by Hammer for the later period of mining (1917-1920) yielded 12,546 ore-tons averaging 18.5 troy ounces of silver per ton. Thus, total production for the Silver King mine 1875-1920 was approximately 6.2 million ounces of silver from about 160,546 estimated tons of ore, at an average grade of 38.5 troy ounces per ton.

The closest producing copper mine is the Ray open pit Mine, approximately 9 miles (13 km) south of Resolution along the same mountain range ([www.asarco.com](http://www.asarco.com), Grupo Mexico). The Pinto Valley open pit

copper mine, approximately 14 miles (20 km) (14 miles) to the northeast of Resolution, was recently restarted ([www.capstonemining.com/operations](http://www.capstonemining.com/operations)). Unlike Magma and Silver King, both Ray and Pinto Valley are copper porphyry deposits, with large volumes and relatively low copper grade, much like the current Resolution Copper deposit.

## 4.2 Non-metallic and industrial minerals

Perlite is mined from several pits in the Arnett Rhyolite, nearly 3 miles (4 km) southwest of Superior. The perlite occurs as broad zones of light grey to milky white silicate minerals which are the products of natural alteration/hydration of rhyolitic volcanic flows, and commonly include accumulations of glassy spheroids, a mm to a cm in diameter. 'Expanded' perlite today is mainly used for construction.

Chrysotile asbestos occurrences are found in the southern part of the Superior quadrangle. Contact metamorphic bedding parallel veins occur in the magnesium-bearing Mescal Limestone where it is intruded by the Apache diabase (Peterson, 1969). Known deposits and notable occurrences in Arizona are summarized in an open file report by the Arizona Geological Survey (Harris, 2003). This report mentions 'several occurrences' of chrysotile asbestos near Superior, referring to Phillips (1987), and asbestos mined from Mescal Limestone at Putnam Wash, some 60 km south of Superior along route 77, referring to Stewart (1955), Krieger (1968) and Phillips (1987).

Uranium occurrences are reported in the vicinity to Resolution. They are the Lucky Boy and the Sky deposit, 6 mi and 10 mi (10 km and 15 km) southeast of Superior, respectively (Figure 1 in Granger and Raup, 1969). More than 100 significant occurrences were identified in the '50s, most of them in the Sierra Ancha Region in Gila County, some 100 km (60 miles) north of Resolution. Occurrences are typically in stratabound in diagenetically altered, potassium-rich and carbonaceous volcanogenic siltstones of the Proterozoic Dripping Spring Quartzite. They are in veins or strataform deposits in close proximity to the Apache Diabase intrusion, which is thought to have provided the U-concentrating fluids (Nutt, 1984) if not also the uranium itself (Granger and Raup, 1969). The age of the U mineralization is thought to be circa 1.1 Ga, i.e. the age of the diabase (Granger and Raup, 1969).

Copper deposit-related uranium is found in some copper deposits in Northern Arizona, including that in the Moenkopi Formation (Lukachukai Mountains, Apache County) and the Orphan copper mine in collapsed breccia pipes near the south rim of the Grand Canyon (Scarborough, 1981). The Twin Buttes copper mine in Pima County recovered uranium as a byproduct from leach solutions recovering copper from waste material (Scarborough, 1981). Nutt (1984) notes that the association of uranium, copper, and molybdenum in these deposits may either be indicative of deposition of copper and molybdenum from the same circulating fluid that carried uranium, or may be a result of separate period(s) of fluid movement along the same structures.

Note that the copper mineralization at Resolution (62-64 Ma) is much younger than the Arizona uranium deposits 1.1 Ga (~1,100 Ma), or their host strata 1.4 Ga (>1,400 Ma). Even though the diabase intrusions associated with the known U deposits in Arizona are similar in age to the diabase intrusions at Resolution (the Apache diabase is approximately 1.1 Ga everywhere in Arizona) no anomalous uranium has been encountered at surface or in Resolution drill holes to date (see the whole rock geochemical results presented in Appendix 2).

A spatial correlation of uranium occurrences with the trend of monoclines and monocline-bounding faults, that locally also host diabase intrusions, was recognized for the Sierra Ancha region. This was taken to point to a central genetic role for these relatively old (pre/syn-1.1 Ga) faults, in both the emplacement of the diabase and possibly as a pathway for U-bearing fluids (Nutt, 1984). See also Williams (1957) for

more on the structural control of uranium deposits in Arizona. Proterozoic monoclines and monocline-bounding faults have not been reported for the Resolution area.

## **5. Geological setting**

### **5.1 Tectonic context**

The region that includes the project area has witnessed multiple tectonic episodes that have led to crustal folding and faulting from as early as the Precambrian to present-day (Bird, 2002). Figure 8 provides tectonic context for the project area in the form of a series of maps that outline the timing and transport directions of the main tectonic phases for the Western US.

The work by Bird (op cit.) shows that two main orogenic phases have dominated the structural development of the project area are (see also Figure 8):

- (i) Late Sevier / Early Laramide orogeny (from 64 Ma onwards), related to the subducting Farallon Plate (Figure 8B), causing NE-SW crustal shortening, folding and thrusting, and following a change in plate configuration: ENE-WSW shortening at 45 Ma.
- (ii) Early Basin and Range extension (from circa 22 Ma), due to roll-back of the subducting Farallon plate, (Figure 8D), causing ENE-WSW extension at first, followed by E-W extension. During this phase (hyper-) extensional fault blocks rotated on kilometre-scale listric faults to form the present-day relief.

The resulting structures in the project district are described per tectonic phase below.

For further reading on the regional geology and tectonics see Titley (1982), Keith and Swan (1995), and Leveille and Stegen (2012).

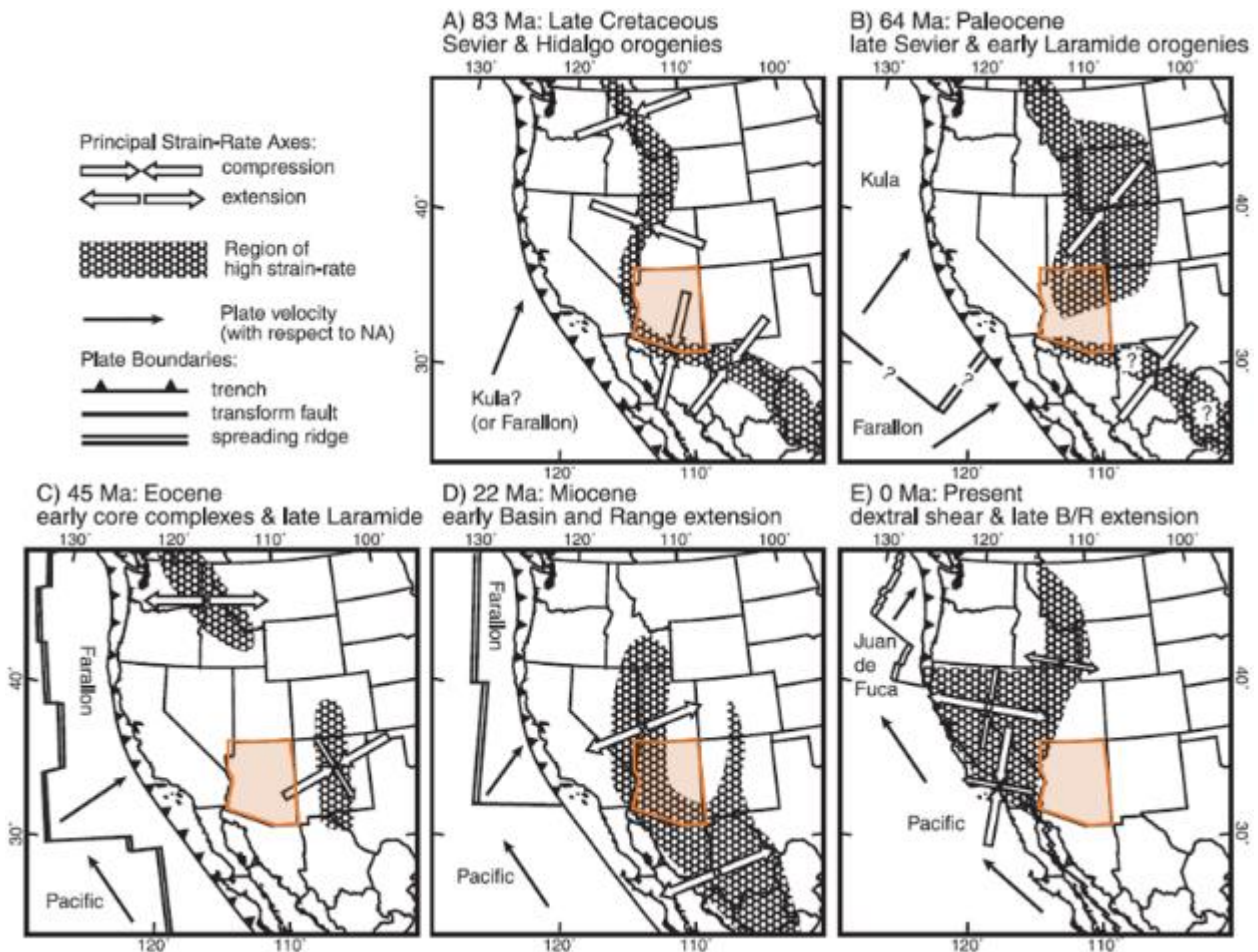


Figure 8: Tectonic history of the western U.S. and Arizona (indicated with red polygon), showing the orientation of the main strain axes, with either compression or extension indicated (From: Bird, 2002). Figure D shows the last deformation to affect the Resolution area, during early, ENE-WSW, Basin and Range extension, as a result of the subduction and roll-back of the Farallon plate. Present-day, dextral lateral movement of the Pacific plate causes contraction in southern California, further extension in the Basin and Range, but no major deformation in Arizona (Bird, 2002).

## 5.2 District structures and structural history

First-order structures in the project area are mainly the result of the Basin and Range extensional tectonic phase. Many kilometre-scale extensional faults are continuous and rotated fault blocks can be easily mapped in outcrop. *Within* these extensional fault blocks are remnants of structures of the Laramide orogeny, and of Proterozoic age - formed during emplacement of the 1.1 Ga diabase dikes and sills. These older structures are dismembered and may be rotated during Basin and Range extension and this must be taken into account when describing and analysing their kinematics. Pre- Laramide structures, including the inherited (Precambrian) basement architecture, as well as the Palaeozoic and Mesoproterozoic faults, are not well understood, but are likely to have influenced the location and geometry of subsequent structures. Influence of inherited structures must be taken into account when making predictions on fault shapes with depth based on limited surface and drill hole data.

### **5.2.1 Inherited basement architecture**

A northeast- to east-northeast-trending structural fabric in east-central Arizona is long recognised in the anomalous regional-scale magnetic and gravity grain that corresponds to trend of a range of Precambrian-aged, accretion-related tectono-magmatic terrains, including continental edge, island arc, oceanic arc and fore-arc basins (Lund et al., 2015 and references therein). A prominent geophysical feature is the **Salt River – Jemez Lineament**, a presumed crustal-scale Paleoproterozoic accretionary boundary that runs parallel to these terrains, and has been described as a potential zone of weakness with episodic reactivation at least 1.1 Ga and 1.4 Ga (Aldrich et al., 1986, Strickland et al., 2003). The Resolution project area is located on this lineament. In the project area this northeastern trend is reflected in the dominant trend of the metamorphic foliation in Pinal Schist, and the trend of the 1.4 billion-year-old (Ga) Ruin Granite (Hehnke et al. 2012 and references therein). It is postulated that the distribution of many minerals deposits in the district and the orientation of most mineralized veins in the area, including those of Magma and the range front, reflect this grain (Heidrick and Titley, 1982). In addition, the distribution and elongation of Laramide intrusions follows this trend. These inherited crustal structures, including those which may be associated with the Salt River – Jemez lineament, must be taken into account when assessing the kinematics and linkage of mapped structures in the project area.

### **5.2.2 Proterozoic diabase emplacement dikes and sills along extensional faults**

Proterozoic steep normal faults are preserved in the Proterozoic Apache Group sedimentary sequences, best observed in the Apache Leap range front. The geological map shows that these faults were exploited by dikes of the regionally extensive 1.1 Ga diabase complex. These dykes facilitated sills to step up and intrude into younger stratigraphy, best observed in the range front. Whether these faults were the effect of local stresses due to igneous inflation, or due to tectonic stresses is not known. Many faults are now intrusive contacts. Later, but before the period of mineralization, some of the old faults followed by these contacts were reopened, and additional displacement occurred (Peterson, 1962). The orientations of these faults and their tectonic significance is not known.

### **5.2.3 Palaeozoic extensional faults**

Stratigraphic offsets and thickness differences across faults in the basal Palaeozoic Bolsa Quartzite Formation and Martin Limestone, seen in the range front, suggest subtle syn-depositional extension and development of small horsts and grabens at the time of deposition (initial rifting before platform development?). The character of these faults in the project area is significant because these rocks overly the deposit, and the structures have an influence on subsidence and groundwater movement.

### **5.2.4 Laramide orogeny, folds and thrust, intrusions and erosion**

Early Tertiary-aged structures associated with the Laramide orogeny (~64 to ~45 Ma) are preserved within the kilometer (km)-scale Basin and Range fault blocks in the vicinity of the Resolution deposit. They include meter- to 10s of meters-scale folds and thrusts, observed locally in the range front. Larger and more continuous, km-scale thrusts are mapped in Telegraph Canyon, southwest of Superior, and near the Ray mine (Richard and Spencer, 1998), and Laramide-aged reverse movement is described along the N-NE-trending Sleeping Beauty fault north of Ray (Keith, 1986). Possible footwall fault splays and folds of the Elm Canyon Overthrust (Short et al., 1943) are located 1.5 miles west of the Resolution deposit, at the base of Apache Leap.

Intrusions associated with the Laramide orogeny crop out within 20km of Resolution, including the Silver King quartz diorite north of Resolution, a swarm of dikes and sills in the range front east of Superior town, and within the Resolution deposit itself (Hehnke, 2012, and references therein). The geological maps

show a strong spatial relationship with these intrusions and regional lineaments, which are interpreted to be deep-seated transcurrent fault zones that likely formed the conduits for these intrusions.

#### **5.2.5 Tertiary Basin and Range extension, listric faults, (half) grabens and rotated fault blocks**

The most prominent structures in the project area are the <22 Ma Basin and Range extensional faults and associated km-scale rotated fault blocks. Faults that crop out include the Concentrator Fault, the Main fault, and the Conley Springs fault near the range front, as well as the Devils Canyon Fault east of the deposit (Hehnke et al. 2012), see Figure 9 and Figure 10. These faults in the range front show a dominant set of slicken-lines that plunge to the WSW, consistent with the eastward tilt of the post-Laramide fault blocks in the range.

For Resolution, down-to-the-west displacement along the listric Devils Canyon Fault, and related faults, of at least 5900 ft (1800 m), tilted a large block encompassing the Resolution deposit (currently known 1% copper shell) approximately 25 degrees to the east-northeast.

In the western project area, in the Superior Basin, blocks dominantly tilt to the southeast, which is different from the east-northeast tilt of the blocks in the range front. Looking at the map, it can be seen that some extensional faults have acted as side-wall faults during extension. The section in Figure 9 illustrates how the SE dipping tilted fault block sits between the Roblas Canyon and the Concentrator Faults (section: Figure 3 from Spencer and Richards, 1995). The rotation of the fault block is well documented and beyond doubt. It is not possible, however, to create that tilt on the bounding faults as drawn on the map (see the SE trends of both the Concentrator and Roblas Canyon Fault on the map where section A-A' intersects these faults). The SE tilt of the block can only be created on NE to NNE-trending listric faults. The section as such is at an unfortunate misleading angle to the faults. At the time of rotation of this block, both the Concentrator and the Roblas Canyon fault segments must have acted as side-walls to (N)NE-trending listric extensional fault segments. This infers a significant strike slip component for both fault segments. Dip slip displacement on these segments at some (earlier?) point cannot be ruled out, but this is not what caused the rotation that we see today. For Resolution, the thickening of conglomerates towards the South Boundary Fault may be the local expression of this component of extension.

Regional extension, normal faulting, and fault block tilting ended after Tertiary volcanism and during the deposition of conglomerate and sandstone (QTg) (Spencer and Richard 1995).

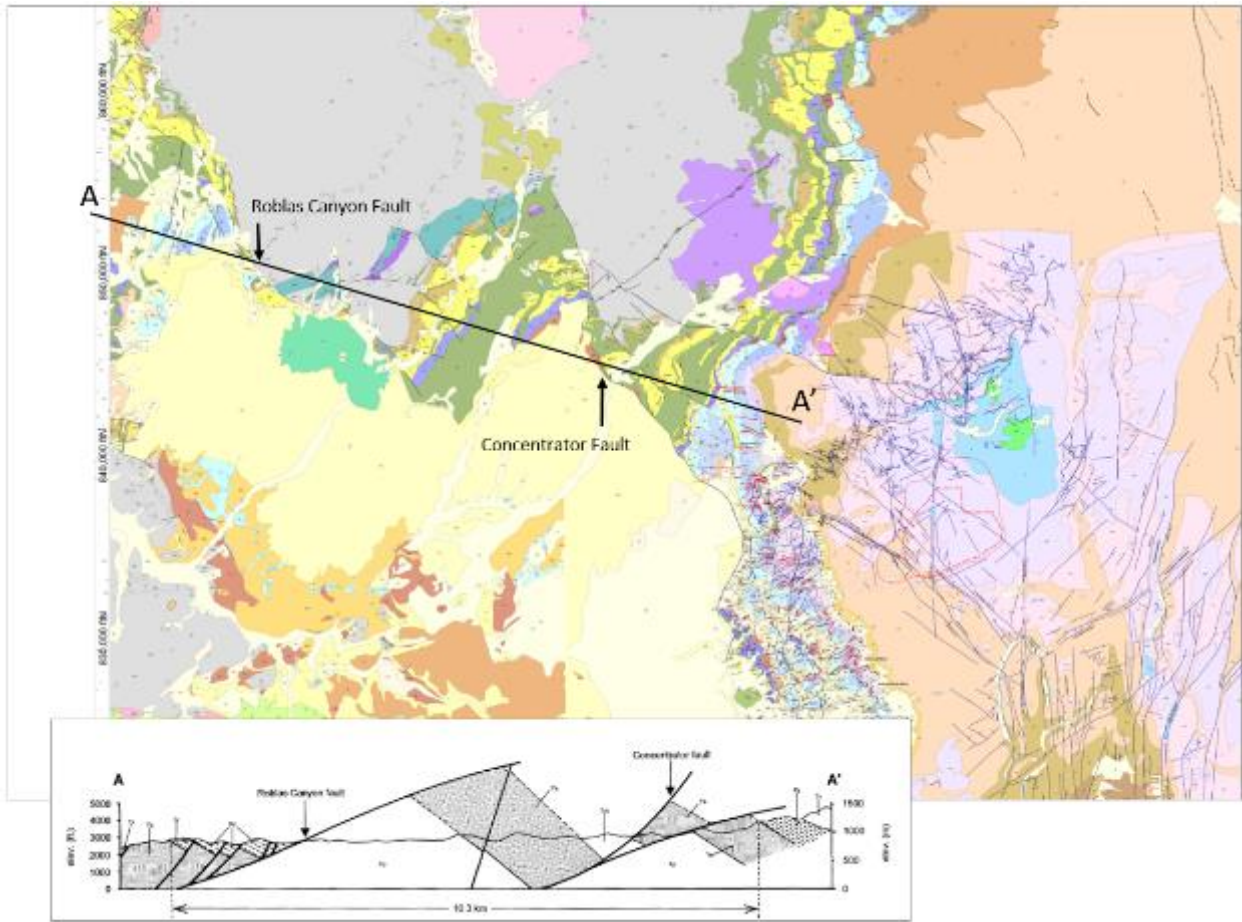


*Figure 9: Map and regional section illustrating the SE dipping tilted fault block between the Roblas and the Concentrator Faults (Figure 3 from Spencer and Richards, 1995), and the ENE-dipping fault blocks in the Range Front, illustrating the interplay between WSW and NW-SE extension, and the likelihood of reactivation of some extensional faults as extensional side-wall ramps. See text for further discussion.*

### **5.2.6 Newly documented regional faults, structures and kinematics**

Figure 10 illustrates the recently updated geological map over the deposit area and across Oak Flat, highlighting the published faults on the left, with on the right the additional faults and structures that have been integrated, mapped and analysed, to inform the geological framework modelling (paragraph 6). Here the nature of these faults and their significance for the geological model is described.

the upward continuation of the West Boundary Fault. The significance of this is further discussed in Section 6.4.2.

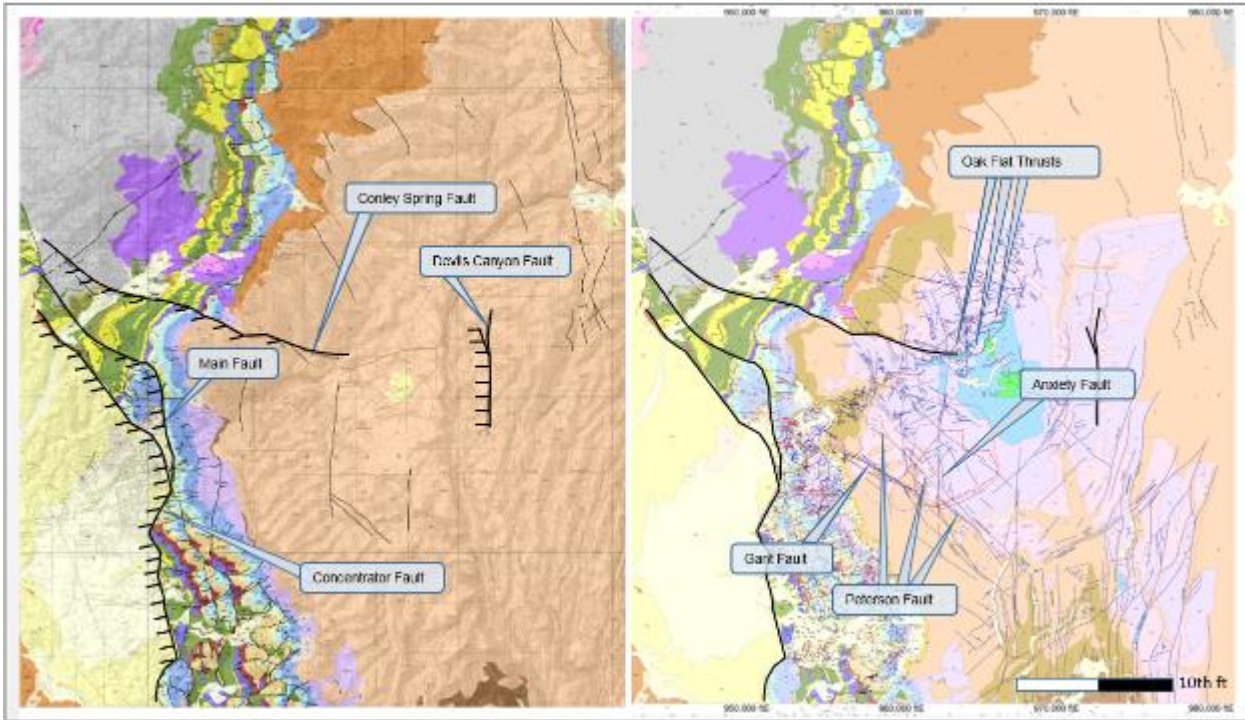


Figure 10: Illustrating results of the continued effort to identify, map and analyse faults over the deposit area. Left: zoom-in of the 1969 USGS geological map (Peterson) highlighting published Basin and Range extensional fault traces significant for the Resolution deposit area. Right: zoom-in of the updated geological map with newer, in-house mapped fault traces in dark-blue (right). The most significant faults are labeled and discussed in the text. Note the 1% copper shell footprint for reference. See Figure 5 for regional context and Appendix 1 for the complete updated map at full resolution.

## Gant fault zone

The Gant Fault is a zone of fault splays that collectively form a circa 2 km long corridor on Oak Flat. The zone was mapped by Gant and Wilkins (2003-2005). Exposures along a 50-70m wide Gant Fault splay that runs up against the Apache Leap ridge are rare because of the generally low relief (Figure 11). Exposures with kinematics indicators are particularly rare. On the margin of this zone, S/C foliations of which the most continuous one is parallel to the Gant Fault zone are interpreted as an S/C pair, with a tentative sinistral horizontal component of displacement with sub-horizontal striae. It is parallel to the NW-trending segments of the Concentrator Fault (and the Roblas Canyon Fault), making it likely that it has some dip-slip as well as strike-slip component to its displacement. The Gant Fault is a candidate for being



Figure 11: Typical low relief of one of the Gant fault strands. Kinematic indicators are rare. Horizontal (sinistral?) displacement is interpreted based on S/C relationships.

## Peterson Fault

The Peterson Fault was mapped by Gant and Wilkins (2003-2005) (Figure 12). It is a collection of fault strands that form a corridor across a large portion of Oak Flat. The strands in weathered surface outcrop reveal little structure to interpret kinematics, but fresh road cut outcrop shows shear foliation with shallowly plunging stretching lineations. No evidence for down-dip slip was found. It is cross cut by the Anxiety Fault.



*Figure 12: The Peterson Fault is a collection of fault strands that forms a corridor across a large portion of Oak Flat. The strands reveal little structure to interpret kinematics in weathered surface outcrop, but fresh road cut outcrop shows shear foliation with shallowly plunging stretching lineations. No evidence for down-dip slip was found.*

## Anxiety Fault

The well-defined Anxiety fault zone crops out along a fresh road cut showing vertical shear foliation with mainly horizontal slickenside lineations on the Anxiety Fault (Figure 13). Steps on slickensides indicating sinistral displacement. No evidence of dip-slip displacement was found. It is different from the Gant and Peterson Fault zones because of its widespread red staining.

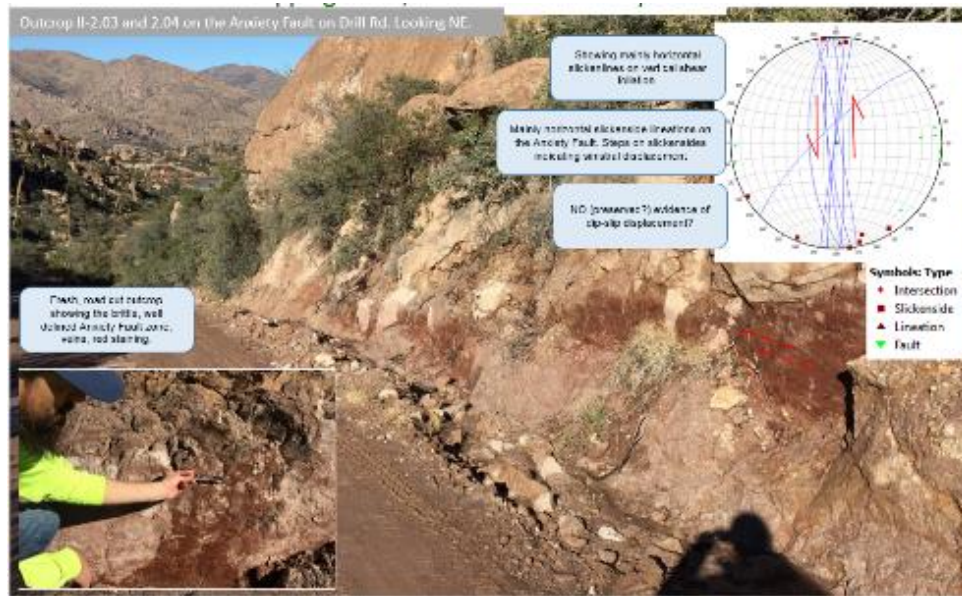


Figure 13: The Anxiety Fault along a road outcrop showing steep shear foliation with horizontal stretching lineations and a dominantly sinistral sense of shear.

## Conley Spring Fault

The Conley Spring Fault is a zone of steep anastomosing foliations, fractures and shear zones with generally shallowly plunging lineations, either to the NW or SE, confirming a significant strike-slip component to its displacement. No steeply dipping lineations were observed (yet) that would suggest a significant component of normal or thrust displacement. In detail, the zone contains at least two sets of structures related to two phases of activity: the youngest set indicates dextral displacement, an older set indicates sinistral shear.

Dextral strike-slip on the steep fault zone is interpreted from S/C foliation relationships in local outcrops. It is consistent with the dextral offset as seen on the range front. But locally, complications occur. Vertical linkage of the steep shears in to shallower, more flat lying side-wall ramps with hangingwall and footwall blocks, were seen where outcrop allowed (Outcrop I-703, Figure 14). On the map, the eastern fault tip of the Conley Springs shears is where a set of shallow thrusts is interpreted as horse-tail thrusts dissipating local strain (Figure 15). Kinematics of both are consistent with dextral displacement on the Conley Spring Fault. Because these structures are the most prominent, they are likely to have developed last.

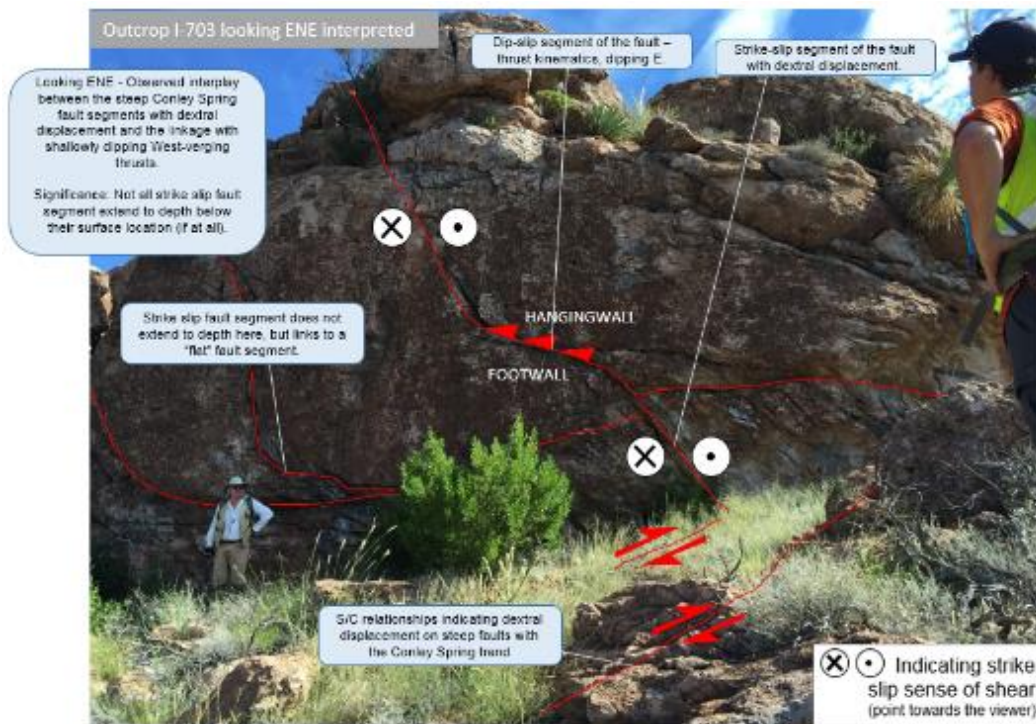


Figure 14: Outcrop I-703 on Oak Flat illustrating the spatial relationship and interplay between dextral strike-slip on the steep shears of the Conley Spring Fault and the sidewall ramps and shallow thrusts in the Tertiary Apache Leap tuff.

## Oak Flat Thrusts

Near the eastern tip of the Conley Springs Fault, on Oak Flat, shallowly NW dipping, narrow brittle thrusts verge dominantly SE but, locally, also NW. Lineations on the thrusts like on the Conley Springs Fault are generally shallowly plunging, either to the NW or SE, confirming that the two are kinematically related. The thrusts are interpreted to have accommodated dextral displacement at the fault tip of the Conley Springs shears. Southwesterly extensions of some of the thrust faults into the area of rugged terrain just south of the eastern portion of Conley Springs fault suggests a possible additional Conley Spring Fault splay south of the main fault as mapped.

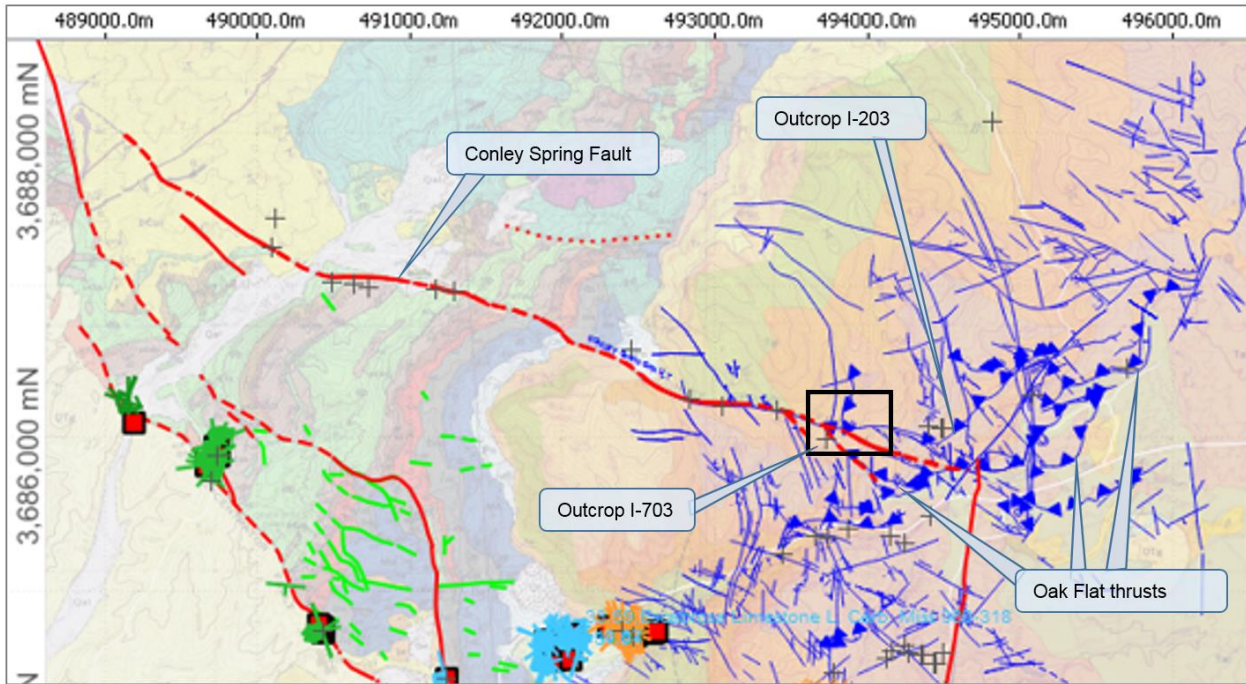


Figure 15: Mapped thrusts on Oak Flat and outcrop I-703 showing the spatial relationship and interplay between the steep Conley Spring Fault and the NE-trending thrust splays.

## Sinistral shear on the Conley Spring Fault

Sinistral shears are found in the fine-grained core of the Conley Spring Fault, with well-developed foliations with S/C domains and horizontal stretching lineations (Figure 16). Sinistral shear on this fault is consistent with Late Basin and Range NW-SE extension (Figure 8E), if the fault is considered as an accommodating strike-slip fault.

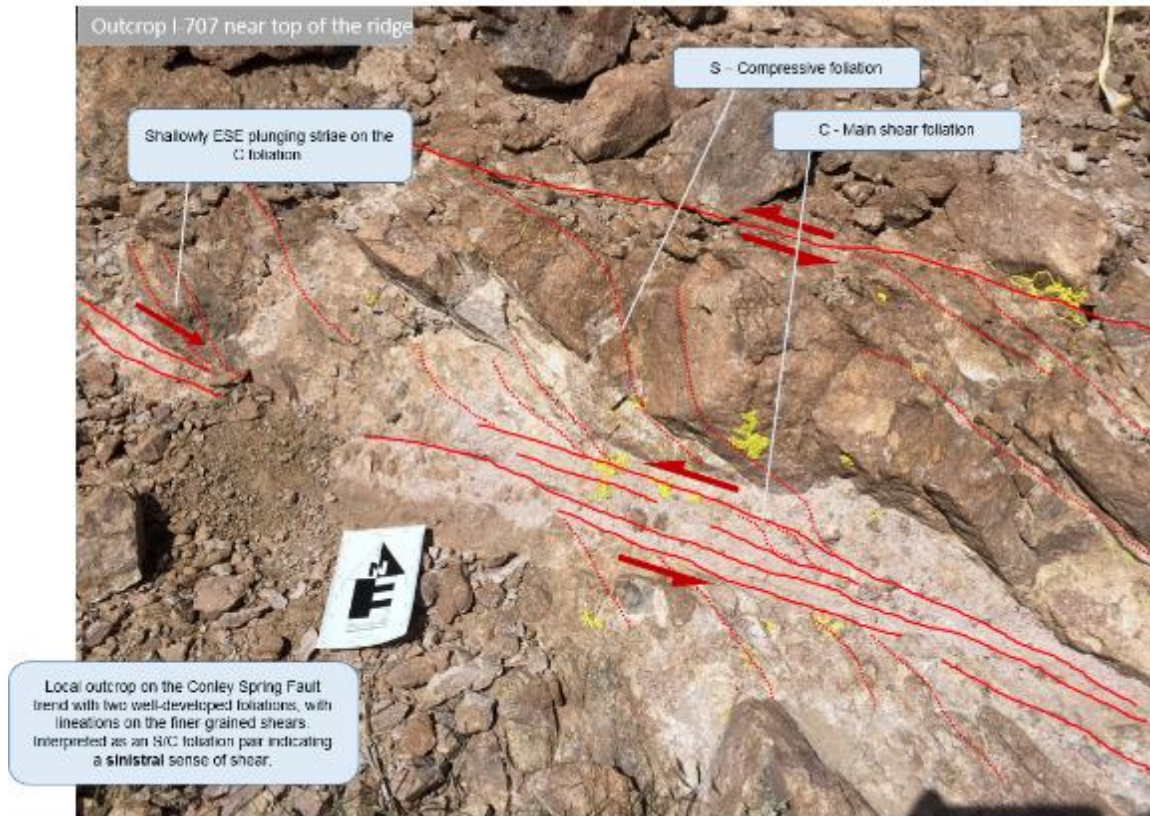


Figure 16: Outcrop I-707 on the Conley Spring Fault near the ridge, showing with two well-developed foliations, with lineations on the finer-grained shears, interpreted as an S/C foliation pair indicating a sinistral sense of shear.

## The Roblas Canyon fault zone

The Near West area with Proterozoic and Palaeozoic rock units is bounded on the northeast side by extensive exposures of Pinal Schist. On the existing geological map this contact is part of a regional NW-trending fault zone that extends for tens of kilometres (Figure 17). It has a similar trend to the Conley Spring fault system. As such, it is expected to have had similar, transcurrent displacement during possible reactivation after originating as a more purely extensional fault. To the south of the Proterozoic/Palaeozoic rocks is an area covered with younger sediments – the proposed tailings location in the mine plan of operations. Knowing the nature of the Roblas Canyon fault zone (hereafter abbreviated as “Roblas fault”) may help to predict the possible existence and the trends of faults beneath the sediments.

Two end-member scenarios are considered: (1) the contact between the Pinal Schists and the overlying sediments is a low angle extensional fault with dip slip displacement, (2) The Roblas fault zone is part of a steep transcurrent shear zone that has formed a complex array of structures, including vertical shear foliation, cataclasites and second order thrusts and normal faults.

Observed structures include a shallowly dipping schistosity of the Pinal Schist near the contact, but also steeply dipping mylonitised shears, fractures and cataclasite, and smaller shallowly dipping thrusts that appear to have mutual cross-cutting relationships. Slickensides are generally near-horizontal on the poorly exposed steeply dipping shears and trend down-dip on the small thrusts. This suggests that the Roblas Fault may have originated as a shallowly dipping extensional fault, and was reactivated as, or cut by, a transcurrent fault zone composed of more steeply dipping shears. The fault shows no evidence for movement since deposition of Tertiary-aged sediments and volcanic rocks that overly portions of the fault, and modern seismicity on this fault has not been recorded (see Section 5.3.3). Location and nature of this structural zone will be further refined once the characterization work in the area has been completed.

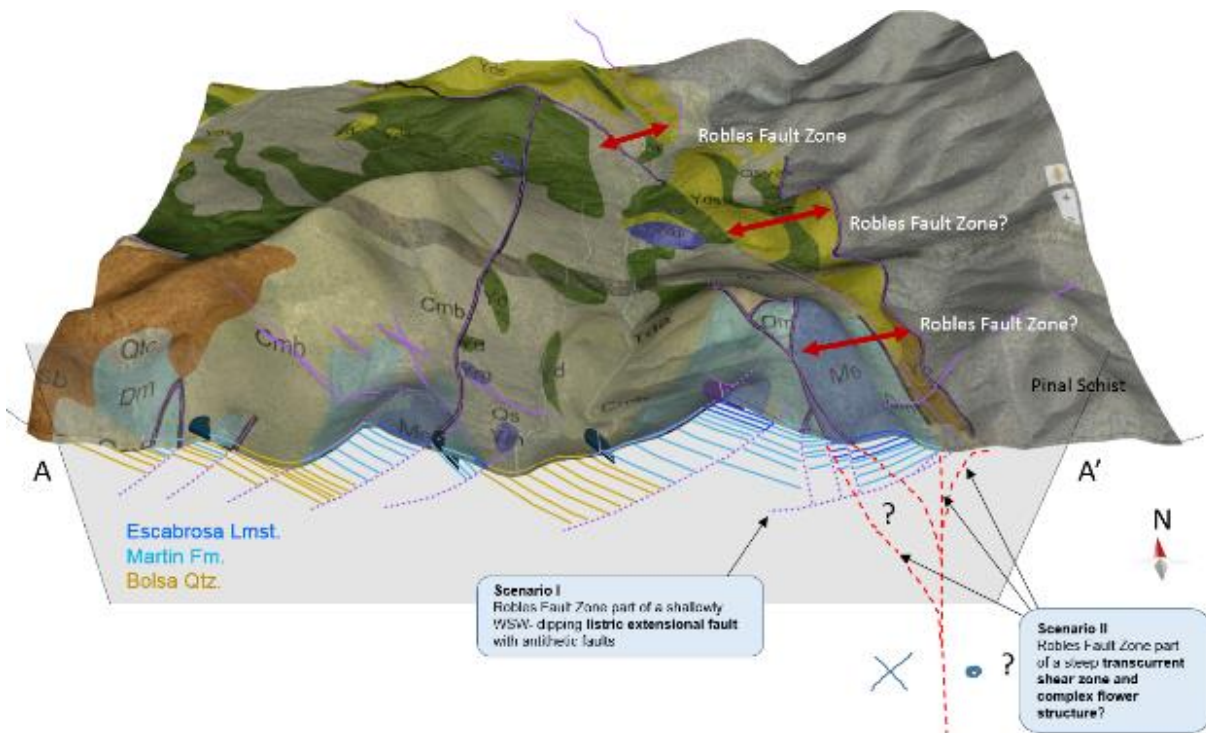


Figure 17: Based on the structural style of the fault blocks west of the fault, the Roblas Fault may either be an extensional fault with antithetic faults near the contact with the Pinal Schist, or may (also) have

acted as a steep transcurrent fault zone. The nature of this structural zone will be further refined once the characterization work in the area has been completed.

### 5.3 Present-day tectonics, stresses and seismicity

#### 5.3.1 Regional tectonic stresses

In the late stage development of the western U.S, the tectonic strains (and inferred stresses) in Arizona have evolved from ENE-WSW extension due to Farallon plate roll-back at 22 Ma, to transcurrent movement of the Pacific plate northward causing NNE-SSW contraction in California and strike-slip displacement on the San Andreas fault system today (Bird, 2002), see Figure 8. Further north, in Nevada, the dominant maximum horizontal stresses are ESE-WNW extensional, attributed to the roll-back of the subducting Farallon plate there, causing Late Basin and Range extension in this area (Bird, 2002). Compared to California and Nevada, Arizona and the project area are not much affected by either of the transcurrent slip or the roll-back related extension.

Across Arizona, measured present-day tectonic stresses (from geological indicators) are illustrated in the 2008 World Stress Map by Heidbach et al. (2009) (Figure 18). For Arizona, first-order, NW-SE trending maximum horizontal stresses dominate (marked in red on Figure 19), and are part of an overall stress environment that results in normal faults. In contrast, to the east in New Mexico, the dominant horizontal compression direction has a NE-trend, at right angles to the main trend in Arizona, and parallel to those in Nevada. These measurements are located along a NE-trending crustal scale structural lineament, with Resolution near its SW tip. Similar but smaller lineaments occur to the NW of Resolution: one through central Arizona and one at the NW corner of the project area. Both are associated with extension and with strike slip faulting, and leaving the deposit in a stress (strain) shadow.

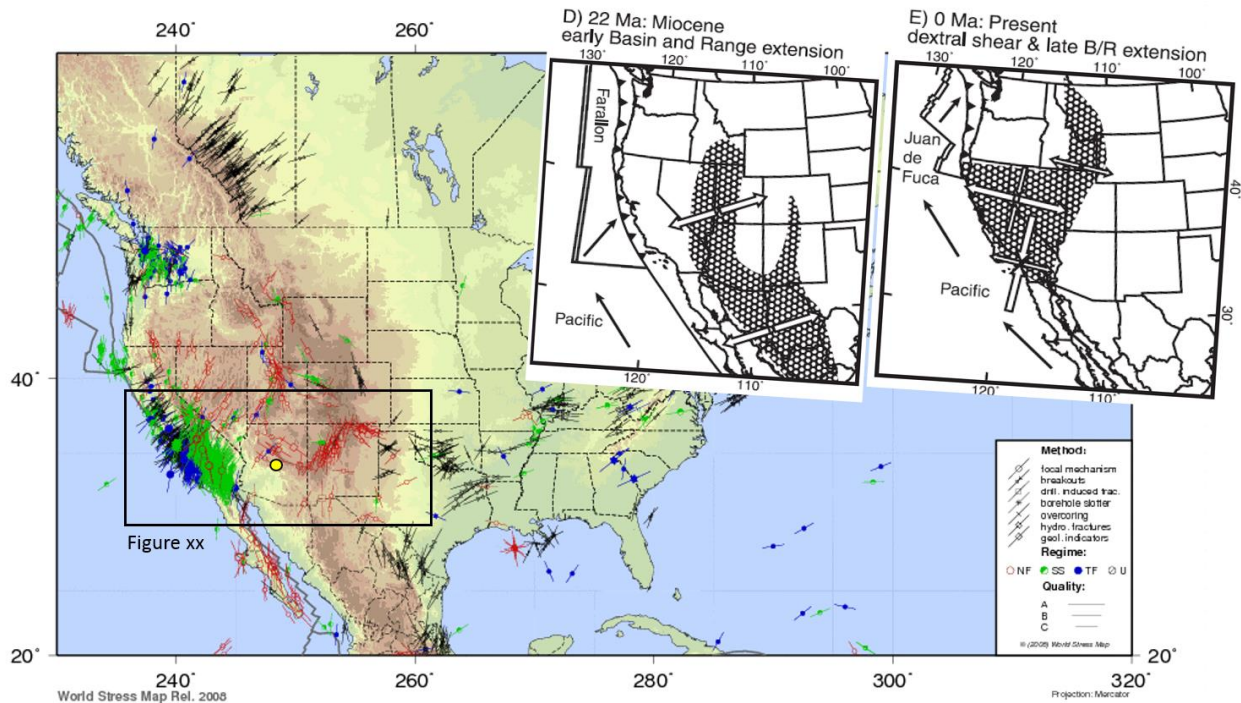


Figure 18: Present-day stress orientations, displaying the orientations of the maximum horizontal compressive stress  $S_H$ . The tectonic regimes include normal faulting (red), SS for strike-slip faulting (green), TF for thrust faulting (blue), and U for an unknown regime. Map from the World Stress Map (Heidbach et al. 2009).

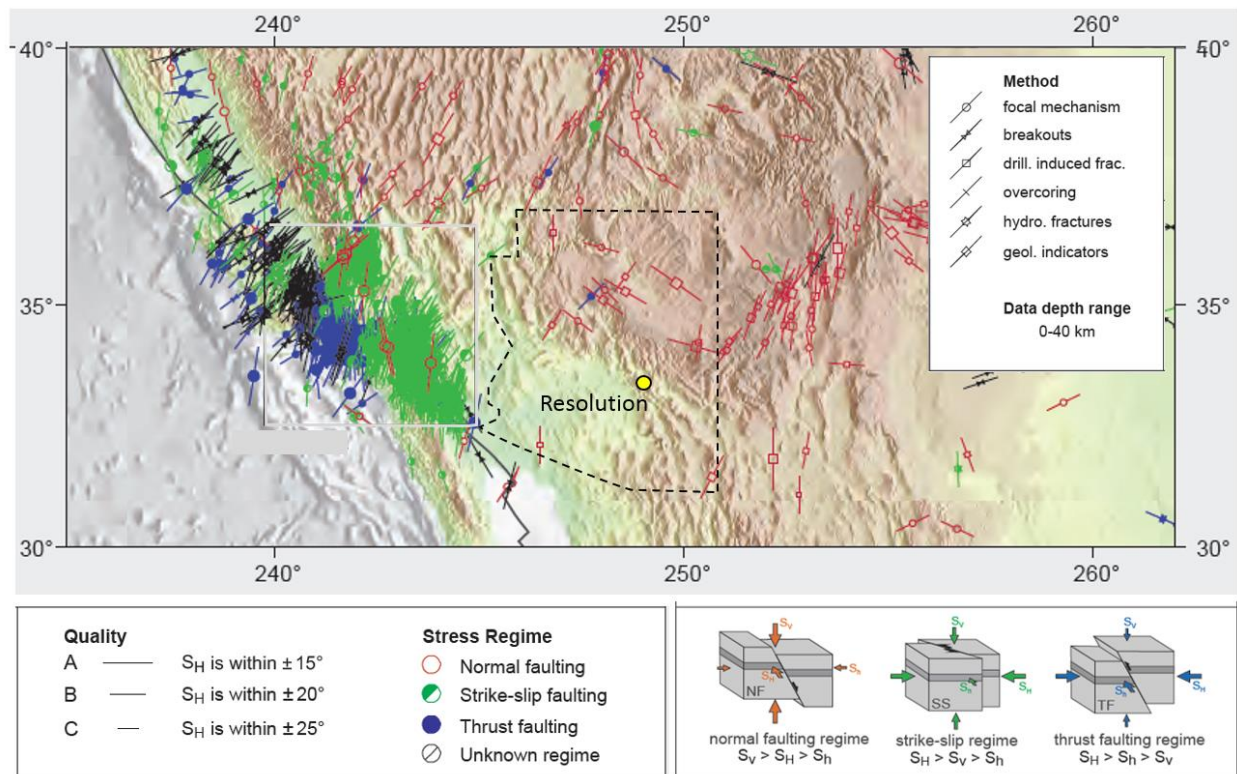


Figure 19: Present-day maximum horizontal compressive stress  $S_{Hmax}$  (World Stress Map, Heidback, 2009) derived from geological indicators such as fault, veins and dykes, showing NW-SE maximum horizontal stresses for the region of Resolution resulting in NE-SW directed normal faults. Note that Resolution is situated in a generally low-stress domain with NW-SE directed compressional stresses, and note the strong deflection of stresses from NW-SE to NE-SW along crustal scale lineaments.

### 5.3.2 Measured in situ stresses at Resolution

For the Resolution project area, a model for the in-situ stresses, both orientation and magnitude, was proposed by GeoMechanics International (GMI, 2007). The direction of the maximum horizontal stress ( $S_{Hmax}$ ) was reported to be NNW-SSE, based on well bore failure data, including bore hole breakouts and tensile wall fractures observed in 10 drill holes, as is illustrated in Figure 20. This orientation is not dissimilar to what the world stress map proposes.

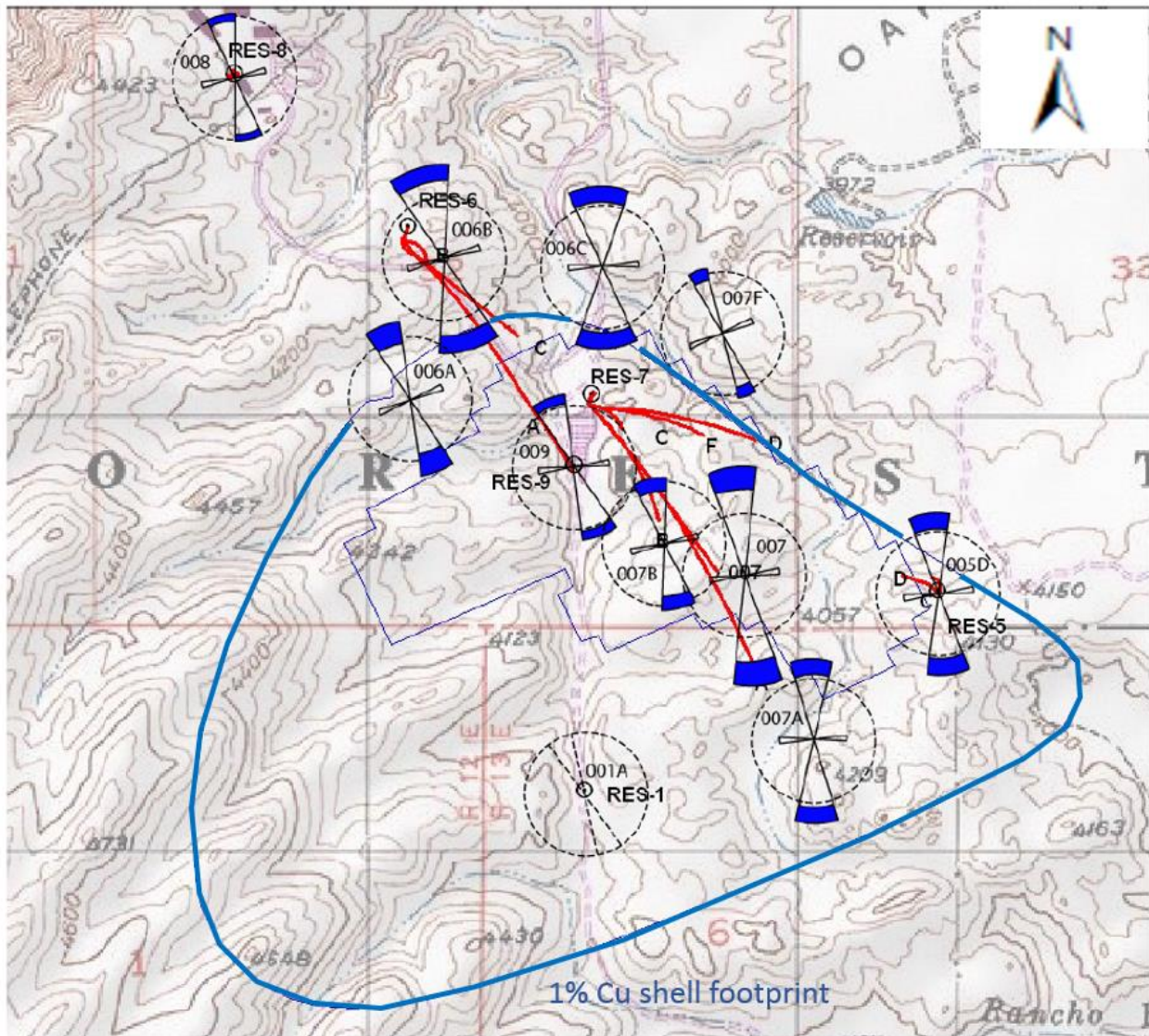


Figure 20: Present-day stress orientation and magnitude, deduced from observed oriented borehole breakouts and tensile fractures, as a function of well location at the Resolution Copper site. See the 1% Cu shell footprint for location reference.

Whether rock fails is a function of (i) imposed (differential) stresses, in part due to the weight of the rock, and in part due to possible tectonic stresses, and (ii) rock strength, taking into account the (iii) pore fluid pressure weakening the rock. It was noted that, where wellbore breakouts are observed, they are generally pervasive between land surface and 1000 meters depth, i.e. in the Whitetail Formation and Cretaceous volcanoclastics, and they are sparse below a 1000 m depth.

GMI (2007) concluded that the modelled maximum horizontal stress ( $SH_{max}$ ) indicates a stress regime that changes from strike-slip at surface to normal faulting with depth. Their model took into account an approximately linear overburden pressure gradient, a sub-hydrostatic pore fluid pressure with the water table at 700 m depth below land surface, rock strength that is highly variable and is a function of both lithology and variation within the same lithological unit due to pre-existing fractures. The change was explained largely as the result of variations in rock strength. An alternative explanation is that the increasing vertical stress due to the weight of the rocks at a certain depth overrules the (small) horizontal differential stresses of tectonic origin.



various magnitudes occurring on those sources, and the likelihood of the earthquakes producing ground motions over a specified level for the project area.

Seven events have been recorded within a 200 km radius of the project area with an intensity larger than M5 (MM V-VI), the largest was of magnitude M7 (MM VII-IX), some 185 km southeast of the project area, in 1830. The most notable earthquake was the 1887 Sonora, Mexico earthquake at M7.5 (MM IX-X) which occurred about 285 km southeast of the project area, off this map. This event was estimated to have resulted in an M5-6 (MM VI) for the project area based on an iso-seismal map (Wong et al., 2013).

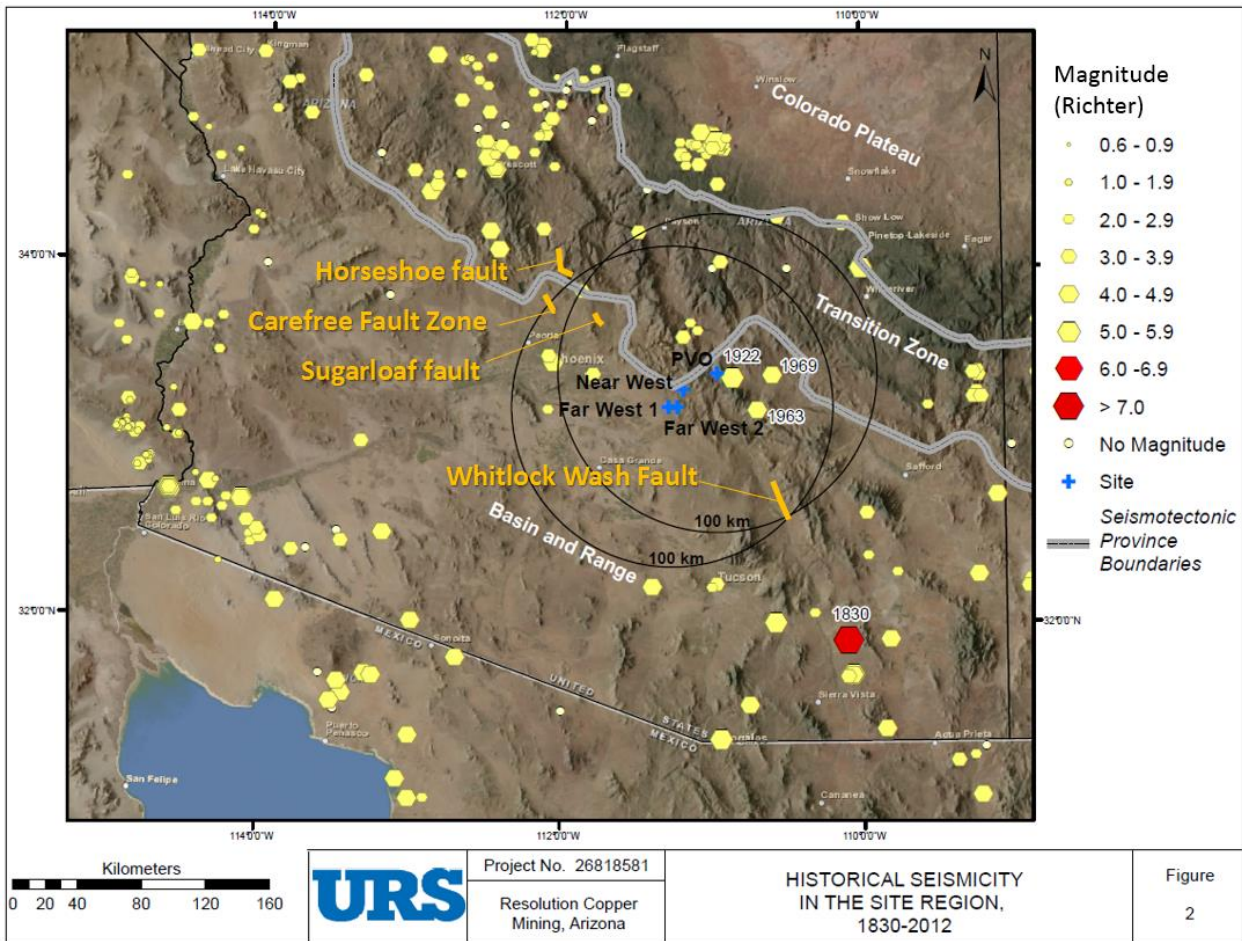


Figure 22: Historical seismicity in Southern Arizona, showing past earthquake epicenters and magnitude in and around the project region between the years 1830 – 2012. In orange are the currently active faults, which are potential future seismic sources. They are outside or near a 100 km radius of the project area. (From: Wong et al, 2013).

Seventeen events were recorded within 100 km of the project area. The largest and closest was an M5-6 (MM VI) event in 1922 near the town of Miami. Wong and co-workers note that two centuries of historic data is not a long time compared to the lifespan of active tectonic faults.

Larger, Basin and Range extensional faults in the project area, i.e. the Concentrator Fault, the Conley Spring Fault, do not show evidence of recent movement (Wong and co-workers, op cit.). As such they are not identified as a potential source for earthquakes. Four potential sources for earthquakes are identified within a 100 km radius: The Horseshoe fault, the Carefree fault zone, the Sugarloaf fault and the Whitlock Wash fault. They are near to or outside a 100 km radius of the project area (see Figure 22).

## 6. Deposit-scale geology and structures

### 6.1 Background

A 3D digital geological framework model is constructed for the deposit area. This model is the basis for accurate resource estimations, mine design, and associated evaluations of potential geotechnical and hydrogeological impacts.

Given the great depth to the deposit (4,500 to 7,000 feet below surface), and the great thickness of the post-mineral cover rocks (1,500 to 3,000 feet), the 3D digital geological framework model and the understanding of the local geology relies mostly on the available deep drill holes.

A 3D digital geological framework model is constructed largely on drill hole data and interpretation of the data. Since 2001 the Resolution team has been collecting and integrating drill hole data in 3D digital space, to interpret and construct a 3D digital framework model. A total of 438 drill holes are available. Drilling is ongoing and the model is regularly updated, with the latest update occurring in 2016.

The 2016 framework model is constructed over an area of about 4.2 km (14,000 ft) by 2.7 km (9,000 ft) wide, an area that is defined by the faults that define the local graben that hosts the deposit. The model extends to a depth of 1 km (3,500 ft) below sea level, which is the minimum elevation of known, potentially economic mineralization. Key ingredients of this model are the location and geometry of stratigraphic beds, intrusive bodies, and fault surfaces.

Because of the importance of the drill hole data, Resolution has an extensive core logging workflow and interpretation methodology, designed to observe and interpret lithology and stratigraphy, as well as alteration and in particular oriented structures, in a consistent and repeatable fashion further described below (Figure 23).

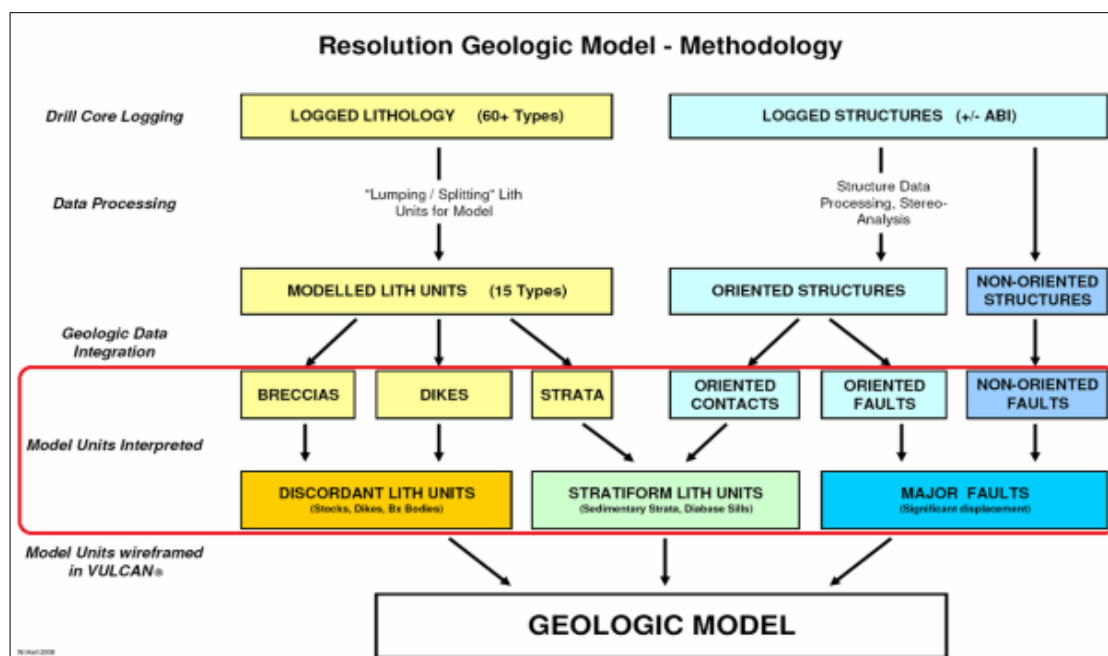


Figure 23: Summary workflow diagram for the construction of a digital 3D geological model from drill core data analysis and integration, and interpretation of lithological units and structures, followed by construction of 3D objects as wireframes in VULCAN software.

The drill holes at Resolution are relatively wide-spaced because of their depth, and also due to the requirement to limit surface disturbance from data collection within the Tonto National Forest. The aim is to arrive at a 3D model that is not only consistent with drill hole data, but also consistent with the regional geological history including the timing of tectonic phases and the style of faulting and kinematics of key faults.

The model has been and is continuously subjected to peer review and third party audits. The most current review is summarized by Amec Foster Wheeler (March 2017).

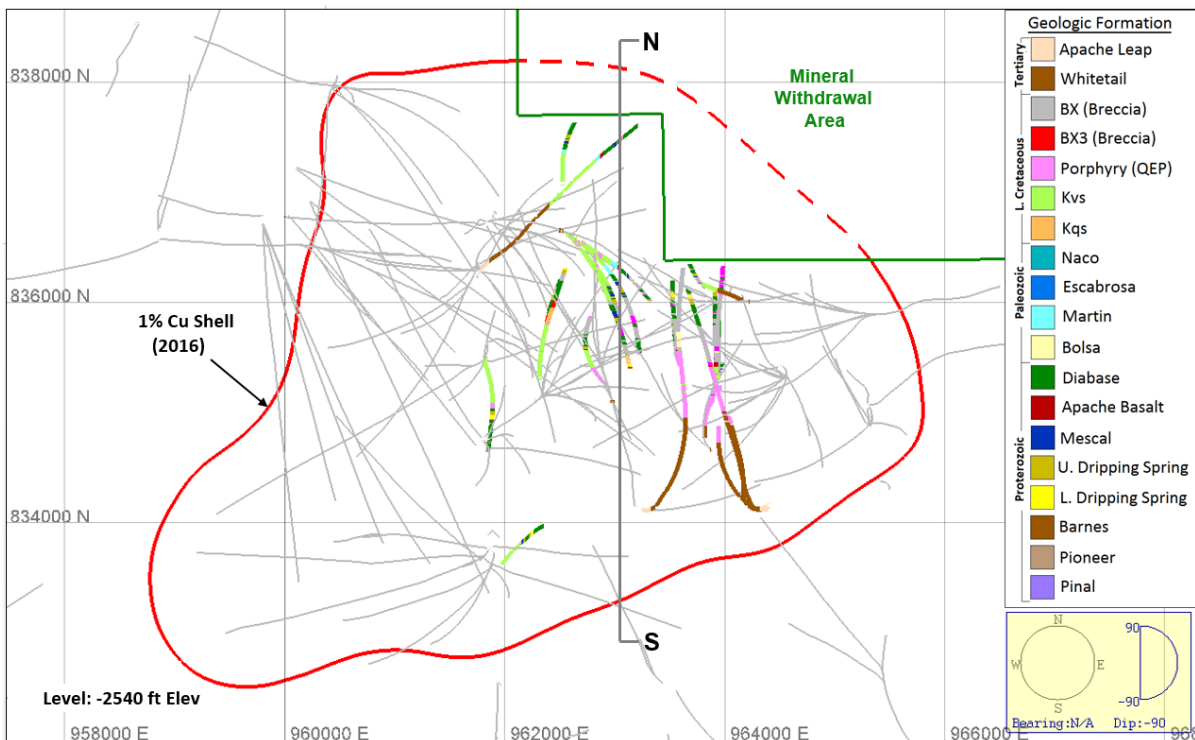
## 6.2 Input data

### 6.2.1 Data sets used for the geological model

The current geological model honors detailed geologic logging information from all 438 available drill holes plus archival geologic data from five of Magma's nine mine shafts, and new data from the one new RCC shaft, for a total of 729,234' core, with 381,354' being assayed. Figure 24 illustrates the drill hole depth and spacing with respect to the modelled 1% copper shell (red polygon).

From all holes, in addition to lithology, Cu analyses were available. Molybdenum analyses were available for all RES- core holes and most MB- holes for use in defining Cu and Mo grade shells.

Oriented structural measurements from drill holes form a significant source of information. They are acquired either via down-hole oriented acoustic borehole image logs (ABI) and/or analysis of recovered core from most of the exploration holes drilled at Resolution since 2005. A total of 25,112 oriented geologic structures (including fault, joints, veins, folds, slickensides, stretching lineations) were available for use in the latest 2016 geo-structural interpretation.



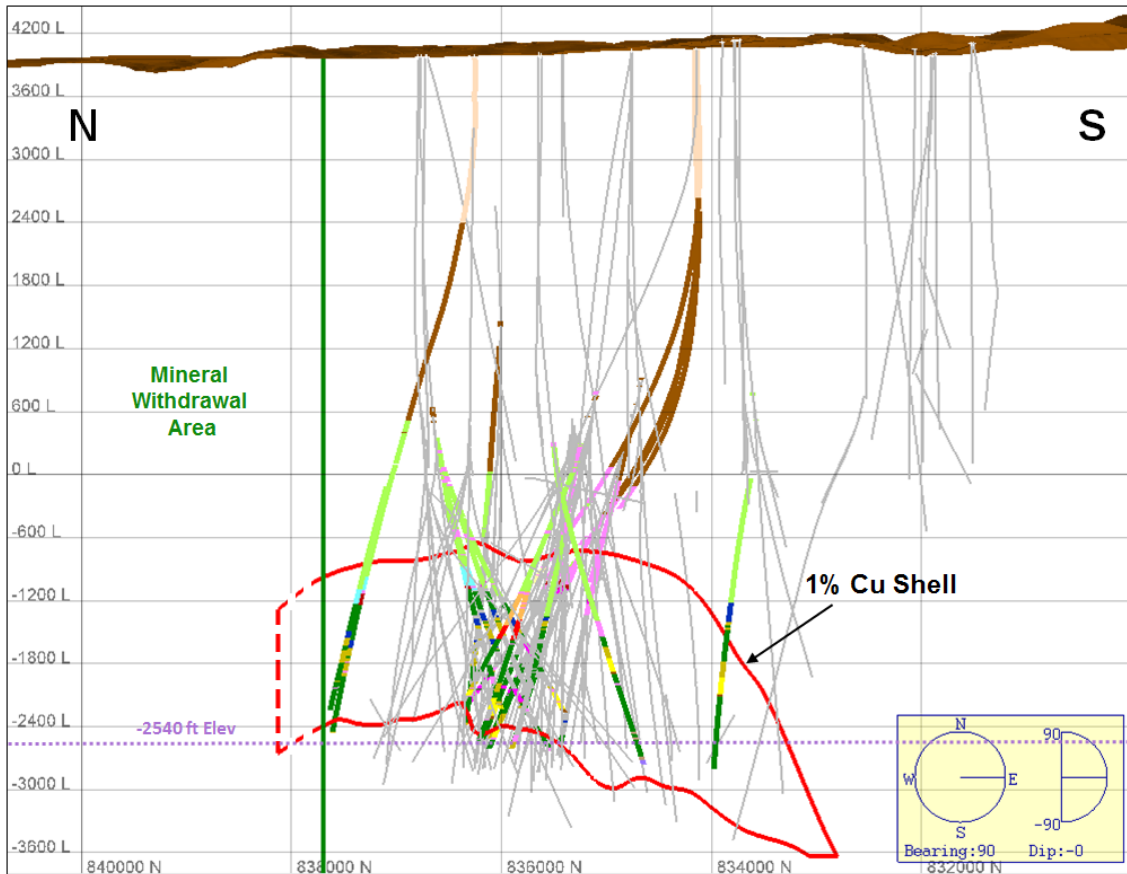


Figure 24: Plan view (at -2540 ft below sea level) (top) and cross-section view (bottom, looking East) across the 2016 geologic model showing the depth and the spacing of the drill holes with respect to the 2016 JORC compliant 1% copper shell (red polygon). The latest (post-2012) drill holes shown as thicker, multi-colored traces. Drill holes pass within 300 feet north or south of the plane of the section. Elevation grid lines are spaced at 1000 feet; note the lateral and vertical (+4,000 to -3,600 ft above mean sea level) extents of the model. The -2540 ft level is the current lower mining limit.

Multi-element drill hole whole rock geochemical analysis yielded average abundances for a 49 elements in parts-per-million or weight percent including the elements arsenic, mercury, lead, and uranium. Data for the full set of 49 elements and their average crustal abundances are listed in the table in Appendix 2 (Data modified from: MWH, 2013). The spatial coverage of the samples with respect to the volume of rocks to be moved in the mining process is illustrated on the map in Figure 25.

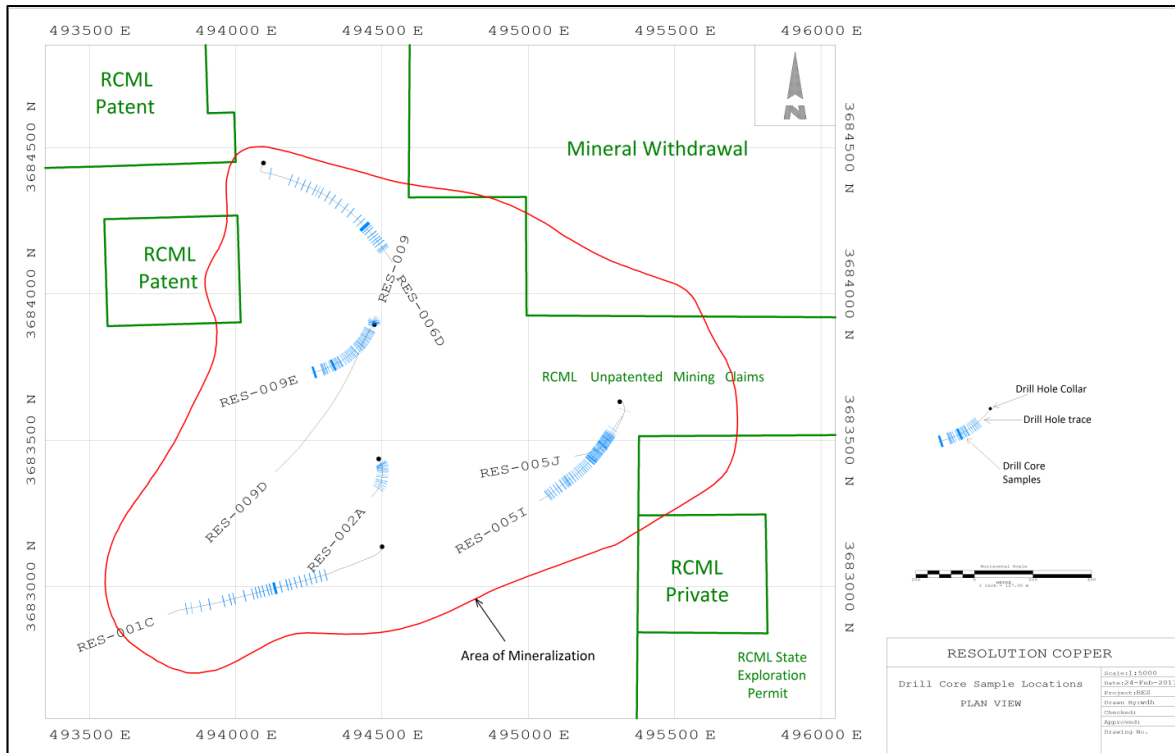


Figure 25: Map of geochemical sample locations within the Area of Mineralization (red polygon) illustrating the spatial coverage of the samples with respect to the volume of rocks to be moved in the mining process.

## 6.2.2 Types of data sets used in alteration and mineralization modelling

**Loggers silicate minerals estimation** – Up to 18 silicate minerals are logged at the domain level (40 ft) on a semi-quantitative basis. To assist the loggers, a Terraspec (and prior to this PIMA) instrument or infrared spectrometer is available.

**Hylogger** - or infrared spectroscopy analyzed by CSIRO in Australia, was performed routinely on assay sized samples ( $\leq 10$  ft) during 2011-13. Hylogger identifies white phyllosilicates/clay minerals, such as dickite, pyrophyllite, that are diagnostic of advanced argillic alteration. Darker minerals are more challenging to confidently identify.

**PIMA (infrared spectrometry)** is used primarily to identify zones of advanced argillic alteration where these intervals may not have been clearly recorded in the original logs.

**Quantitative Evaluation of Minerals by Scanning Electron Microscopy (QEMSCAN)** is used mainly on rocks from within the 1% Cu GS. Chalcopyrite, chalcocite and bornite are identified and reported in weight (and volume) percent. Additionally, low amounts of covellite and trace amounts of enargite are identified locally. Concerning alteration minerals, QEMSCAN is unable to detect individual clay species (e.g. dickite, pyrophyllite that are diagnostic of advanced argillic alteration), but it does identify secondary k-spar that is commonly missed during the logging stage and not identified by infrared spectroscopy.

**XRD (X-ray Diffraction)** analyses are used to confirm secondary k-spar (orthoclase) identified by QEMSCAN.

**Petrography** directs our attention to specific features i.e. significant secondary relict k-spar within marginal chlorite + epidote (propylitic) altered rock volumes.

**Loggers sulphide estimation** - The loggers record three copper sulfide species (chalcopyrite, chalcocite and bornite) on a domain level ( $\leq 40$  ft). These are estimated as veins and disseminations individually to give a total volume %.

**Loggers pyrite estimation** - Quantitative estimation to be used only within the anhydrite zone for block estimation.

### **6.3 Modeling techniques, constraints and assumptions, handling uncertainty**

The main tasks and data types involved in the construction of the 2016 geologic model at Resolution is detailed below.

#### **6.3.1 Modeling of stratigraphic domains**

Lithological domains are constructed following in-house validation and domaining by the Chief Geologist of drill hole lithologic data. This process includes interpretation, translation and recoding of loggers' lithology and formation combinations into 15 distinctive primary lithologic units.

Construction of the wireframe solids for these stratiform lithologic units follows a series of documented steps, including an optional cross section interpretation on paper plots, through digitization of electronic scans registered in Vulcan 3D, to the construction in Vulcan of 3D wireframe solids representing the stratiform lithologic units in a single fault block.

#### **6.3.2 Modeling of intrusive bodies**

Laramide-aged intrusive bodies known from drilling at Resolution include intermediate to felsic porphyry sills, dikes, and small stocks which intrude all pre-Tw lithologies except BX, and are modeled as individual wireframe solids. Intrusive bodies are typically constructed by digitizing polygons in section view and then generating wireframes that enclose the polygons. Existing wireframes may also be updated when new drill hole data becomes available. The current model comprises four solids representing the 4 largest-volume Laramide porphyry intrusive bodies ("QEP"), see Figure 26 (left).

#### **6.3.3 Modeling of breccia bodies**

Hydrothermal breccia volumes are known to exist within and immediately peripheral to the Resolution deposit. Only the larger breccia bodies are modeled. Methodology is similar to that used for intrusive bodies (see above), even though breccia bodies are typically more irregular. The current model comprises three larger and numerous smaller breccia bodies (BX), see Figure 26(right).

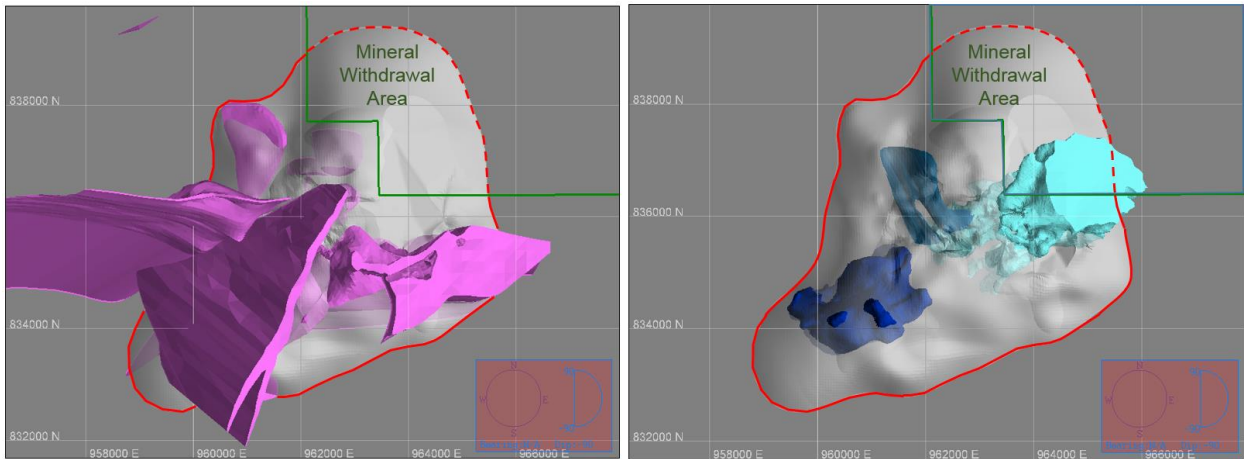


Figure 26: Map view of the 3D modelled intrusions in pink (left) and breccia bodies in blue (right). Light grey ovoid surface is the top 1% Cu shell outlined in red.

#### 6.3.4 Modeling of structures and orientation data

Structures and orientation data are seen as essential for the confident interpretation and modeling of the geo-structural framework concealed beneath a thick cover. They are routinely collected, interpreted and analysed by Senior Geologists. These include true dip and dip direction values for the top and bottom surfaces of planar structures such as faults, joints, breccia zones, and shear/slickenside lineations, as well as bedding orientations and contacts of intrusive dikes or sills. Oriented structures are statistically evaluated via stereographic projection, and displayed in 3D for use in the structural interpretations and construction of the major faults and relevant geologic contacts.

##### 6.3.4.1 Discretisation of Faults

Faults or discrete shears of various orientations and character are recorded consistently, following internal documented procedures. A single, typical drill hole of 7,000 feet in length may intersect up to several hundred individual faults, ranging from discrete shears less than 1" thickness to continuous intervals of faulting exceeding several tens of feet in true thickness. Textural and geotechnical characteristics of these faults vary greatly and may include one or more of the following:

- Discrete shear - a single, isolated "joint" with only shear lineations (striae/grooves, slickensides);
- Shear zone – an interval of multiple, discrete, closely-spaced sub-parallel shears;
- Fault with breccia - an interval of coarse, tectonically crushed/ brecciated rock;
- Fault with gouge - an interval of finer, granular "rock flour" or clay ("fault gouge");
- Various combinations of types 1-4;
- Annealed forms of any fault type.

Thicker log intervals that consist entirely of faulted rock are highlighted for future geotechnical focus. A fault that delineates significant offset (>100 ft) in adjacent geologic units is modeled as an individual wireframe surface which represents the approximate mid-plane of the interpreted zone of faulting. Other faults which exhibit significant "damage", but only minor demonstrable offset (<100 ft) are modeled as

individual, tabular wireframe solids which roughly delineate zones or corridors of anomalous fault/fracture/vein intensity, and are informally termed “geotechnical” faults.

#### **6.3.4.2 Annealed vs Non-annealed Faults**

Most individual faults observed in drill core at Resolution constitute roughly planar/tabular zones of relatively weaker, less cohesive rock material than the adjacent host rock, commonly known as a “damage” zone. But this is not true for all faults, or for all portions of a “major” fault. A fault of any of the types listed above may have been partially or entirely “healed” or annealed by new minerals forming within associated fractures/voids, and may have thus become relatively strong, and in some cases even stronger than the un-faulted rock. Such a fault is *geologically* still a fault, and will be modeled as a Major Fault if it can be demonstrated it has displaced host rock units by a significant distance.

#### **6.3.5 Constraints and assumptions for the 2D and 3D modelling of faults**

Because of the exceptionally large number of “thin”, closely-spaced faults and discrete shears of unknown lateral extent, combined with relatively widely-spaced drill holes, it is impractical, if not impossible, to construct individual wireframe surfaces to define every fault logged in core. It is thus important to rank and select for modeling the key faults that will support accurate resource estimations, mine design, and associated evaluations of potential geotechnical and hydrogeologic impacts.

The spatial distribution, orientation, and potential impacts of the remaining and far more abundant, but generally less persistent faults must then be accounted for and evaluated by other means. For example, geotechnical evaluations of these non-modeled faults may be accomplished via construction of a DFN (Discrete Fracture Network) model, or by treatment of these structures via the “Major Structures” parameters available in the RMR/IRMR (rock mass rating) system.

Considering the above criteria, the faults selected for modeling as individual wireframe surfaces in the geologic model are mainly those which delineate abrupt and significant (generally >100 ft) changes in the position of an otherwise continuous geologic contact. In some cases, an important fault may be recognized by an abrupt change in *thickness* of a rock unit, or an abrupt change in the orientation/attitude of a lithologic contact.

Most of the faults interpreted in the current model are intersected by at least one drill hole. The final pierce points delineating these faults were selected on the basis of detailed geological and structural logs, and in many cases, true orientations of one or more shear planes defining the fault. A few of the faults in the model do not have an actual drillhole intersection, but are instead inferred to exist by information in holes drilled either side. Most faults in the current model are interpreted on the basis of a combination of pierce points and abrupt changes in elevation or 3D position of distinctive marker beds or other lithologic contacts (Figure 27).

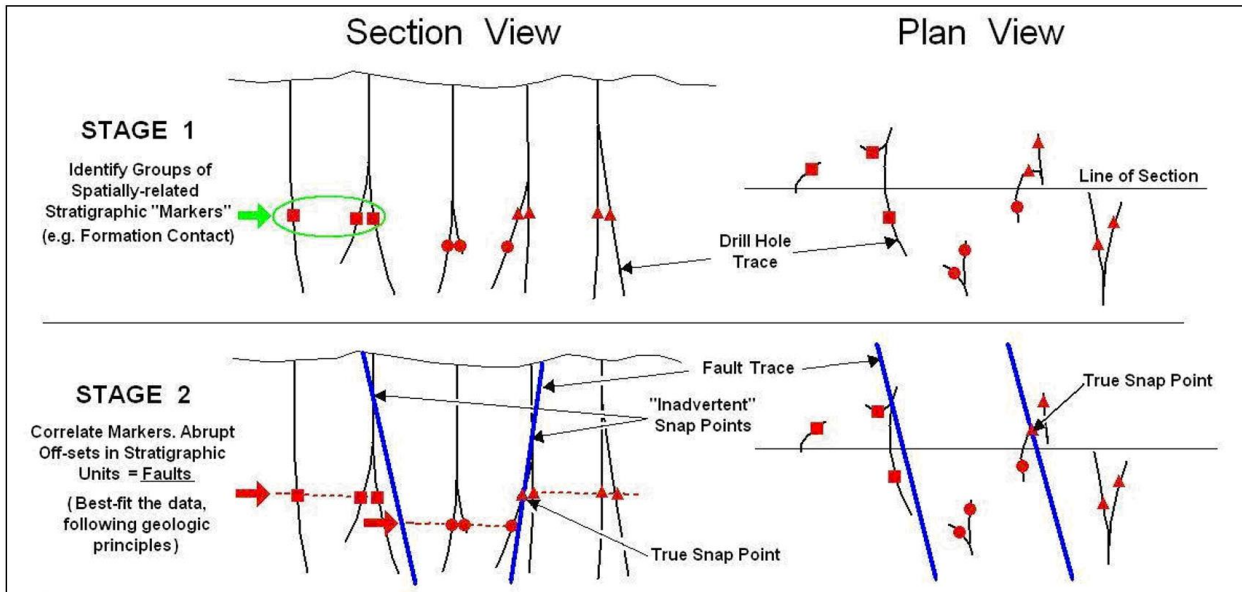


Figure 27: Conventional, two-stage method for interpretation and construction of major faults (blue) between spatially related stratigraphic markers (red) identified in multiple drill holes.

### 6.3.6 From section interpretation to 3D geological framework model

All drill hole interpretations – in the form of color-coded drill hole traces with lithology and faults, plus symbols denoting orientations of contacts and bedding - are plotted on paper sections and levels to be sketch-interpreted, digitally scanned, and imported as registered section panels in Vulcan. Key faults and geologic contacts are identified in 3D and in section views, then manually digitized as vector line-work which forms the framework for construction of 3D wireframe surfaces representing faults and geologic contacts. Fault surface wireframes are used to digitally slice a large model solid into individual fault block solids which are in turn sliced with wireframe surfaces representing the lithologic contacts to produce the final lithologic domains.

## 6.4 The 3D geological framework model

Here we summarize the modelled geological units and the main structures. For an outline on the mineralization and alteration please refer to the publication by Hehnke et al. (2012). The 2016 geological framework model consists of hundreds of digital 3D Vulcan wireframe surfaces and solids (closed 3D wireframes) representing:

- 21 geologic units (including stratigraphic units, intrusive dykes and sills, and breccia zones);
- 21 major faults (fault planes, damage zones, and geotechnical faults);
- Published inferred and indicated resource boundaries for Cu and Mo;
- Zones for alteration, oxidation, and dominant sulphide mineral species.

The extents of the Resolution geologic model are directly related to the natural geologic configuration of the host sequence and the distribution and extent of known mineralization. The zone of known economic Cu-Mo-Ag mineralization appears roughly centred within, and restricted to, a structurally down-dropped

block that is delineated on the north, west, south (and possibly on the east) by steeply dipping faults (Hehnke, 2012). The lateral extent of the model is restricted to these bounding faults, which roughly define an oval-shaped area with an east-west dimension of about 4.2 km (14,000 ft), and a north-south dimension of 2.7 km (9,000 ft). The vertical extent of the model is determined by the maximum elevation of the local topography of ~1400 m (~4,500 ft) above sea-level, the minimum elevation of known, potentially economic mineralization at 1 km (-3,500 ft) below sea-level, and the current technical limits of deep wire-line core drilling (approximately 2700 m / 9,000 ft). Thus, as has been done in previous models, the base elevation of the 2016 model was set at 1 km below sea-level (see Figure 28).

#### 6.4.1 Interpreted geological units

The general geological configuration of the pre-mineral stratiform geologic units interpreted in the Resolution Deposit area is that of a gently east-northeast dipping stratified / paraconformable sequence of Precambrian- and Paleozoic-aged quartzite, conglomerate, limestone and basalt. This is overlain by a westward thickening wedge of immature Cretaceous-aged sandstone and tuffaceous sediments (Kqs, Kvs). Post-mineral units include an overlying east-northeast thickening wedge of immature Tertiary-aged conglomerate, sandstone, and siltstone, capped by a very gently east-dipping accumulation of younger, Tertiary-aged welded dacite tuffs.

This structural complexity is documented in a section A - A' that runs NW-SE, Figure 28 (from:Hehnke et al. 2002). Also here thickness variations are seen in the Cretaceous Kqs and Kvs, suggesting that the ENE-trending faults also had a control on creating depositional space at this point. Thickness variations in the underlying Paleozoic sequence suggests that ENE-trending faults are originally Paleozoic, pre-mineralisation. It must be noted that uplift and erosion may have influences on the thickness distribution. Laramide intrusions exploited these Paleozoic faults.

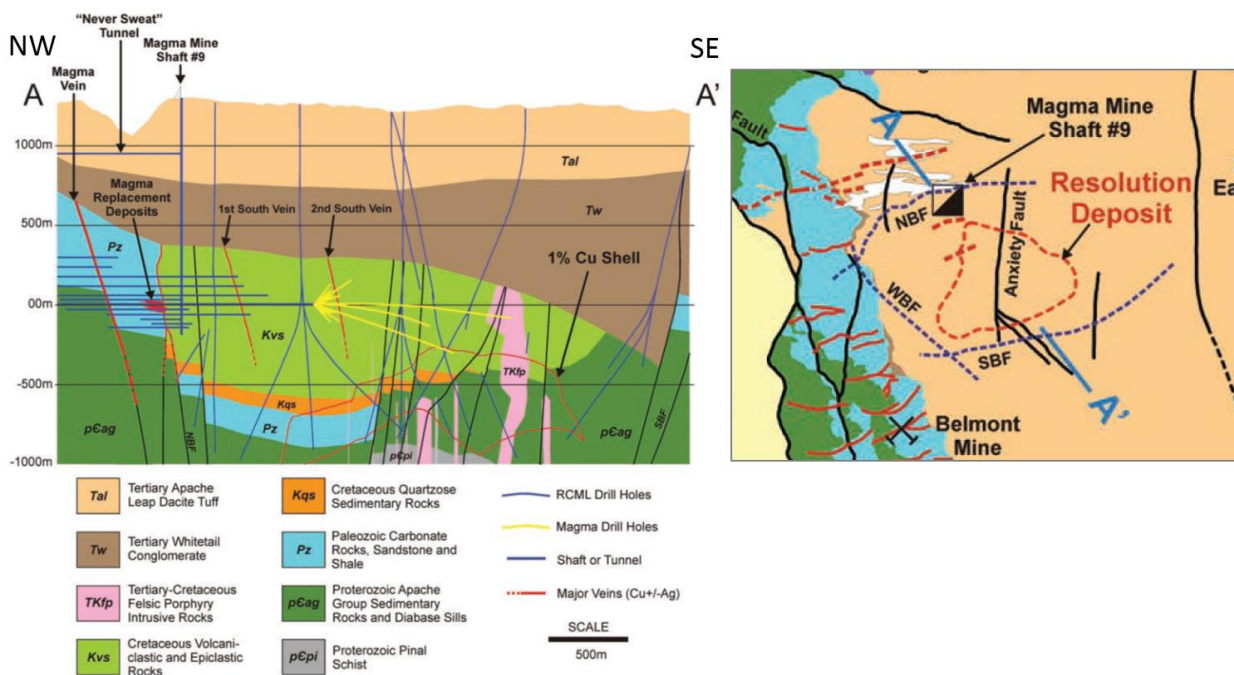


Figure 28: (Left) Representative section A – A' viewed toward NE through the central portion of the Resolution deposit showing modeled strata (colors), Laramide felsic intrusions (pink), the major faults (black lines) and drill holes in blue. The red polygon outlines the extent of significant Cu mineralization (+1% Cu grade zone). (Right) Map showing the location of the section in context with the graben bounding faults and the 1% Cu footprint polygon (Hehnke et al. 2002).

The plan view in Figure 29 shows the complex fault pattern at that level. Three section are cut across to illustrate the complexity in the lithologic and structural configuration of the rock sequence hosting the Resolution Deposit. Figure 30 shows a vertical cross section trending approximately east-west (looking north). It illustrates how faults were interpreted where differences in elevation of stratigraphic units and/or orientation so required. This is further discussed in Section 6.4.2. Figure 31 has a N60E trend. It is well suited to illustrate how Laramide intrusive dykes exploit the Palaeozoic extensional faults, and how the mineralization is located around a local horst block. Figure 32 trends NW and illustrates the nature of the South and the North Boundary Fault.

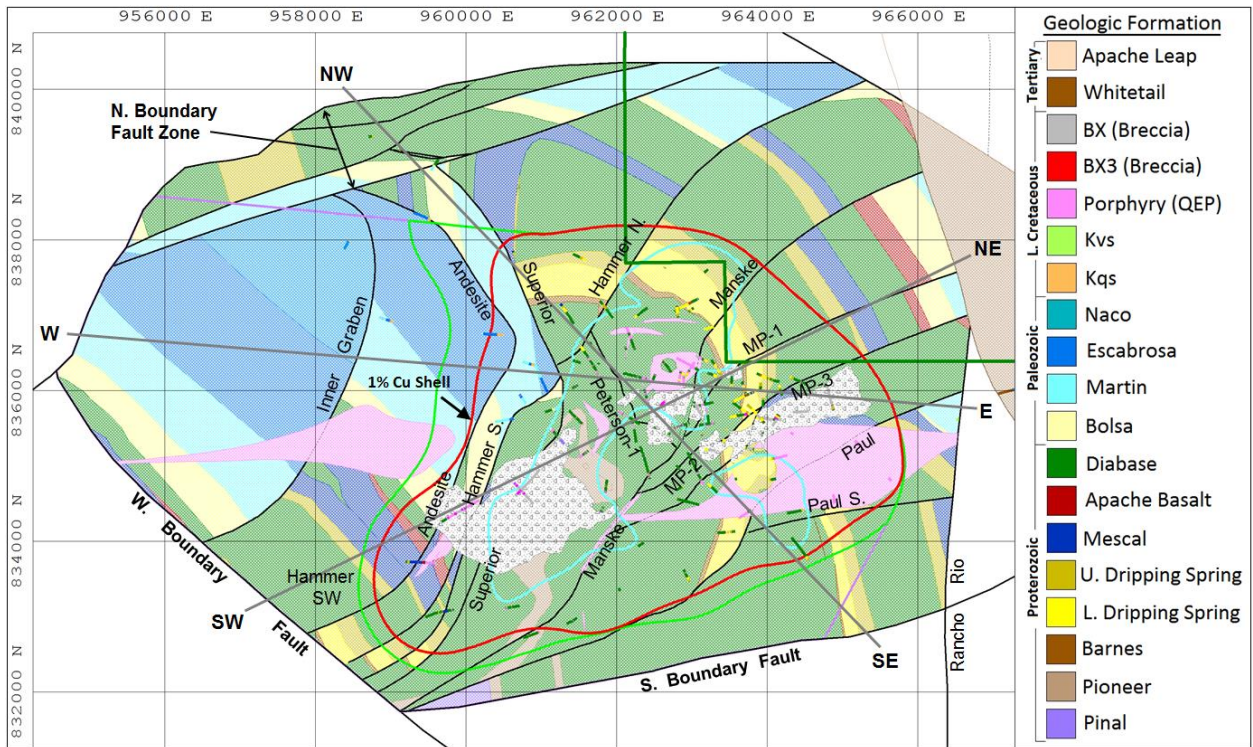


Figure 29: Plan view at -2540 ft elevation of the 2016 geologic wireframe model. Different colors denote the various stratiform and discordant geologic units within multiple fault blocks. These include: Laramide felsic intrusions (pink), breccia bodies (gray patterns), and major faults (black lines) as modeled in 2016. Extent of significant Cu mineralization is shown as a red polygon (+1% Cu grade zone). The section traces shown are for vertical cross sections seen in Figure 30, Figure 31 and Figure 32, below. The reference grid shown is AZ State Plane, in feet.

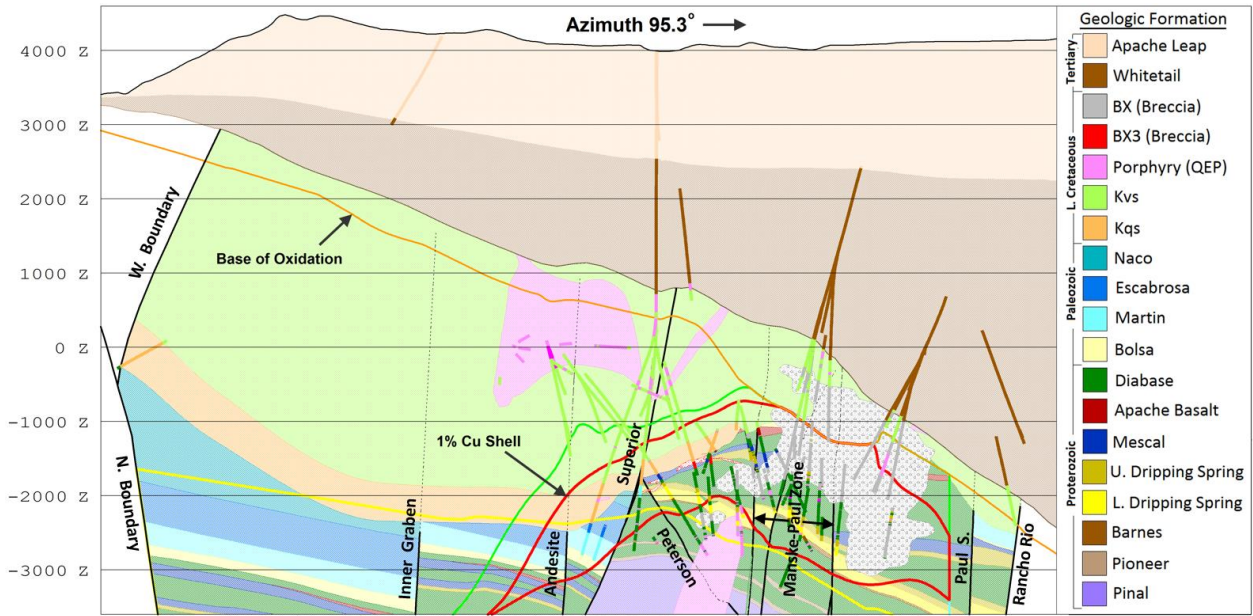


Figure 30: Approximate E-W trending (azimuth 093.5 deg) vertical cross section from the 2016 geologic model showing lithological and structural configurations of stratigraphy, Laramide felsic intrusions (pink), breccia bodies (gray patterns), and major faults (black lines). Red polygon indicates extent of 1% Cu grade zone. Drill holes passing within 300 feet north or south of the plane of this section appear as multicolored traces. Elevation grid lines shown are spaced at 1000 feet.

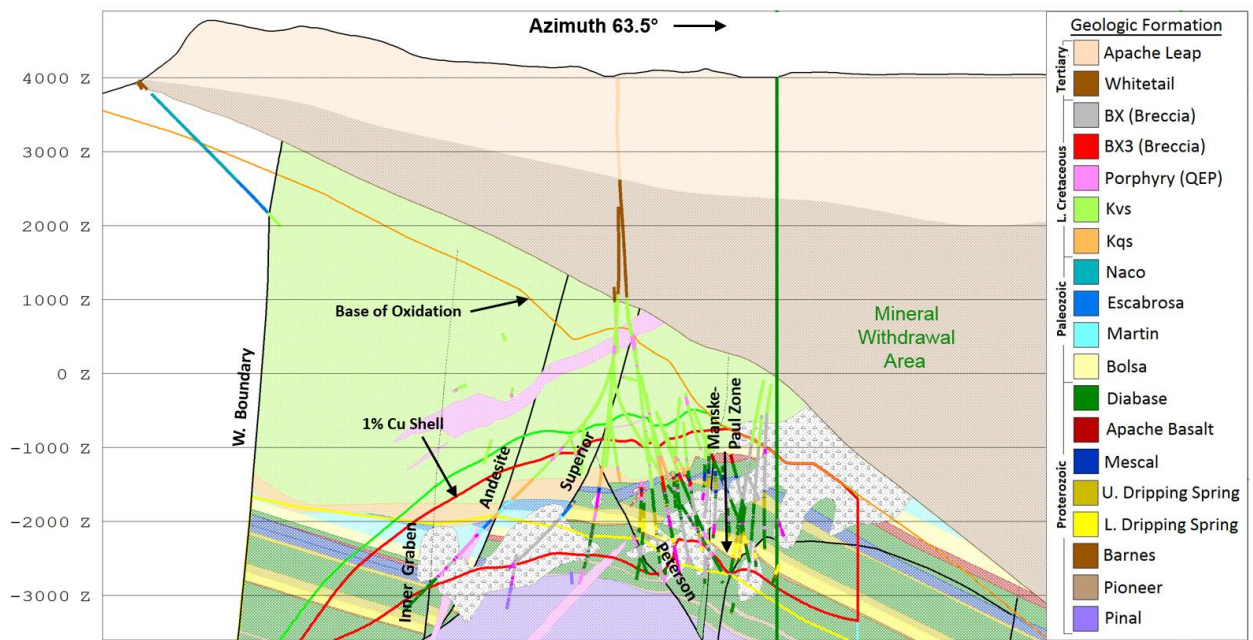


Figure 31: SW-NE trending cross section (trending at Azimuth 63.5 deg, viewed toward NW) through the central portion of the Resolution deposit showing modeled strata (colors), Laramide felsic intrusions (pink), breccia bodies (gray patterns), and major faults (black lines) as modeled in the 2016 geological model. Extent of the 1% Cu grade zone is shown in red. Reference line for this section is shown in Figure 29. Base of model is 3600 ft below mean sea level. Elevation grid lines shown are spaced at 1000 feet.

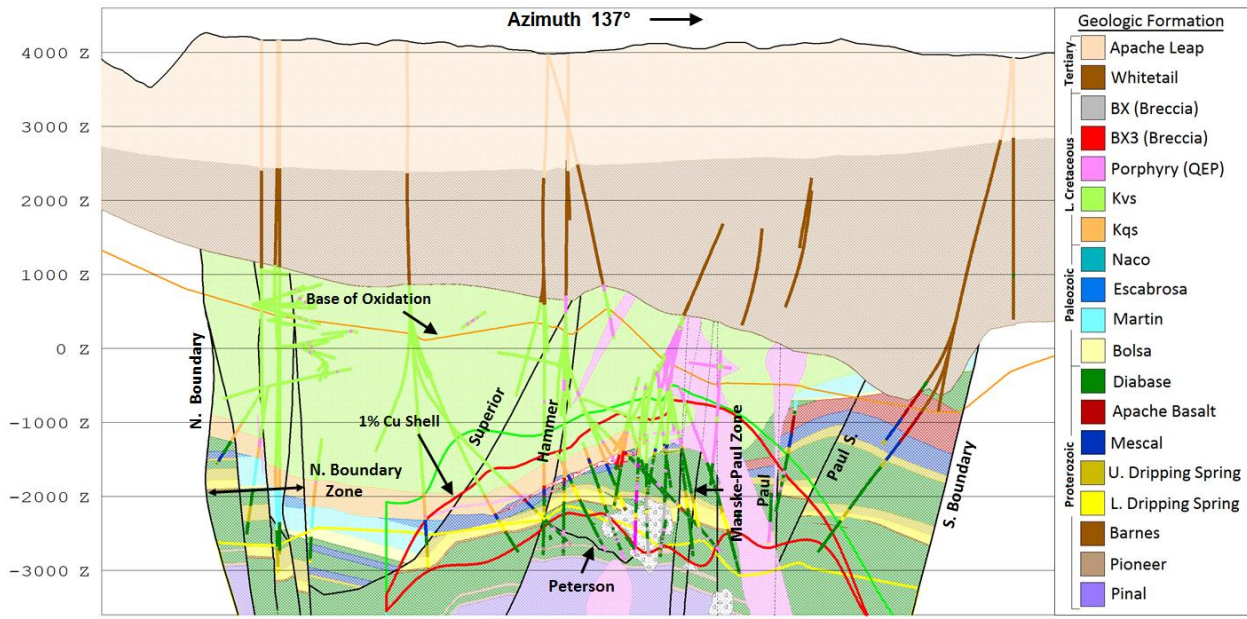


Figure 32: NW-SE trending cross section (trending at Azimuth 137 deg, viewed toward NE) of modeled strata (colors), Laramide felsic intrusions (pink), breccia bodies (gray patterns), and major faults (black lines) as modeled in the 2016 geological model. Extent of significant Cu mineralization is shown in red (+1% Cu grade zone). Reference line for this section is shown in Figure 29. Elevation grid lines shown are spaced at 1000 feet.

**6.4.2 Interpreted faults and fault blocks**

Most faults in the current model were interpreted on the basis of a combination of controlling drill hole pierce points and abrupt changes in elevation (typically >100 feet of offset) or a change in the 3D position of a distinctive stratiform bed or other lithologic contact. In some cases, an important fault may be recognized by an abrupt change in thickness of a rock unit or an abrupt change in the orientation/attitude of a lithologic contact. Such faults are required for the three dimensional interpretation, and are important to the distribution of host rock types which could in turn impact the distribution of lithology-controlled mineralization, but do not necessarily represent zones of recent movement or zones of geotechnical weakness. In some cases, the annealing effects of some forms of mineralization may increase the strength of faulted rock relative to the adjacent rock mass. In addition to these pre- or syn-mineral faults, some zones of faulting, gouge, and strong shearing (geotechnical faults) are recognized. All the interpreted faults are then modeled in Vulcan by digitizing lines in cross section views, regularly spaced at 150 feet or 300 feet, then creating a 3D surface along these control lines. With ongoing drilling new faults are being identified. Figure 33 shows a level plan at -2100 ft illustrating the fault pattern at this depth. The five new faults most recently modeled are shown with red labels.

Surface mapping and drilling information evidence suggests that three of these faults, Anxiety, Gant W. and Gant E. (Figure 33), intersect both mineralized and post-mineral rock units (Tal and Tw), but exhibit mainly strike-slip displacement, with only a minor component of vertical offset (<100 ft). These faults are considered geotechnically important, and are interpreted as narrow 3D “corridors” of relatively greater fracturing and potential faulting, but with no offset of adjacent, bounding rock units is actually modeled, and thus they do not currently serve as physical boundaries for the modeled fault blocks.

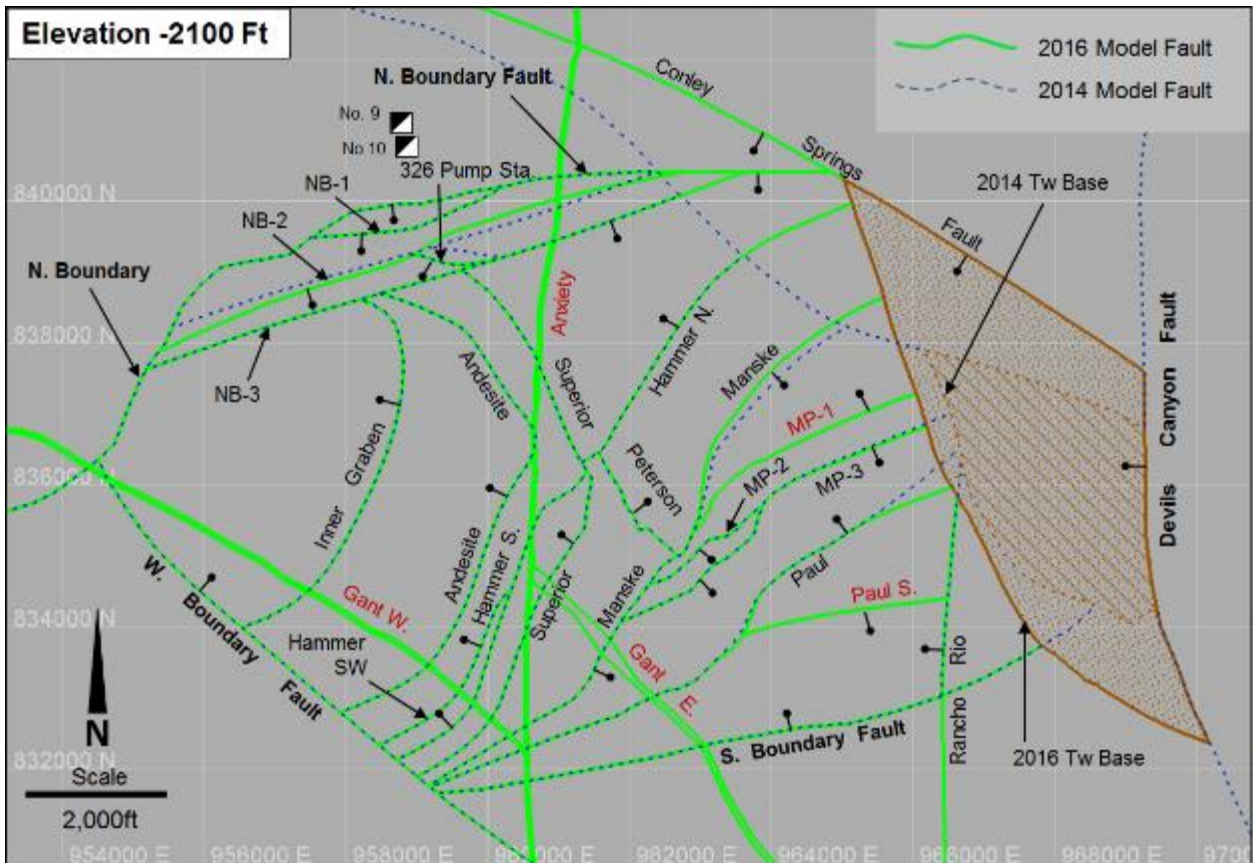


Figure 33: Subsurface 2D plan view of modeled faults (at -2,100 ft elevation). Solid green lines are 2016 model fault traces, thin dashed blue lines are the 2014 faults. Five new faults modeled in 2016 are shown with red labels. The reference grid shown is AZ State Plane, feet.

The Resolution “graben” is delineated by the North, West and South Boundary faults, and tentatively, a southeast-ward projection of the Conley Springs fault. Four major zones of faulting are interpreted to intersect the known ore deposit, comprising 16 individual faults internal to graben. The best constrained of these faults are described individually below.

**Superior - 326 Pumpstation Fault Zone** - (Includes previously named “Shaft Fault”)

This fault is interpreted as being strongly curving (in plan view), and concave-to-the-west, with 1,250 to 1,500 feet of pre-Kqs (pre-97 Ma) down-to-the-west normal displacement, with relatively minor post-Kqs reactivation with 100-300 feet of additional normal, down-to-the-west displacement. The northern portion of the fault, which has the best drilling support, strikes northwest toward Shaft No. 10 and is interpreted to terminate at, or be offset by, N. Boundary-3 fault, then possibly continuing to the northwest as the 326 Pumpstation fault which intersects Shaft No. 10 at a depth of 6,519.5 ft below the shaft collar. The “Superior-326 Pumpstation fault zone” may continue toward the northwest as a steeply SW-dipping fault which cuts the Never Sweat tunnel near Shaft No. 9 and which conducts significant ground water in this area. Currently, inadequate drilling control at moderate depths below the bottom of Shaft No. 9 limits confidence in resolving this question. Farther along its trajectory toward the SE, the Superior fault is interpreted to cut and offset the SW portion of the northeast-striking Hammer fault zone, down-to-the-west.

**Hammer Fault Zone** - The existence of this important NNE striking fault zone, now comprising three separate fault splays, has been interpreted or inferred in every geologic model constructed since mid-2006 (Zulliger and Hart, 2006). Prior to 2012, the fault was named the “N30E Fault”, denoting its average strike direction, and was interpreted to pass between several widely-spaced core holes but with no actual drill-hole intersections. This fault zone, which is bisected and offset by the Superior Fault, displaced the pre-Cretaceous strata down-to-the-NW by 600 to 800 ft, and was later reactivated during the Cretaceous and/or early Tertiary, displacing the Kqs and Kvs by another 100 to 200 ft, also down-to-the-NW.

**Manske - Paul Fault Zone** - This broad zone of multiple steeply NW-dipping faults is interpreted to comprise at least five, NNE- to ENE-striking, steeply NW-dipping faults with numerous drill holes providing evidence for both reverse and normal apparent displacements of up to 400 ft. Oriented shear lineations (including shear fibres and slickensides) measured in drill core vary greatly in orientation and sense but most plunge steeply toward the NW, raking approximately 90° within the average fault plane, with shear sense indicators that would suggest the latest displacements on most of these faults was normal. The various fault splays are currently modeled to gradually merge toward the southwest, ultimately merging with the ENE-striking South Boundary fault zone.

Based on the geometry and relative sense of shear displacements observed, the current interpretation for the overall Manske-Paul fault zone is that this structural zone initially comprised several steep oblique-reverse fault splays defining a positive flower structure formed during sinistral shear on an ENE regional lineament, resulting from pre- to syn-mineral NE-SW Laramide compression. The structure then inverted to a negative flower structure during post-mineral extensional collapse and coeval ENE tilting, with resultant normal re-activation along some of the former reverse faults. Alternatively, due to the clockwise rotation of the compressive stress field due to changing tectonic plate configuration (Bird, 2002), the constraining fault bend changed into a releasing bend with the maximum compressive horizontal stresses now with an E-W orientation, and the ENE regional lineament now suffering dextral horizontal shear.

**Peterson Fault** – The Peterson fault strikes NW-SE, and divides an otherwise continuous NE trending fault block into two “compartments”, i.e. fault blocks 7A and 7B. The fault dips at approximately 60 deg toward the NE, and displaces NE-dipping host strata down-to-the NE by ~200 ft. During the modeling, similar, though less obvious, drill hole evidence for down-to-the-NE offset occurs in the two adjacent fault blocks to the south, (FB08B and FB09), suggesting that the Peterson fault, or faulted segments of this fault may persist toward the southeast, passing between drill holes. Additional drilling may help resolve this.

#### **6.4.3 Concept for the structural evolution of the Resolution “graben”**

The rationale for the current 3D geo-structural configuration of the framework model is four-fold:

1. Knowledge and application of the established tectono-stratigraphic history for the Resolution (Pioneer) district and surrounding region regarding expected or permissible geo-structural architectures and kinematics.
2. Identification of dominant structural trends and structural style in statistical analysis of oriented structures logged in drill holes, including: bedding, contacts between different strata, intrusive contacts, faults, folds, veins and joints).
3. Comparison of mineralogical associations, 3D patterns of alteration and mineralization, and associated age dates observed at Resolution with other deposits of similar age in the regions, and with established models for porphyry Cu-Mo deposits world-wide.

4. Construction of a geometrically valid and geologically sound wireframe model for the Resolution deposit.

Based on these four aspects, the following structural 3D fault configuration of the Resolution “graben” is proposed. This configuration is important for the location and geometry of the mineralisation, potential offsets of the mineralised volume, rock-mass characterisation for the mine design and subsidence predictions.

#### **6.4.3.1 Pre-mineralization extensional faulting**

Clear evidence exist for at least two stages of significant pre-mineral faulting across the “blind” Superior, Hammer, Andesite, and N. Boundary faults, as seen in the geo-structural cross-sections, where the Cretaceous aged Kvs and/or Kqs strata (lime-green Kvs above the orange Kqs unit) are vertically displaced (down-to-the-northwest) only a few tens of feet, whereas the deeper and older strata (e.g. dark blue Precambrian Mescal Ls) are vertically displaced by up to 1,500 feet (also down-to-the-northwest) across these same faults. To what extent these faults are restricted to the graben is not known.

#### **6.4.3.2 Syn - mineralization releasing bend and fault-bounded pull-apart graben**

Mineralisation is during Laramide orogeny and magmatism. During the compression, space for the intrusions can be made by local dilation in a releasing bend of a transcurrent fault system. Bird (2002) shows that Laramide compression rotated clockwise from a NE-SW orientation to more ENE-WSW to E-W. The ENE-trending inherited basement lineament, (parallel to) the Salt River – Jemez lineament, would form a releasing bend by a right-stepover fault geometry with E-W compression. E-W compression is also indicated by the E-trending swarm of mineralised veins in the range front.

A right step-over would also explain the erosion that occurred within the graben prior to Kvs deposition; because the graben would have a constraining bend geometry during earlier NE-SW compression. Its fill would have locally popped-up and eroded.

Contractional structures need not have developed much outside the graben, if the response to crustal shortening was largely by displacement on (conjugate?) strike slip faults.

#### **6.4.3.3 Post-mineralization Basin and Range Extensional faults**

Basin and Range listric extensional faults (Devil’s Canyon Fault, Concentrator Fault, plus the smaller South Boundary Fault) are the main faults responsible for integrally tilting the fault block that hosts the Resolution deposit. At the surface, faults with smaller displacements on the order of 10’s to 100 ft have been documented to affect Tertiary dacite volcanic cover unit (Tal, Apache Leap Formation), but their linkage to the system of main extensional faults is uncertain. Decreasing offsets towards the surface is what is expected with growth-faults, i.e. faults that are active during - and are ultimately overtaken by - deposition. This may explain the change in offset and character from deep to shallow. But, to hard-link these surface faults to faults with large offsets observed at the level of the deposit carries a high uncertainty.

#### **6.4.3.4 Post-mineralisation compressional structures and present-day stresses**

Bore hole break-out observations from drill holes across Resolution indicate present-day NNW-SSE compression. This is not unlike what Bird (2002) indicated for the western US. In the current understanding it is proposed that these stresses caused small thrusts in the Apache Leap tuff on Oak Flat linked with small sinistral strike-slip displacement on the Anxiety Fault.

The present-day stresses are expected to influence geotechnical aspects of the underground mine, as well as the location of subsidence, as it may cause the preferential failure of faults and fractures with a particular orientation with respect to the present-day stresses.

## 7. References

Aldrich, M. J., Laughlin, A. W., Meade, J. S., and Peirce, H. W., 1986. The Jemez Lineament: structural boundaries and control on sedimentary facies, tectonism and mineralization: Proceedings of the 6th International Conference on Basement Tectonics, p.104-113.

Ballantyne, G. H., Marsh, T. M., Hehnke, C., Andrews, D. S., Eichenlaub, A. B., and Krahulec, K. A., 2003. The Resolution copper deposit, a deep, highgrade porphyry copper deposit in the Superior district, Arizona: Marcofest Conference, Golden, Colorado, 3–5 April 2003, Society of Economic Geologists Student Chapter, Colorado School of Mines, CD Publication, 12 pages.

Berger, B.R., Ayuso, R.A., Wynn, J.C., and Seal, R.R., 2008. Preliminary model of porphyry copper deposits: U.S.Geological Survey Open-File Report 2008–1321, 55 p.

BHP Billiton, 2009, Annual Report.

Donadini, F, L.J. Pesonen, K. Korhonen, A. Deutsch, S.S. Harlan, 2011. Paleomagnetism and Paleointensity of the 1.1 Ga Old Diabase Sheets from Central Arizona. *Geophysica*, Vol. 47(1–2), p. 3-30.

Ferguson, C. A. and S. J. Skotnicki., 1996. Geologic Map of the Florence Junction and Southern Portion of the Weavers Needle 7.5' Quadrangles, Pinal County, Arizona (revised 1996). Arizona Geological Survey, Open-File Report 95-10.

Ferguson, C.A. and R.A. Trapp, 2001. Stratigraphic Nomenclature of the Miocene Superstition Volcanic Field, Central Arizona. Arizona Geological Survey, Open-File Report 01-06, P. 103.

Granger, H.C., and Raup, R.B., 1969. Geology of Uranium Deposits in the Dripping Springs Quartzite, Gila County, Arizona. US Geological Survey Professional paper 595.

Grupo Mexico, 2010 Annual Report.

Hammer D.F., 2011, The Silver King Mine, Pioneer Mining District, Pinal County, Arizona; unpublished internal consultant's report, Magma Mining Company, Superior, Arizona.

Hammer D.F., and Peterson, D. W., 1968. Geology of the Magma Mine area, Arizona, in: Ridge, J. P., ed., *Ore Deposits of the United States, 1933-1967: A.I.M.E. Graton-Sales volume*, p. 1282-1310.

Harris, R.C., 2003. Is asbestos present in Agua Fria River sand and gravel? Arizona Geological Survey Open File Report, OFR-03-06, 15 pages.

Heidbach, O., Tingay, M., Barth, A., Reinecker, J., Kurfeß, D., Müller, B., 2009. The World Stress Map based on the database release 2008, equatorial scale 1:46,000,000, Commission for the Geological Map of the World, Paris.

Hehnke, C., Ballantyne, G., Martin, H., Hart, W., Schwartz, A., and Stein, H., 2012. Geology and Exploration Progress at the Resolution Porphyry Cu-Mo Deposit: Society of Economic Geologists Special Publication 16, p. 147-156.

John, D.A., Ayuso, R.A., Barton, M.D., Blakely, R.J., Bodnar, R.J., Dilles, J.H., Gray, F., Graybeal, F.T., Mars, J.C., McPhee, D.K., Seal, R.R., Taylor, R.D., and Vikre, P.G., 2010, Porphyry copper deposit model, chap. B of Mineral deposit models for resource assessment: U.S. Geological Survey Scientific Investigations Report 2010–5070–B, 169 pages.

Keep, M., 1996, The Pinal Schist, southeast Arizona, USA: Contraction of a Palaeoproterozoic rift basin: *Journal of the Geological Society of London*, v. 153, p. 979–993.

Kesler, S.E., Chryssoulis, S.L., and Simon, G., 2002. Gold in porphyry copper deposits: its abundance and fate: *Ore Geology Reviews*, v. 21, p. 103-124.

Lowell, J.D., and Guilbert, J.M., 1970, Lateral and vertical alteration-mineralization zoning in porphyry ore deposits: *Economic Geology*, v. 65, p. 373-408.

Lund, Karen, Box, S.E., Holm-Denoma, C.S., San Juan, C.A., Blakely, R.J., Saltus, R.W., Anderson, E.D., and DeWitt, E.H., 2015. Basement domain map of the conterminous United States and Alaska: U.S. Geological Survey Data Series 898, 41 pages.

Manske, S.L., and Paul, A.H., 2002. Geology of a major new porphyry copper centre in the Superior (Pioneer) district, Arizona: *Economic Geology*, v. 97, p. 197–220.

MWH, 2013. Resolution Copper Mining, LLC Geochemical Characterization Data Summary Report , 461 pages (**Submitted as an appendix to the Resolution Copper Mine Plan of Operations**).

Nutt, C., J., 1984. Strata-bound uranium deposits in the Dripping Spring Quartzite, Gila County, Arizona, USA: A model for their formation. In: *Proterozoic Unconformity and stratabound uranium deposits – Report of the working group on uranium geology organised by the International Atomic Energy Agency by Ferguson (ed.)*, p 95-115.

Peterson, D.W., 1969. Geologic map of the Superior quadrangle, Pinal County, Arizona: U.S. Geological Survey Quadrangle Map GQ-818, scale 1:24,000.

Phillips, K.A., 1987. Arizona Industrial Minerals, 2nd. Edition, Arizona Department of Mines & Minerals Mineral Report 4, 185 pages.

Richard, S.M. and Spencer, J.E., 1998. Compilation Geologic Map of the Ray-Superior area, Central Arizona: Arizona Geological Survey Open-file Report 98-13, 47 pages.

Scarborough, R.B., 1981. Radioactive Occurrences and Uranium Production in Arizona, US Dept. of Energy, GJBX-143(81), 93 pages.

Seal, R. R., 2012. Geologic and Environmental Characteristics of Porphyry Copper Deposits with Emphasis on Potential Future Development in the Bristol Bay Watershed, Alaska. USGS Report, 2012.

Seedorff, E., Barton, M.D., Gehrels, G.E., Johnson, D.A., Maher, D.J., Stavast, W.J.A., and Flesch, E., 2005. Implications of new U-Pb dates from porphyry copper related plutons in the Superior-Globe-Ray-Christmas area, Arizona. *Geological Society of America Abstracts with Programs*, v. 37, no. 7, p. 164.

Seedorff, E., Dilles, J.H., Proffett, J.M., Jr., Einaudi, M.T., Zurcher, L., Stavast, W.J.A., Johnson, D.A., and Barton, M.D., 2005, Porphyry deposits: Characteristics and origin of hypogene features: Economic Geology 100th Anniversary Volume, p. 251-298.

Short, M., et al, 1943; Geology and Ore Deposits of the Superior Mining Area, Arizona; Arizona Bureau of Mines Geological Series No. 16, Bulletin No. 151, p. 139-154.

Sinclair, W.D., 2007. Porphyry deposits, in Goodfellow, W.D., ed., Mineral Deposits of Canada: A Synthesis of Major Deposit-Types, District Metallogeny, the Evolution of Geological Provinces, and Exploration Methods: Geological Association of Canada, Mineral Deposits Division, Special Publication No. 5, p. 223-243.

Spencer, J.E., Richard, S.M. and Pearthree, P.A. (digitized by S.M. Kneale). 1998. DI-11 Geologic Map of the Mesa 30' x 60' Quadrangle, Arizona, compiled by, 15 p., 3 disks. Arc/INFO export file (.e00) format.

Spencer, J.E., and Richard, S. 1995. Geologic map of the Picketpost Mountain and the southern part of the Iron Mountain 7 1/2' Quadrangles, Pinal County, Arizona (complementary notes): U.S. Geological Survey Open-File Report 95-15, 16 pages.

Stewart, L.A., 1955. Chrysotile-Asbestos Deposits of Arizona, U.S. Bureau of Mines Information Circular 7706, p. 118-119.

Strickland, D., M. Heizler, J. Selverstone, K.E. Karlstrom. 2003. Proterozoic evolution of the Zuni Mountains Western New Mexico: Relationship to the Jemez lineament and implications for a complex cooling history. New Mexico Geological Society Guidebook, 54th Field Conference, Geology of the Zuni Plateau, 2003, p. 109-117.

Tenney, J.B., 1929. History of Mining in Arizona. Arizona Bureau of Mines. v1, P. 514 (two volumes). Edited and prepared by the Special Collections Division, University of Arizona Library, 1959-1960. Collection Number AZ 198.

Williams, F. J., 1957. Structural control of uranium deposits, Sierra Ancha region, Gila County, Arizona: U.S. Atomic Energy Commission RME-3152, Technical Information Service, Oak Ridge, Tenn., 21 pages.

Wong, I., E. Nemser, M. Dober, S. Olig, J. Bott, F. Terra, R. Darragh and W. Silva, 2013. Site-specific seismic hazard analyses for the Resolution Mining Company tailings storage facilities options, Southern Arizona. Report prepared for Resolution Copper Mining by URS Seismic Hazard Group and Pacific Engineering & Analysis, June 2013, 192 pages (**Submitted to the USFS in support of the EIS**).

Wrucke, C.T., 1989. The Middle Proterozoic Apache Group, Troy Quartzite, and associated diabase of Arizona: Arizona Geological Society Digest v. 17, p. 239-258.

Zulliger, G.A., 2007. Mid-late Cretaceous stratigraphy and volcanic-intrusive transition at the Resolution porphyry Cu-Mo deposit, SW Arizona: Age and timing constraints based on U/Pb, Re/Os and <sup>40</sup>Ar/<sup>39</sup>Ar dating: Internal report to Resolution Copper Mining L.L.C., 41 pages.

**APPENDIX 1. Geological map compiled for the project area at 1: 15,000 scale (W. Hart, Resolution Copper, 2016).**



APPENDIX 2: ELEMENT ABUNDANCE OF THE RESOLUTION COPPER OREBODY (MULTI-ELEMENT GEOCHEMICAL ANALYSIS) COMPARED TO AVERAGE CRUSTAL ABUNDANCE (DATA FROM: MWH, 2013)

WHOLE ROCK ANALYSIS		Al	Sb	As	Ba	Be	Bi	Cd	Ca	Ce	Cs	Cr	Co	Cu	Ga	Ge	In	Fe	La	Pb	Li	Mg	Mo	P	K	Rb	Sulfide	Th	Sn	Ti	Y	Zr	Mn	Ni	Nb	Se	Ag	Na	Sr	Ta	Te	Tl	W	U	V	Zn	
Hole ID	Sample ID	%	PPM	PPM	PPM	PPM	PPM	PPM	%	PPM	PPM	PPM	PPM	PPM	PPM	PPM	PPM	%	PPM	PPM	PPM	%	PPM	PPM	%	%	PPM	PPM	PPM	PPM	PPM	PPM	PPM	PPM	PPM	PPM	PPM	%	PPM	PPM	PPM	PPM	PPM	PPM	PPM	PPM	PPM
Crustal Average		8.36	0.2	1.8	390	2	0.0082	0.16	4.66	66.4	3 <sup>1</sup>	122	29	68	19	1.5	0.1 <sup>1</sup>	6.22	34.6	13	20	2.76	1.2	1120	1.84	78	0.034	8.1	2	0.63	33	162	1060	99	20	0.05	0.08	2.27	384	1.7	0.01 <sup>1</sup>	0.72	1.2	2.3	136	76	
RES-001C	RES-001C 1502-1505	7.2	0.22	1.3	600	2.64	5.71	1.15	0.14	48.7	2.9	175	13.6	2450	23.3	0.11	0.727	2.99	24.3	21.3	17.2	0.44	11.75	490	3.39	153	2.8	3.7	5.4	0.166	8.6	14.8	78	12.1	3.6	5	0.99	0.07	184	0.28	2.8	0.81	25.5	2.4	56	716	
	RES-001C 1530-1533	6.38	0.24	0.6	480	2.21	2.64	0.29	0.36	45.8	5.86	200	14.6	1685	22	0.13	0.339	4.2	22	16.7	15	0.88	17.75	560	3.8	168	3.45	3.9	5.1	0.154	11.5	15.3	274	19.6	3.5	6	0.89	0.38	149.5	0.26	1.58	0.82	17.4	2	54	435	
	RES-001C 1557-1560	6.24	0.31	0.6	320	2.51	1.19	0.04	0.47	46	3.36	203	21.4	906	20.2	0.15	0.086	5.36	22.6	6.1	18.5	0.72	61.2	520	3.53	154	4.82	3.9	6.3	0.124	10.9	12.4	275	15.2	2.6	9	0.28	0.51	121	0.21	0.68	0.53	18.3	1.7	56	221	
	RES-001C 1584-1587	6.82	0.28	0.4	560	2.32	0.55	0.08	0.48	48	4.07	198	24.2	720	20.7	0.13	0.218	5.04	23.2	6.9	25.2	1.03	24	630	3.65	158	2.85	3.8	4	0.166	10.9	11.6	443	24.7	3.5	6	0.25	0.48	146.5	0.27	0.48	0.73	19.5	1.6	59	552	
	RES-001C 1611-1614	6.21	1.07	3.8	530	2.68	8.69	1.66	0.78	47.4	3.98	181	29.5	3360	20.8	0.14	1.615	4.64	23.7	285	19.1	0.81	62.9	590	3.39	159.5	2.57	3.6	3.8	0.175	10.6	11.3	659	18.8	3.8	7	16	0.25	186	0.28	0.7	0.85	25.2	3.3	57	1420	
	RES-001C 1639-1642	6.72	0.54	1.4	610	2.94	0.87	0.71	0.63	48.7	4.92	235	27.2	1270	20.8	0.14	0.759	5.57	25	179	17.9	0.97	29.9	530	3.56	177	2	4	3.8	0.165	10.7	11.5	2390	21.5	3.9	5	1.1	0.3	145.5	0.29	0.4	0.94	16.5	1.6	57	1110	
	RES-001C 1666-1669	6.36	0.39	0.5	540	2.69	0.53	0.22	0.7	46.2	5.72	167	21.5	1690	20	0.13	0.171	4.37	23	29.8	20.3	0.9	93.2	560	3.53	169.5	2.16	3.5	4.7	0.161	10.2	13.5	1465	18.2	3.4	6	0.63	0.2	96.6	0.25	0.2	0.82	16.7	1.5	64	645	
	RES-001C 1693-1696	6.58	0.53	3.7	630	2.81	2.27	0.72	0.58	45	5.82	171	20	2000	21.2	0.12	0.454	3.97	21.4	126	20.8	1.07	68.4	530	3.77	183	1.87	4.1	3.5	0.175	10.3	10.4	1030	17.8	3.7	6	1.15	0.09	96.1	0.28	0.45	1.06	15.5	1.8	61	715	
	RES-001C 1711-1714.96	7.39	0.39	1.1	590	2.28	0.51	0.19	2.95	50.9	6.22	168	18.8	993	22.2	0.13	0.116	4.05	22.9	10.5	15.4	1.15	37.9	920	3.47	166.5	1.98	4.2	3.5	0.345	21	15.8	589	6.2	4.7	5	0.35	1.31	217	0.31	0.22	0.88	8.7	1.2	97	125	
	RES-001C 1745-1748	6.72	0.29	1.1	480	2.85	0.52	0.08	4.36	48.8	5.47	236	14.2	1040	21.1	0.13	0.337	3.77	22.9	8.2	19.1	1.57	116.5	780	3.01	142.5	2.82	4.1	5.3	0.412	20.4	19	756	13.3	7	5	0.48	1.1	257	0.46	0.27	0.71	14	1.7	110	125	
	RES-001C 1771.75-1791.4	1.02	0.63	36	10	7.84	43.3	1.64	17.35	21.6	0.83	182	8.9	2620	13.1	0.18	1.75	4.77	15.8	17.8	23.2	6.42	184.5	500	0.21	17.7	1.92	1.8	9.1	0.058	24.2	32.5	3850	16.2	1.8	7	1.69	0.03	42.4	0.12	21.6	0.07	103	3.9	28	624	
	RES-001C 1781-1784	0.75	0.9	10	10	9.63	25.2	0.9	15.4	31	0.94	14	6.3	1300	7.17	0.1	0.749	1.86	22.3	5.8	13.1	10.25	44.1	360	0.27	24.1	2.42	1.5	4.3	0.054	16.5	27.8	2810	12.9	1.5	5	0.75	0.02	25	11	4.43	0.06	19.6	3.9	18	386	
	RES-001C 1799-1802	0.74	4.47	<5	10	3.79	2.54	2.97	19.05	5.42	0.32	171	17.7	9160	30.7	0.34	5.59	13.6	2.8	6.3	19.5	2.29	532	320	0.03	2.9	3.61	1.4	39.6	0.055	10.8	32.9	3420	7.1	1.7	14	5.09	<0.01	29.8	0.12	1.38	0.04	184.5	9.8	40	659	
	RES-001C 1814-1817	7.24	0.84	1.4	110	12.65	0.38	0.14	8.51	70.9	7.22	71	11.7	2140	28.2	0.15	0.634	3.62	34.8	6.7	20.3	6.06	94.5	1000	2.35	116.5	1.73	12.1	16.7	0.405	23	54.3	2300	21.5	14.1	6	0.8	0.18	129	1.06	0.15	0.52	41.3	6.8	100	126	
	RES-001C 1837-1840	3.77	1.48	<5	50	5.18	0.87	0.55	11.8	50.2	3.18	174	18.2	4270	17.65	0.13	0.791	4.07	25.9	47.5	15.4	7.31	89.4	400	1.34	82.2	2.36	6.5	8.3	0.193	16.9	27.2	3870	15.6	6.8	7	1.24	0.13	81.6	0.53	0.35	0.35	24.4	3.3	49	325	
	RES-001C 1855-1858	2.32	0.61	7	90	8.71	3.05	0.66	14.15	41.8	0.44	212	13.2	3780	28.7	0.16	4	10.4	19.2	29.1	28.8	4.02	34	320	0.3	16.5	1.14	4.3	36.1	0.118	13.3	54.6	4610	9.5	4.6	6	1.12	0.03	51.2	0.35	0.97	0.08	129.5	4.8	41	306	
	RES-001C 1873-1876	4.12	0.48	0.7	170	8.23	0.86	0.84	4.83	34.3	5.81	108	34.3	10000	32.5	0.16	1.255	6.09	14.4	36.2	36.7	7.73	64.6	650	2.39	155.5	1.96	7.8	19.5	0.23	19.8	55.6	1505	21.3	8.7	14	2.79	0.05	90	0.71	0.47	0.49	66.9	9	77	285	
	RES-001C 1892.5-1895	1.58	0.61	3	20	6.92	22.1	11.55	8.9	17.95	2.46	48	20	10000	17.95	0.12	4.09	4.72	8.5	7.7	72.4	11.8	125.5	420	0.7	58	2.59	2.8	12.9	0.087	9.8	22.1	2360	14.5	3.7	11	3.67	0.04	38.2	0.29	12.3	0.27	73.2	5	40	2880	
	RES-001C 1934-1937	0.87	1.11	<0.2	30	0.93	7.84	<0.02	0.1	14.2	0.28	719	20.4	8900	4.5	0.18	0.298	3.61	5.3	13.3	2.1	0.12	910	60	0.41	18.5	3.38	1.9	4.8	0.051	4	15.5	86	28.4	1.1	17	3.95	<0.01	3.7	11	0.59	0.03	13.2	0.9	35	12	
	RES-001C 1987-1990	6.18	0.94	<0.2	190	3.92	1.75	0.38	0.63	19.95	7.31	426	73.9	10000	27.4	0.39	1	9.19	8	9.6	16.5	2.79	1105	1090	3.81	242	3.59	0.3	9.3	0.608	17.5	61.7	1125	96.5	1.2	18	3.93	0.01	19.5	0.11	0.79	0.99	21.8	2.3	214	313	
	RES-001C 2007-2010	6.59	0.21	0.9	500	2.38	1.4	0.42	1.48	22.2	9.23	328	73.2	10000	26.5	0.19	0.646	9.72	9.3	5.9	21.3	3.07	291	1090	4.53	217	2.96	0.8	7.3	0.66	19.5	21	1175	88.9	1.7	14	3.77	0.04	66.2	0.14	1	1.36	14.9	1.4	192	223	
	RES-001C 2041-2044	7.74	0.38	0.3	430	3.09	1.58	0.7	2.07	31.7	9.61	296	63.1	10000	25.1	0.2	0.549	9.73	14	4.2	37.3	3.78	345	1210	3.9	254	3.9	0.9	7.4	0.516	19.9	27.7	1120	108	3	15	4.46	0.06	122.5	0.23	0.71	1.26	17.3	1.2	209	259	
	RES-001C 2115-2118	4.16	0.99	<0.2	70	5.49	3.85	0.8	8.3	39.2	4.53	123	40.1	10000	30.1	0.34	0.997	7.29	17.7	4.2	21	5.17	736	750	1.63	121.5	4.86	2	18.4	0.304	22.3	50	2280	28.2	4.2	18	4.77	<0.01	59.5	0.23	0.98	0.56	41.4	3.2	97	299	
	RES-001C 2164.4-2166.3	0.58	3.75	17.1	70	0.25	23.6	0.11	0.14	17.95	0.06	525	88.2	10000	1.64	0.49	0.992	36.6	7.2	212	2.8	0.05	40.1	200	0.06	2.9	10	1.4	20.6	0.006	0.9	0.5	53	63.6	0.2	49	36.3	<0.01	61.6	0.05	39.5	0.08	5.6	0.6	18	80	
	RES-001C 2214-2215	0.47	0.27	<5	<10	4.39	1.82	3.42	10.5	4.82	0.06	175	32.8	10000	7.62	0.12	2.36	7.12	2.1	5.4	1.6	9.03	102	130	0.06	3.4	6.92	0.9	7.9	0.015	4.1	11.3	3040	7.7	0.6	15	7.47	0.01	35.3	0.05	1.62	0.03	161.5	1.9	22	868	
	RES-001C 2242-2244	5.96	0.96	<0.2	210	3.75	18.95	0.02	3.28	57.7	2.2	383	57.6	10000	29.9	0.32	1.1	9.82	23.4	2.2	5.1	2.04	673	3330	2.74	146.5	8.5	2.1	13.8	0.546	19.1	29.7	455	58.4	2	19	4.37	<0.01	118.5	0.18	1.62	0.55	45.6	3.7	220	96	
RES-002A	RES-002A 858-861	8.31	0.78	20.1	1320	1.55	2.77	0.05	0.06	58.9	2.14	129	0.7	198.5	26.5	0.05	1.4	1.63	28.7	54.6	8.1	0.25	2.67	240	5.7																						

WHOLE ROCK ANALYSIS		Al	Sb	As	Ba	Be	Bi	Cd	Ca	Ce	Cs	Cr	Co	Cu	Ga	Ge	In	Fe	La	Pb	Li	Mg	Mo	P	K	Rb	Sulfide	Th	Sn	Ti	Y	Zr	Mn	Ni	Nb	Se	Ag	Na	Sr	Ta	Te	Tl	W	U	V	Zn			
Hole ID	Sample ID	%	PPM	PPM	PPM	PPM	PPM	PPM	%	PPM	PPM	PPM	PPM	PPM	PPM	PPM	PPM	%	PPM	PPM	PPM	%	PPM	PPM	%	PPM	PPM	PPM	PPM	PPM	PPM	PPM	PPM	PPM	PPM	PPM	PPM	PPM	PPM	PPM	PPM	PPM	PPM	PPM	PPM	PPM	PPM	PPM	PPM
Crustal Average		8.36	0.2	1.8	390	2	0.0082	0.16	4.66	66.4	3 <sup>1</sup>	122	29	68	19	1.5	0.1 <sup>1</sup>	6.22	34.6	13	20	2.76	1.2	1120	1.84	78	0.034	8.1	2	0.63	33	162	1060	99	20	0.05	0.08	2.27	384	1.7	0.01 <sup>1</sup>	0.72	1.2	2.3	136	76			
RES-005I	RES-005I 1473.13-1476.13	3.85	--	17	1200	--	2.9	0.03	0.08	--	0.37	--	0.7	80.6	11.9	0.2	0.111	5.45	--	14.8	0.7	--	70.5	270	1.67	62.9	--	3.7	7.7	0.089	2.2	18.5	51	2.2	2.9	8	2.79	0.04	42.6	0.23	2.86	0.21	--	0.9	35	19			
	RES-005I 1481-1482.66	2.82	--	25.2	180	--	5.85	<0.02	0.06	--	0.43	--	1.8	60.4	12.05	0.22	0.107	6	--	121	0.8	--	35.5	460	1.22	59.6	--	4.5	11.6	0.109	2.2	18.1	34	6	3.3	9	3.48	0.03	115	0.27	4.18	0.17	--	0.8	23	17			
	RES-005I 1485.5-1486.51	2.81	--	24.7	180	--	5.8	0.1	0.06	--	0.42	--	1.7	61.7	11.95	0.21	0.106	5.96	--	119	0.8	--	35.1	440	1.18	58.7	--	4.5	11.4	0.104	2.1	17.6	32	5.7	3.1	9	5.04	0.03	113.5	0.26	4.08	0.17	--	0.8	22	17			
	RES-005I 1487.1-1490.1	6.22	--	7.5	3630	--	2.19	0.02	0.07	--	0.71	--	0.6	144	23.1	0.19	0.332	2.81	--	15.8	0.9	--	29.6	410	2.87	120	--	4.4	7.8	0.112	3.3	17.4	43	1.5	3.8	4	3.44	0.06	52.9	0.31	1.28	0.41	--	1.1	35	23			
	RES-005I 1490.1-1493.1	6.15	--	13.8	820	--	2.45	0.02	0.07	--	0.79	--	0.6	82.1	24.4	0.23	0.16	4.33	--	55.4	0.9	--	51	430	2.87	121	--	4.5	8.8	0.105	3	19.8	40	1.5	3.4	6	2.35	0.05	84.1	0.3	1.9	0.4	--	1.1	38	25			
	RES-005I 1499-1502	7.03	--	11.4	500	--	1.22	<0.02	0.07	--	0.95	--	0.5	41.7	25.4	0.21	0.115	2.61	--	48.3	1.4	--	19.1	510	3.27	138.5	--	4.4	7.3	0.131	3.3	29.6	38	1.4	4.4	7	1.84	0.05	120	0.35	0.61	0.5	--	1.1	47	24			
	RES-005I 1506.56-1509.47	6.41	--	8.6	530	--	0.86	<0.02	0.13	--	0.86	--	0.6	64.4	21.6	0.23	0.201	2.28	--	44.1	1.1	--	18.4	800	2.97	122.5	--	6	7.8	0.237	4.4	33.1	37	1.7	5.8	11	2.8	0.05	111.5	0.39	2.77	0.42	--	1.2	91	28			
	RES-005I 1515.47-1518.47	6.69	--	4.6	580	--	1.65	<0.02	0.08	--	0.84	--	0.6	59.5	24.8	0.2	0.157	1.82	--	26.1	1	--	14.5	440	3.06	130.5	--	4.8	7.5	0.129	3.1	16.1	41	1.6	5.3	7	1.43	0.05	96.1	0.42	0.88	0.43	--	0.9	37	26			
	RES-005I 1524.47-1527.47	6.56	--	15	750	--	2.74	0.02	0.03	--	0.87	--	0.5	5130	24.4	0.25	0.112	3.2	--	12.6	1	--	33	290	2.96	126.5	--	4	9.2	0.103	2.2	12.7	41	1.9	3.9	9	3.91	0.05	56.6	0.32	1.38	0.4	--	0.8	37	21			
	RES-005I 1532.98-1534.97	6.77	--	5.7	510	--	2.38	<0.02	0.12	--	0.77	--	0.6	887	24	0.18	0.108	1.39	--	81.8	0.8	--	9.26	380	3.21	132	--	4	11.5	0.128	2.4	15.8	43	1.3	5.3	3	3.94	0.06	116	0.42	0.67	0.39	--	0.8	38	30			
	RES-005I 1544-1546.55	3.48	--	20.3	470	--	4.86	<0.02	0.05	--	0.37	--	0.5	441	19.6	0.24	0.237	3.1	--	392	4.9	--	23.7	710	1.26	60.7	--	6.2	26	0.136	1.9	15.8	49	1.3	5	8	22.8	0.03	611	0.38	2.28	0.16	--	1	31	15			
	RES-005I 1552.55-1555.58	5.24	--	11.9	350	--	4.04	<0.02	0.05	--	0.7	--	0.9	95.3	23	0.29	0.18	4.71	--	64.7	2.1	--	34.1	450	2.24	98.7	--	5	16	0.105	2.3	13.4	52	2.2	3.9	8	4.02	0.05	184	0.28	1.22	0.3	--	0.8	41	26			
	RES-005I 1559.46-1562.46	5.84	--	7.5	380	--	2.96	<0.02	0.04	--	0.7	--	1.9	202	25.5	0.24	0.134	3.43	--	41.9	0.9	--	32.2	330	2.64	111	--	3.9	12.5	0.104	2.4	14.7	64	2.1	4.2	10	2.1	0.05	117.5	0.32	1.37	0.31	--	0.8	44	31			
	RES-005I 1568.46-1571.46	6.21	--	8.2	380	--	1.53	0.02	0.04	--	0.61	--	1	147	22.4	0.18	0.118	3.56	--	20.1	1	--	33.3	390	2.84	112.5	--	3.8	10.8	0.098	2.2	14.8	61	3.1	3.3	11	1.29	0.05	85.6	0.27	0.75	0.3	--	0.8	40	26			
	RES-005I 1586.46-1589.46	6.4	--	12.9	610	--	1.89	<0.02	0.04	--	0.66	--	1.4	230	26	0.09	0.155	3.78	--	22.8	1.2	--	25.1	390	2.96	118	--	3.8	10.3	0.094	2.6	15.5	43	3	2.8	10	6.77	0.05	110	0.24	1.43	0.35	--	0.8	51	35			
	RES-005I 1604.46-1607.46	6.9	--	6.3	640	--	1.77	<0.02	0.05	--	0.74	--	1.2	37.6	31.1	0.08	0.194	1.58	--	60.5	1.1	--	13.8	530	3.24	128.5	--	4.5	11.5	0.116	2.8	15.1	41	2	3.9	9	7.53	0.06	210	0.32	1.11	0.36	--	0.8	55	22			
	RES-005I 1613.46-1616.46	7.41	--	15.7	620	--	1.96	<0.02	0.05	--	0.73	--	2.2	40.4	32.9	0.09	0.317	2.16	--	31	1	--	29.5	590	3.49	137.5	--	4.5	13.1	0.112	2.7	15.6	15	5.7	3.3	8	1.59	0.06	186.5	0.29	2.01	0.37	--	1	60	22			
	RES-005I 1616.46-1619	7.25	--	9.5	580	--	1.54	<0.02	0.05	--	0.68	--	1.4	47	34.3	0.08	0.409	1.47	--	32	0.9	--	14.25	630	3.4	127.5	--	4.9	12.2	0.113	3.1	14.5	26	2.2	4	7	0.91	0.05	287	0.35	9.54	0.35	--	1	60	31			
	RES-005I 1626.54-1627.16	2.29	--	84.3	570	--	9.77	<0.02	0.04	--	0.61	--	1.4	158.5	18.8	0.18	1.285	8.86	--	72.8	1.8	--	144.5	630	0.96	37.6	--	5.3	10.3	0.089	2.6	20.3	90	3.5	2.6	24	3.2	0.02	327	0.18	45.5	0.15	--	1.5	63	24			
	RES-005I 1627.16-1630	7.02	--	21.4	570	--	2.09	<0.02	0.03	--	0.78	--	2.1	630	27.9	0.09	0.268	2.4	--	7.5	2.9	--	30.6	380	3.35	130.5	--	3.5	11.6	0.101	2.1	14.8	39	5.5	3.1	14	0.61	0.06	112	0.27	1.76	0.38	--	0.7	60	21			
	RES-005I 1630.5-1631.5	7.2	--	17.8	580	--	2.15	<0.02	0.02	--	0.79	--	2.1	280	28	0.17	0.257	2.68	--	7.7	3.1	--	36	390	3.42	122.5	--	3.7	12.1	0.104	2.2	15.6	31	5.5	3.2	13	0.49	0.05	117.5	0.27	1.87	0.39	--	0.8	60	14			
	RES-005I 1632.56-1635.56	7.2	--	2.4	250	--	0.79	0.23	0.01	--	0.76	--	20	3080	24.7	0.24	0.097	4.85	--	4.2	3.3	--	28.2	300	3.55	122.5	--	3.8	10.4	0.091	3.5	17	39	6.3	3.4	18	0.91	0.04	131.5	0.27	0.56	0.35	--	1.1	43	53			
	RES-005I 1638.37-1641	7.82	--	4.7	250	--	1.08	0.3	0.02	--	0.9	--	26.1	3930	26.8	0.28	0.115	5.85	--	4.6	4.3	--	65.6	390	3.87	133	--	5.4	11.6	0.156	5.6	53.2	31	11.7	3	19	2.74	0.04	237	0.22	0.47	0.41	--	1.7	74	61			
	RES-005I 1645.84-1648.08	7.33	--	34.9	640	--	3.77	0.19	0.04	--	1.02	--	5.9	1385	35.6	0.54	0.518	3.59	--	48	2.8	--	32.1	470	3.46	128.5	--	4.6	10.7	0.097	2.7	14.7	49	3.2	3.6	109	33.6	0.04	238	0.28	4.07	0.45	--	1	64	25			
	RES-005I 1652-1654.93	7.13	--	3.2	310	--	1.36	0.04	0.02	--	0.81	--	33.2	2320	27.2	0.39	0.163	5.83	--	43.7	2.7	--	60.4	370	3.41	122	--	4.2	10.3	0.098	3	16.1	50	6.2	3.8	53	1.67	0.03	99.5	0.29	0.63	0.4	--	1.2	50	2			
	RES-005I 1654.93-1657.3	5.92	--	7.4	130	--	4.42	<0.02	0.06	--	0.61	--	29.5	10000	26.9	0.62	0.237	6.4	--	304	3.2	--	223	680	2.56	91.4	--	5.7	15.1	0.095	2.4	17.1	48	8.1	3.6	116	7.72	0.02	475	0.27	1.07	0.31	--	2.1	53	7			
	RES-005I 1677.8-1680.8	7.89	--	55.7	370	--	8.29	<0.02	0.02	--	1	--	36.6	10000	36.9	0.31	0.409	5.11	--	73.8	5.4	--	414	520	3.75	146.5	--	4	13.1	0.104	3.5	18.8	35	11.1	3.6	26	1.43	0.04	205	0.32	1.91	0.48	--	1.6	96	28			
	RES-005I 1695.23-1697.23	7.78	--	98.7	550	--	1.39	0.39	0.02	--	0.92	--	15.4	10000	27.7	0.24	0.148	3.13	--	4.6	3.4	--	166	520	3.83	130	--	4.8	17	0.144	4	51.5	30	9.5	3.5	15	1.86	0.04	194.5	0.24	5.37	0.41	--	2	84	25			
	RES-005I 1711.23-1713.23	6.21	--	15.4	270	--	2.52	<0.02	<0.01	--	0.68	--	28	10000	20.4	0.26	0.103	5.06	--	3.6	2.6	--	160.5	240	2.96	103.5	--	2.8	15.3	0.082	2.2	12.8	60	6.8															

WHOLE ROCK ANALYSIS		Al	Sb	As	Ba	Be	Bi	Cd	Ca	Ce	Cs	Cr	Co	Cu	Ga	Ge	In	Fe	La	Pb	Li	Mg	Mo	P	K	Rb	Sulfide	Th	Sn	Ti	Y	Zr	Mn	Ni	Nb	Se	Ag	Na	Sr	Ta	Te	Tl	W	U	V	Zn		
Hole ID	Sample ID	%	PPM	PPM	PPM	PPM	PPM	PPM	%	PPM	PPM	PPM	PPM	PPM	PPM	PPM	PPM	%	PPM	PPM	PPM	%	PPM	PPM	%	PPM	PPM	PPM	PPM	PPM	PPM	PPM	PPM	PPM	PPM	PPM	PPM	PPM	PPM	PPM	PPM	PPM	PPM	PPM	PPM	PPM	PPM	PPM
Crustal Average		8.36	0.2	1.8	390	2	0.0082	0.16	4.66	66.4	3 <sup>1</sup>	122	29	68	19	1.5	0.1 <sup>1</sup>	6.22	34.6	13	20	2.76	1.2	1120	1.84	78	0.034	8.1	2	0.63	33	162	1060	99	20	0.05	0.08	2.27	384	1.7	0.01 <sup>1</sup>	0.72	1.2	2.3	136	76		
RES-006D	1954.83-1972	5.20	--	18.5	160	--	20.60	<0.02	0.07	--	0.5	--	21.0	6170	25.4	0.22	0.570	4.35	--	284.0	8.8	--	347	500	2.05	76.7	--	3.9	18.6	0.144	5.1	27.3	46	14.3	3.7	13	2.81	0.01	271.0	0.33	0.98	0.17	--	1.6	118	7		
RES-006D	1980.6-1983.6	3.96	--	3.6	90	--	2.28	3.53	0.11	--	0.5	--	80.5	4190	18.8	0.35	1.060	12.15	--	271.0	4.5	--	440	610	1.61	65.1	--	4.5	13.6	0.082	6.9	13.7	75	30.5	2.6	31	1.32	0.02	138.5	0.12	0.76	0.21	--	2.5	122	345		
RES-006D	1995.6-1998.6	3.97	--	0.8	110	--	8.00	<0.02	0.28	--	0.5	--	86.5	10000	21.4	0.48	4.360	10.35	--	322.0	5.6	--	1530	980	1.22	57.7	--	4.1	22.5	0.082	9.2	15.3	82	35.3	2.9	39	4.97	0.02	179.5	0.14	3.14	0.24	--	5.6	107	443		
RES-006D	2022.66-2025.66	6.24	--	<0.2	120	--	4.01	<0.02	0.22	--	0.8	--	80.6	10000	20.8	0.96	0.755	9.05	--	60.0	6.1	--	5980	1130	2.79	135.0	--	0.5	65.3	0.142	11.6	7.0	70	83.4	2.2	49	3.03	0.04	301.0	<0.05	1.92	0.44	--	1.2	167	213		
RES-006D	2040.66-2043.66	7.77	--	1.4	170	--	1.36	<0.02	0.28	--	2.4	--	55.1	10000	21.6	0.36	0.903	6.42	--	92.1	6.8	--	661	1220	3.76	181.0	--	0.5	21.7	0.261	46.6	27.7	148	46.5	1.6	27	2.29	0.07	154.5	0.10	0.31	0.59	--	1.9	202	374		
RES-006D	2058.16-2061.16	7.29	--	1.3	150	--	0.90	<0.02	0.66	--	5.9	--	46.7	10000	23.4	0.27	0.308	6.97	--	7.6	22.2	--	102	1700	4.01	163.5	--	0.5	14.1	0.480	11.0	11.5	289	67.5	2.2	22	2.83	0.08	31.7	0.16	1.54	1.10	--	0.6	211	96		
RES-006D	2073.13-2076.13	6.17	--	2.0	160	--	1.38	0.5	0.47	--	4.9	--	43.8	10000	22.5	0.33	0.755	8.45	--	19.6	11.9	--	121	1540	4.04	134.0	--	0.4	21.4	0.382	11.0	10.7	410	64.5	1.5	38	2.95	0.08	20.5	0.12	0.32	0.96	--	0.8	204	394		
RES-006D	2091.13-2094.13	8.40	--	0.7	250	--	0.42	<0.02	0.56	--	8.0	--	30.5	10000	24.7	0.26	0.467	5.67	--	17.7	26.6	--	417	1730	4.94	292.0	--	0.6	15.5	0.463	12.3	12.9	489	61.6	1.8	20	2.59	0.08	59.2	0.14	0.33	1.23	--	0.7	204	151		
RES-006D	2115.47-2118.47	5.06	--	<0.2	150	--	37.50	0.26	0.22	--	0.6	--	12.4	8870	15.7	0.43	0.639	4.46	--	147.0	6.5	--	595	310	2.19	87.7	--	8.4	22.9	0.089	8.4	18.0	67	19.1	2.1	21	7.69	0.05	84.6	0.16	1.39	0.25	--	1.5	98	26		
RES-006D	2125.45-2128.42	5.54	--	<0.2	310	--	5.56	<0.02	0.11	--	0.6	--	18.9	6140	18.0	0.38	0.282	3.55	--	154.0	5.9	--	556	400	2.62	101.0	--	9.1	23.1	0.112	9.4	18.0	53	15.7	3.3	14	3.38	0.04	93.1	0.22	0.62	0.28	--	1.7	101	30		
RES-006D	2137.08-2138.5	5.81	--	5.1	110	--	34.40	<0.02	0.45	--	0.1	--	35.0	6620	36.7	0.35	0.462	9.49	--	2350.0	36.1	--	361	2080	0.51	18.1	--	10.3	40.9	0.089	7.9	24.6	35	19.3	3.1	19	5.36	0.02	1820.0	0.19	6.83	0.06	--	3.2	104	6		
RES-009	RES-009 7.43-7.96	--	0.28	1	1080	3.08	0.04	0.05	1.41	99.4	4.12	145	4.7	24.2	20.2	0.2	0.058	--	--	20.9	25	0.31	1.58	580	3.07	114.5	0.02	12.2	1.9	0.238	29.9	53	655	4.9	17.2	3	0.01	2.57	348	1.28	<0.05	0.6	1.1	2.3	26	67		
RES-009	RES-009 199.18-199.78	--	0.23	1.4	990	2.44	0.08	0.11	1.59	103.5	3.52	133	4.6	8.6	20.1	0.15	0.051	--	--	18.7	41.8	0.48	1.52	580	2.76	106.5	<0.01	10.2	1.8	0.259	27.9	49.4	638	4.1	20	2	0.06	2.66	373	1.21	<0.05	0.42	1.2	2.4	27	62		
RES-009	RES-009 199.78-200.3	--	0.23	1.1	1000	2.51	0.08	0.12	1.61	102.5	3.6	140	4.7	9.2	20.4	0.15	0.05	--	--	19.4	43	0.5	1.49	590	2.78	110.5	<0.01	10.6	1.9	0.266	28.5	50.6	647	4.6	20.4	2	0.05	2.68	376	1.26	<0.05	0.44	1.2	2.5	28	62		
RES-009	RES-009 281.14-281.64	--	0.23	1.2	990	2.57	0.09	0.06	1.62	102	4.09	139	5	8.5	20.6	0.15	0.051	--	--	20	40.2	0.53	1.05	570	2.76	109	<0.01	10.2	1.8	0.238	28.6	54.8	638	4.6	19.4	2	0.06	2.48	609	1.23	<0.05	0.46	1	2.5	26	64		
RES-009	RES-009 348.3-348.83	--	0.25	1.6	1040	2.62	0.1	0.06	1.7	100	2.95	247	5.2	9.8	20.9	0.16	0.051	--	--	20.1	42.7	0.42	1.44	620	2.9	110	<0.01	10.2	1.9	0.263	28	50.3	722	6.3	20.1	2	0.04	2.96	408	1.21	<0.05	0.5	1.1	2.4	29	64		
RES-009	RES-009 447.23-447.8	--	0.91	7.3	710	1.72	0.27	0.22	3.91	67.5	11.25	165	22.4	63.8	18.55	0.17	0.095	--	--	29.9	65.1	1.71	1.22	910	2.38	97.3	<0.01	6.8	1.6	0.499	24.1	83.9	770	41.3	12.5	2	0.21	1.63	541	0.77	0.26	0.46	1.9	1.8	85	136		
RES-009	RES-009 485.12-485.71	--	0.96	8.8	430	1.23	0.31	0.37	7.23	46.7	4.05	181	22.6	108.5	15.65	0.16	0.163	--	--	31.4	24.9	1.72	3.71	840	1.92	68.2	0.01	4.4	1.5	0.508	19.8	70.9	1110	45.6	8	2	0.14	1.34	508	0.49	0.21	0.39	2.3	2.9	96	186		
RES-009	RES-009 557.06-557.56	--	1.66	26.5	700	4.69	1.89	0.19	0.87	81.8	14.5	82	26.4	2610	37	0.15	0.583	--	--	34.8	45.6	1.48	57.3	940	3.73	190	0.02	11.1	12.3	0.242	17.6	47.1	549	40.8	9.6	3	0.6	0.59	117	0.69	0.96	1.06	14.9	3.4	90	184		
RES-009	RES-009 647.52-648.1	--	1.65	8.4	330	1.88	0.76	0.45	3.4	60.1	6.89	179	34.3	714	20.9	0.15	0.284	--	--	33.6	44.5	2.22	13.05	1030	2.03	101	0.01	6.4	3.1	0.838	21.9	60.8	1275	58.5	9.5	3	0.24	1.24	219	0.63	0.6	0.56	5.2	1.7	158	286		
RES-009	RES-009 718-718.58	--	0.51	14.8	350	2.35	1.8	0.03	0.27	70.9	7.73	390	6.3	1480	24.5	0.21	0.908	--	--	56.9	8.6	0.33	71.6	1260	3.27	130.5	0.02	10.4	7.9	0.382	11.3	46	341	16	4.8	3	0.17	0.11	95.4	0.33	2.12	0.59	9.4	3.2	124	87		
RES-009	RES-009 810.42-810.98	--	1.47	7.5	240	1.44	1.92	0.9	4.93	44.6	3.76	165	31.6	404	20	0.15	0.871	--	--	69.9	17.6	3.23	9.73	1330	1.56	78	0.02	4.2	4	0.705	23.4	58.9	1665	70.4	6.6	2	0.2	0.9	230	0.42	1.92	0.51	5.1	1.3	149	547		
RES-009	RES-009 906.08-906.58	--	0.84	4.1	330	1.49	1.11	0.43	4.69	40.4	2.36	199	27.1	406	20.1	0.18	0.553	--	--	39.6	12.8	2.51	5.02	840	2.14	93.2	0.02	3.6	3.9	0.55	19	66.2	1650	58	5.6	2	0.41	0.73	170	0.35	0.79	0.61	5.8	1.2	141	416		
RES-009	RES-009 987.9-988.45	--	1.86	34.6	210	1.94	6.27	0.27	0.6	44.9	1.73	242	46.8	1210	33.5	0.22	1.385	--	--	151	5.3	0.84	19.85	830	1.9	94.5	0.06	4.7	16.4	0.362	11.6	39.9	641	30.9	3.9	7	2.72	0.1	106	0.25	6.43	0.57	24.2	2.6	147	498		
RES-009	RES-009 994.67-997.67	--	0.95	25.9	990	3.27	2.64	0.15	0.32	45.6	2.29	265	6.7	784	27.4	0.15	2.36	--	--	87.5	5.1	0.44	8.34	410	5.3	251	0.02	5.1	2.1	0.182	9.4	23.8	698	12.5	8	2	0.39	0.11	151	0.56	1.33	2.24	6.6	3.4	51	454		
RES-009	RES-009 1012.16-1014.16	--	0.71	33	1050	2.44	2.13	0.1	0.31	51.7	1.92	267	5.1	934	23.8	0.14	1.76	--	--	132.5	4.1	0.41	4.83	420	5.05	226	0.01	4.4	1.4	0.176	7.6	18	717	10.5	7.3	1	0.6	0.37	174	0.5	0.86	2.03	6.6	2.3	34	946		
RES-009	RES-009 1027.38-1030.3	--	0.69	43.5	1010	2.01	0.96	0.13	0.85	57.4	1.58	270	7	1180	24.9	0.15	0.62	--	--	42.9	4.7	0.35	4.97	620	3.83	157	0.02	4.5	1.4	0.179	11	21.5	1165	9.9	8.1	2	0.67	1.66	442	0.56	0.59	1.27	6.8	2.7	34	649		
RES-009	RES-009 1045.3-1048.3	--	0.4	12.9	920	1.72	0.53	0.02	0.29	57.6	1.01	244	6.5	2600	26.1	0.14	0.712	--	--	19.1	5.5	0.47	2.66	320	3.96	161.5	1	4.7	1.3	0.178	28.2</																	

WHOLE ROCK ANALYSIS		Al	Sb	As	Ba	Be	Bi	Cd	Ca	Ce	Cs	Cr	Co	Cu	Ga	Ge	In	Fe	La	Pb	Li	Mg	Mo	P	K	Rb	Sulfide	Th	Sn	Ti	Y	Zr	Mn	Ni	Nb	Se	Ag	Na	Sr	Ta	Te	Tl	W	U	V	Zn	
Hole ID	Sample ID	%	PPM	PPM	PPM	PPM	PPM	PPM	%	PPM	PPM	PPM	PPM	PPM	PPM	PPM	PPM	%	PPM	PPM	PPM	%	PPM	PPM	%	%	PPM	PPM	PPM	%	PPM	PPM	PPM	PPM	PPM	PPM	%	PPM	PPM	PPM	PPM	PPM	PPM	PPM	PPM	PPM	PPM
Crustal Average		8.36	0.2	1.8	390	2	0.0082	0.16	4.66	66.4	3 <sup>1</sup>	122	29	68	19	1.5	0.1 <sup>1</sup>	6.22	34.6	13	20	2.76	1.2	1120	1.84	78	0.034	8.1	2	0.63	33	162	1060	99	20	0.05	0.08	2.27	384	1.7	0.01 <sup>1</sup>	0.72	1.2	2.3	136	76	
	RES-009E 1846.66-1849.66	2.03	0.58	4.1	20	4.68	3.04	5.82	3.62	26.7	1.1	42	52.1	10000	35.4	0.27	4.47	16.15	15.7	7.9	8	1.23	362	740	0.34	27.9	10	3.4	35.7	0.13	12.9	25.6	1060	23.5	4.8	40	5.34	0.01	14.3	0.28	2.68	0.13	169.5	15.5	125	2440	
	RES-009E 1862.15-1865.15	1.85	0.31	11	10	3.43	3.55	0.34	10.75	25.1	1.15	36	39.3	10000	27.5	0.4	1.825	12.85	16.5	14.5	9.6	1.51	389	760	0.24	25.2	10	2.9	26.3	0.131	14.4	32.9	2580	10.8	4.4	33	3.94	0.01	22.6	0.27	2.57	0.09	82	6.8	79	258	
	RES-009E 1867.87-188	1.63	0.6	6	100	3.03	4.89	5.26	15.6	20.9	1.02	431	50.5	10000	37.9	0.41	4.19	13.4	16	3.3	11.5	1.56	439	980	0.31	32.6	9.26	2.5	31.8	0.089	14.8	37.8	2660	27.5	3.1	39	5.93	<0.01	48.7	0.2	4.04	0.11	119.5	11.7	111	2140	
	RES-009E 1880.15-1882.37	0.94	0.63	5	10	3.68	3.31	3.32	13.8	17.3	0.63	161	38.4	10000	33	0.34	3.52	10.9	13.5	4.8	15.4	1.22	385	830	0.2	18.6	7.36	1.4	28.7	0.059	8.8	20.1	2440	12.5	2	35	6.74	0.01	35.4	0.12	4.23	0.09	132.5	8.2	81	1200	
	RES-009E 1885.5-1886.5	0.92	0.65	5	10	3.96	3.35	3.43	13.95	17.45	0.65	140	41.4	10000	33.8	0.35	3.74	11.25	13.8	3.2	16.8	1.2	389	820	0.19	19.4	7.77	1.4	29.8	0.058	9.3	21	2470	13.4	2.1	38	7	0.01	37	0.12	4.36	0.09	139	8.6	80	1200	
	RES-009E 1899-1901.88	3.03	0.12	2	70	3.45	0.65	0.44	3.05	22.2	1.93	55	49.7	10000	26.5	0.41	1.335	8.84	9.7	2.5	12	1.14	316	320	1.07	67.4	6.71	4.5	20.7	0.151	15.3	20.6	705	36.2	4.5	54	4.35	0.02	16.8	0.28	0.98	0.21	36.8	4.9	138	183	
	RES-009E 1929.76-1932.58	0.64	0.18	12.8	10	2.6	2.83	3.57	6.33	10	0.32	11	41	10000	24.7	0.39	3.49	14.5	5.5	2.5	7.9	0.59	70.1	260	0.14	11.5	8.43	1	23.7	0.039	11.2	8.3	1420	14.2	1.8	45	2.88	0.01	8.4	0.09	2.62	0.06	175.5	4.5	89	1590	
	RES-009E 1947.67-1950.67	4.1	0.48	<0.2	80	4.19	4.48	0.05	4.05	39.7	3.77	29	51.3	10000	22.3	0.3	0.905	7.32	18.8	3.5	11.4	5.07	245	780	2.33	156.5	6.14	5.8	17.5	0.165	14.3	39.2	555	36.9	5.4	25	3.18	0.03	8.3	0.36	1.06	0.54	39.9	3.9	109	82	
	RES-009E 1954.6-1956	3.9	0.45	1.2	260	3.78	0.83	<0.02	2.46	32	2.22	13	28.2	10000	24	0.23	0.597	4.67	16.9	2.7	23.5	3.52	203	760	2.42	117.5	3.45	3.6	16.4	0.111	10.8	18.3	451	23.6	2.8	29	2.75	0.03	24	0.21	0.68	0.43	31.4	3.3	119	78	
	RES-009E 1967.76-1969.72	6.61	0.13	1	580	5.52	0.38	0.02	0.23	39.1	2.24	11	18.9	9650	27	0.18	0.31	2.54	20.7	4.2	12	1.22	36.7	620	5.35	185.5	1.7	4.4	16.6	0.149	6.6	16.2	150	21.4	2.6	14	1.45	0.07	53.9	0.2	0.24	0.65	24.3	1.3	117	30	
	RES-009E 1974.78-1977.89	1.76	0.27	<5	10	4.47	1.81	2.64	13.5	18.95	1.02	13	19.3	10000	25.6	0.2	3.45	6.67	8.7	7.4	3.5	10.7	63.2	450	0.38	34	3.45	2.5	19.9	0.069	9.1	17.7	1755	18.5	2.8	20	3.33	0.02	26.2	0.19	1.17	0.17	123.5	4.3	48	773	
	RES-009E 1984.74-1987.74	0.21	1.44	1.8	10	0.21	503	<0.02	0.96	5.55	<0.05	4	7	10000	0.91	0.27	0.598	2.8	2.2	36	1.2	0.02	643	40	0.01	1.1	3.38	1.1	15.7	0.014	2.1	3.7	88	11	1.3	7	25.9	<0.01	42.7	0.08	1.56	<0.02	3.7	0.3	5	177	
	RES-009E 2056.38-2075	6.35	0.12	1.2	220	4.47	1.01	<0.02	3.33	33.8	5.77	519	28.2	10000	27.9	0.29	0.281	5.71	13.8	2.5	11.3	2.67	202	1280	4.44	187	5.99	1	13.5	0.432	12.8	11	212	82.9	2.3	15	1	0.02	176	0.16	0.39	0.84	23.4	3.7	239	60	

-- Not available  
Crustal Average Price,W., 1997, "Guidelines and Recommended Methods for the Prediction of Metal Leaching and Acid Rock Drainage at Minesites in British Columbia", Appendix 3  
Crustal Average<sup>1</sup> Mason, B. and Moore, C.B., 1982, "Principles of Geochemistry", John Wiley & Sons, New York